UNIVERSIDADE DE LISBOA

FACULDADE DE FARMÁCIA

CHITOSAN SCAFFOLDS CONTAINING CALCIUM PHOSPHATE AND DICLOFENAC FOR BONE REGENERATION

DEVELOPMENT, VALIDATION AND OPTIMIZATION

Lara Mariana Almeida Duarte das Neves

The dissertation was supervised by

José Manuel Ventura, Ms and Lídia Diogo Gonçalves, PhD

Master in Biopharmaceutical Sciences

2018

UNIVERSIDADE DE LISBOA

FACULDADE DE FARMÁCIA

CHITOSAN SCAFFOLDS CONTAINING CALCIUM PHOSPHATE AND DICLOFENAC FOR BONE REGENERATION

DEVELOPMENT, VALIDATION AND OPTIMIZATION

Lara Mariana Almeida Duarte das Neves

The dissertation was supervised by

José Manuel Ventura, Ms and Lídia Diogo Gonçalves, PhD

Master in Biopharmaceutical Sciences

2018

“O sucesso nasce do querer, da determinação e persistência em se chegar a um objetivo. Mesmo não atingindo o alvo, quem busca e vence obstáculos, no mínimo fará coisas admiráveis”

José de Alencar

ABSTRACT

In the last decades a growing need for bone substitutes has been detected. This is mainly related to the increasing aging of the population which leads to the increase of muscle and bones disorder.

Bone loss may result from congenital malformations, tumour resections, trauma, short-term and acute onset pathologies, and chronic diseases or even from aging, which may promote physical incapacity and prolonged pain. The application of implants in order to solve these losses is not always positive and some inconveniences may occur, such as the infection development, immune rejections or local tissues death.

At the moment, the market offers numerous solutions with different biomaterials with singular properties combinations that mimic the original bone tissue constitution. However, cases where bone regeneration is associated with local inflammatory response control after surgery are rare. In order to overcome this limitation, a three-dimensional porous matrix (scaffold) incorporating diclofenac will be developed with the goal of release anti-inflammatory drug in a controlled and localized way as it degrades. This drug promotes the inflammation reduction and it is widely used in the treatment of diseases of bones and joints.

This porous matrix of chitosan, calcium phosphate and sodium diclofenac was subjected to the lyophilization process, and it was later characterized in more detail in terms of porosity and structures surfaces by scanning electron microscopy (SEM), of chemical composition and crystallographic structure of calcium phosphate granules by X-ray diffraction (XRD), of particle size by laser beam diffraction, of release profile measured in phosphate buffered saline (PBS) and determined by UV-Vis spectroscopy and absorption capacity by the captive bubble method.

Since no viable microorganisms should exist in medical devices, the scaffolds were subjected to a sterilization process by gamma radiation, guaranteeing the inactivation of microorganisms and providing biological safety.

The scaffolds ability to release drug was studied for 41 days by the diclofenac release assay, with a faster exchange within the first 7 hours. Through the destruction of the samples it was possible to determine that 20% of diclofenac was still remaining in the non-irradiated samples and 40% in the irradiated ones. In this way, it was verified that the radiation influences the release profile. The swelling assay has demonstrated that the absorption capacities of the different structures exhibit similar behaviours, although the irradiated samples appear to have lower values.

The captive bubble assay has led to the conclusion that all the produced samples are hydrophilic, thus promoting better biological interactions between the cells and the material.

Calcium phosphate granules are the major component of the scaffold and, through XRD analysis, it is a biphasic mixture composition that was found to be around 75% Hap and 25% β-TCP, allowing a more efficient osseointegration. As visualized by the SEM images, the small porosity inside the granules along with the scaffolds porosity will allow a total material vascularization. The SEM images allowed to observe the irregular and rough surface of calcium phosphate granules and the structure of the sterilized and unsterilized scaffolds, allowing to conclude that both have characteristics favorable to cell adhesion. Cytotoxicity assays, evaluated by the direct-contact method, showed moderate cytotoxic effect only in 25kGy scaffolds with L929 fibroblast cells.

According to the results obtained in the several tests that were carried out, it was concluded that the developed scaffold that showed the best performance during the study were the samples sterilized. These scaffolds may be a potential medical device for localized delivery of diclofenac.

Keywords: scaffold, calcium phosphates, chitosan, diclofenac, controlled release.

RESUMO

Nos últimos tempos têm-se vindo a verificar uma crescente necessidade de utilização de substitutos ósseos. Isto deve-se à incapacidade de regeneração óssea acompanhar o aumento do defeito ósseo. A perda óssea pode advir de malformações congénitas, ressecção de tumores, traumatismos, patologias de curta duração, doenças crónicas, patologias de início agudo, ou mesmo do envelhecimento, podendo promover incapacidade física e dor prolongada. O recurso à aplicação de enxertos ósseos ou implantes para resolução destas perdas nem sempre é positivo, surgindo alguns inconvenientes como o desenvolvimento de infeções, rejeições imunológicas e morte dos tecidos locais.

De momento, o mercado disponibiliza inúmeras soluções, com diversas combinações de biomateriais com diferentes propriedades que mimetizam a constituição original do tecido ósseo. No entanto, são raros os que permitem a regeneração óssea associada ao combate da resposta inflamatória local após cirurgia.

Com a finalidade de colmatar esta limitação, desenvolveu-se neste projeto uma matriz tridimensional porosa (*scaffold*), em cuja estrutura se associou um anti-inflamatório não esteróide, que promove a redução da inflamação.

A inflamação é caracterizada como uma complexa cascata de eventos fisiológicos, necessária para o processo de cicatrização. Inicia-se uma hora após a agressão, com a afluência inicial de neutrófilos e posteriormente de linfócitos e macrófagos ao local lesionado. O pico da resposta inflamatória aguda é atingido após 24 horas e é concluído ao fim de sete dias.

A implantação cirúrgica de um biomaterial desencadeia uma resposta à agressão e durante essa fase, as propriedades físicas e químicas do biomaterial vão delimitar a duração do processo inflamatório. Desta forma, propôs-se criar um substituto ósseo que permitisse libertar um anti-inflamatório de forma controlada e localizada, de modo a eliminar as tomas diárias de comprimidos por parte dos utentes. A libertação localizada, faz com que a presença de fármaco no organismo seja menor e mais eficaz, evitando potenciais problemas renais e do trato gastrointestinal.

O *scaffold* desenvolvido, teve de respeitar os seguintes requisitos para poder futuramente ser considerado e utilizado em aplicações médicas: capacidade de libertar de forma controlada e localizada o anti-inflamatório, ser biocompatível, ter uma degradação controlada, apresentar resistência mecânica suficiente para suportar tensões existentes do ambiente onde é inserido, demonstrar poros com tamanho e morfologia apropriada para o transporte de nutrientes, ter propriedades químicas

apropriadas para adesão celular, ser de fácil esterilização e de processar em diferentes geometrias tridimensionais.

A composição da matriz porosa em estudo, conta com a mistura de alguns componentes, como:

- Quitosano, polímero natural desacetilado do polissacarídeo quitina extraído do exoesqueleto de crustáceos, apresenta excelentes propriedades a nível de biodegradabilidade, biocompatibilidade, atividade antibacteriana, baixa toxicidade, imunogenicidade e tem a capacidade de melhorar a neovascularização. É um biopolimero de manipulação relativamente fácil, apresentando solubilidade em soluções aquosas ácidas.
- Fosfatos de cálcio (hidroxiapatite e β-TCP), estruturalmente são semelhantes aos componentes inorgânicos do tecido ósseo, capazes de atuar de forma apropriada, numa aplicação específica, promovendo assim a ligação química com o osso e sua regeneração.
- Diclofenac sódico, anti-inflamatório não esteroide com propriedades anti-inflamatória, analgésica, antipirética e antirreumática. Provoca a inibição da biossíntese de prostaglandinas. Apresenta propriedades higroscópicas e a sua solubilidade varia com o pH, podendo ser mais solúvel no meio básico e pouco solúvel em meio ácido.

A mistura dos fosfatos de cálcio e de quitosano, já é comercializada pela empresa Ceramed S.A, sob a forma de pasta injetável com aspeto pastoso e amarelado, denominada comercialmente por k-IBS® .

No início do processo de fabrico das amostras, estudou-se a melhor forma de incorporar o diclofenac na pasta k-IBS®. Após o sucesso da mistura, seguiu-se o processo de liofilização, colocando a pasta em moldes específicos. Este é um processo estabilizante através do qual a mistura é inicialmente congelada, passando para a fase de secagem primária, onde a quantidade de solvente é reduzida por sublimação seguida da dessorção. A liofilização faz com que ocorra transformação da mistura pastosa para um sólido com porosidade associada, capaz de ser cortado com as dimensões pretendidas.

A ausência de microrganismos viáveis é uma obrigatoriedade para os dispositivos médicos. Todavia, as condições em que foram produzidas as amostras deste trabalho, contam com microrganismos provenientes das matérias-primas, do processo produtivo mais concretamente do operador, dos equipamentos e do ambiente. O processo de esterilização é o método de eliminação de contaminação microbiológica, que permite transformar as amostras produzidas em material estéril. Assim sendo e de acordo com a norma Internacional ISO 11137, esterilizaram-se as amostras liofilizadas com doses de radiação gama a 15kGy e a 25kGy.

O perfil de libertação do diclofenac foi medido em solução salina tamponada de fosfato (PBS) e determinada por espectroscopia UV-Vis. A capacidade que os *scaffolds* têm de libertar fármaco foi estudada durante 41 dias. Observou-se uma libertação mais rápida nas primeiras 7 horas, como expectável. Ao fim dos 41 dias, verificou-se que para os *scaffolds* não irradiados faltava libertar 20% do fármaco e para os *scaffolds* irradiados, tanto a 15 como 25kGy, faltava libertar 40% de diclofenac. Desta forma, comprovou-se que a radiação influencia o perfil de libertação. Este facto, pode advir da reticulação provocada pela radiação gama na cadeia do quitosano. De certa forma, os resultados dos ensaios de *swelling*, vieram corroborar os ensaios de libertação, exibindo uma capacidade de absorção inferior para as amostras irradiadas. Uma vez que o diclofenac parece ser libertado quando há desagregação de matéria, a expansão do *scaffold* promovida pela absorção de líquido, leva a um aumento de volume que promove a libertação de fármaco.

O ensaio da bolha cativa permitiu chegar à conclusão, de que todas as amostras produzidas eram hidrofílicas. A nível biológico este parâmetro é essencial. As interações biológicas (adesão e proliferação celular) ocorrem de forma positiva, quanto mais hidrofílico for o material.

Os grânulos de fosfato de cálcio são a maior componente do *scaffold* e através da análise de DRX, verificou-se que a sua composição de mistura bifásica ronda os 75%HAp e 25%β-TCP com alto grau de pureza e ausência de outras fases cristalográficas. Desta forma, e devido à semelhança da composição com a fase mineral do osso humano, a osteointegração ocorrerá de forma rápida. O fosfato tricálcico ao dissolver-se mais rapidamente que a hidroxiapatite acelera o processo de reabsorção e formação de novo osso. E como visualizado pelas imagens SEM, a pequena porosidade existente no interior dos grânulos juntamente com a porosidade do *scaffold* irá permitir uma vascularização total do material.

As imagens de SEM juntamente com a análise FTIR, não permitiram observar a presença do diclofenac nos *scaffolds* irradiados e não irradiados. A quantidade de fármaco adicionado à matriz é inferior a 1%, podendo apenas ser identificada nos ensaios de libertação.

As imagens SEM permitiram observar a superfície dos *scaffolds* esterilizados e não esterilizados e os grânulos de fosfatos de cálcio. A estrutura dos grânulos esféricos apresenta uma superfície irregular e rugosa que quando ampliada, pode-se visualizar uma estrutura com pouca compactação e desarranjo das partículas de grandes dimensões. Estas características são favoráveis à adesão celular.

Comprovou-se através da análise granulométrica, que os tamanhos dos grânulos utilizados no processo variam entre os 135µm e 355µm. Os resultados obtidos revelaram a existência de homogeneidade de tamanhos.

Os ensaios de citotoxicidade, avaliados através do método de contacto direto, revelaram ser citotóxicos para as células MG63 e L929 fibroblastos, quando o poço se encontrava coberto por 1/10 da amostra. Realizou-se novo ensaio apenas com as células L929, onde a amostra ocupava 1/20 do poço. Os *scaffolds* com diclofenac esterilizados a 25kGy deram moderadamente citotóxicos, com viabilidade entre os 60-65% As restantes amostras, com e sem fármaco esterilizadas a 15kGy e não esterilizadas, e as amostras sem diclofenac irradiadas a 25kGy, não tinham evidencias de efeitos citotóxicos, apresentando uma viabilidade celular entre 70%-82%, que estão acima do limite citotóxico definido pela ISO standard.

De acordo com os resultados obtidos nos vários ensaios realizados, concluiu-se que os *scaffolds* desenvolvidos que melhores performances demonstraram ao longo do estudo, foram as amostras esterilizadas, tanto a 15kGy como 25kGy.

Estes *scaffolds* podem ser um potencial dispositivo médico para entrega localizada de diclofenac.

Palavras-chave: scaffold, fosfatos de cálcio, quitosano, diclofenac, libertação controlada.

ACKNOWLEDGEMENTS

To all those who contributed to the realization of this master's thesis directly or indirectly, my sincere thanks.

First of all, I am deeply grateful to my supervisor José Ventura, who has been tireless throughout this project and has always demonstrated an extraordinary availability. I would like to thank you for all the knowledge you have transmitted to me, all the help and guidance you have given me, which has been contributed to my personal and professional growth.

To Doctor Lídia Gonçalves I would like to thank for his availability, help and wisdom when it was needed.

To Ceramed – Cerâmicos para aplicações médicas S.A. for providing the raw material for the development of this project and for the availability it demonstrated in relation to the accomplishment of analyzes.

My gratitude goes also to all my co-workers and friends, Thierry, Sara, Carlos, Ana, Andreia L., Alexandre, Telma, Vanessa, Pedro, Joel and Mário, for all the help, guidance and good disposition. Thanks you also to Dr.Eduardo Pires, CEO of Ceramed S.A, for the help and financial support.

To Doctor Lígia Figueiredo, Doctor Luis Pinto and Doctor Andreia Pimenta, for their help, knowledge and friendship.

A special thanks goes to Doctor Ana Paula Serro (IST), who opened the doors of his laboratory to help me with several techniques, all support and transmitted knowledge.

To Eng. Ana Topete (IST) and Eng.Diana Silva (IST), for help with the equipment and all the knowledge transmitted. Eng.Isabel Nogueira (IST), for her help in SEM analysis, Prof. Amélia Almeida (IST), who helped perform the specimens to be analyzed in SEM.

To Doctor Nuno Faria and Ricardo Pereira (IST) for all assistance with the centrifuge and the lyophilization processes.

To Doctor Helena Gil and Doctor Jorge Guiomar (U.Coimbra) for providing the diclofenac and help.

Last, but definitely not least, a huge thank you to my family for understanding my absences and for all the unconditional support during this journey, especially to my parents, brothers and Ana Almeida. To my friend Miguel for all patience, strength, support and help. You have always motivated me to achieve more.

Thank you very much to all who have accompanied me.

CONTENTS

ABSTRACT iv

RESUMO vi

ACKNOWLEDGEMENTS x

CONTENTS xi

LIST OF FIGURES xiii

LIST OF TABLES xvi

ABREVIATIONS xvii

INTRODUCTION 1

MOTIVATION AND GOALS 3

1. THEORETICAL FUNDAMENTS 4

1.1. Tissue Engineering 4

1.2. Contributing Factors to the Clinical Success of Bone Substitutes Scaffolds 4

1.3. Bone Tissue 5

1.4. Mechanism of Bone Growth 7

1.5. Regeneration Process 8

1.6. Bone Substitutes 9

1.6.1. Biomaterials 11

1.6.1.1. Synthetics Biphasic Bones Substitutes 12

1.6.1.2. Synthetic Biphasic Bones Substitutes with Chitosan Incorporation 13

1.6.1.2.1. Chitosan 14

1.7. Nonsteroidal Anti-Inflammatory Drugs 16

1.8. Mechanisms of Action of NSAIDs 16

1.8.1. Diclofenac Sodium – Structure and main properties 18

1.9. Incorporation of an Active Substance 20

1.10. Controlled Drug Delivery 20

1.10.1. Polymers in Drug Delivery Systems 21

1.10.2. Mathematical Description of the Drug Release Kinetics from the Scaffolds .. 24

1.11. Sterilization 29

1.11.1. Gamma Radiation 29
1.11.2. Gamma sterilization influence in drug release 30
2. PROCESS, MATERIALS AND METHODS 31
2.1. Freeze Drying Process 31
2.2. Scaffolds Preparations 32
2.2.1. Optimization Process 34
2.2.2. Sterilization Process 36
2.3. Diclofenac Controlled Release Experiments 36
2.4. Chemical and Structural Scaffold Characterization 38
2.4.1. Microscopy 39
2.4.2. X-ray Diffraction Method 42
2.4.3. Particle Size Analyser 43
2.4.4. Wettability – Contact Angle (Captive bubble) 44
2.4.5. Swelling 47
2.4.6. FTIR - Fourier-transform Infrared Spectroscopy 48
2.5. Biological Analysis 50
2.5.1. *In Vitro* cytotoxicity test 50
3. RESULTS AND DISCUSSION 54
3.1. Diclofenac Release System on CaPs and CS Scaffolds 54
3.2. Scaffolds and Components Characterization Analysis 61
3.2.1. XRD Analysis 61
3.2.2. Particle Size Distributions 62
3.2.3. Wettability 63
3.2.4. Swelling 64
3.2.5. Scanning Electron Microscopy / Energy Dispersive X-Ray Spectroscopy 66
3.2.6. FTIR 67
3.2.7. *In Vitro* cytotoxicity test 69
4. CONCLUSION AND FUTURE WORK 73
5. BIBLIOGRAPHY 77

LIST OF FIGURES

Figure 1 - Example of scaffold application developed in this project. 3
Figure 2 - Composition of bone tissue 6
Figure 3 – Structure cortical and cancellous bone. 7
Figure 4 - Bone matrix and cells that constitute it . 8
Figure 5 - Chemical structure of chitin. 14
Figure 6 - Chemical structure of chitosan. 15
Figure 7 – Mechanism of action of non-steroidal anti-inflammatory drugs. 18
Figure 8 - Chemical structure of DF. 19
Figure 9 - Schematic representation of chemically controlled release. a) biodegradable system; b) pendant-chain system. 22
Figure 10 - Schematic representation of osmotically controlled release systems and swelling system. a) Type A contains an osmotic core with drugs; b) Type B contains a drug reservoir surrounded by osmotic core. 23
Figure 11 - Schematic representation: a) reservoir diffusion-controlled release systems, b) monolithic diffusion-controlled release systems 23
Figure 12 - Water's phase diagram 32
Figure 13- Schematic illustration of scaffolds production (adapted Asadian-Ardakani et al.). 34
Figure 14 - Example of irradiated scaffolds. These were inserted in Tyvek bags with yellow gamma indicator and sent to Aragogamma. After the radiation, the indicator gets red, as a sign that the radiation occurred. 36
Figure 15 - Preparation of the irradiated and non-irradiated samples with and without diclofenac, to the release assay and subsequent spectrophotometer analysis. 37
Figure 16 - overnight shaking of the tubes that contains scaffolds emerged in PBS. 38
Figure 17 –A) scaffold emerged in PBS before the shaking. b) Scaffold destroyed after the centrifugation. 38
Figure 18 - epoxy formers with granules of calcium phosphates, on the left and with scaffolds on the right. 39
Figure 19 - Scanning Electron Microscope from HITACHI, model S-2400 by IST. 41
Figure 20 – A) scaffolds half's without DF (1, 2 and 3) and with DF (4, 5 and 6) on the SEM support; B) Epoxy former of the CaPs granules overlayed with gold-palladium. 41
Figure 21 - Sessile drop (left image); Captive bubble (right image). 44

Figure 22 - The water contact angle (θ) on a hydrophilic surface and a hydrophobic surface. 45
Figure 23 - Hydrophobic and hydrophilic water contact angle 45
Figure 24 - Micrometer syringe with a needle inverted in the edge and the liquid cell. 46
Figure 25 – Goniometer: 1) Light source 2) Micrometer syringe 3) Liquid cell 4) Video camera. 46
Figure 26 - Scaffold dried used in swelling assay. 47
Figure 27 - IRAffinity-1 Shimadzu equipment. 49
Figure 28 – Example of KBr tablet with scaffold powder blend. 49
Figure 29 – 24-well plate real and layout for the MTT cytotoxicity test, accounting for the 6 different samples of scaffolds and respective positive and negative controls. 52
Figure 30 - SEM image of the lyophilized scaffold, obtained from the dissolution of DF in 1/3 of water and lactic acid in 2/3 of water. Resolution of 20.0kV and magnification of 60x. 54
Figure 31 – A – CaPs granule exterior; B,C CaPs granule interior with different amplifications; D – scaffold's porosity. 55
Figure 32 - DF release profiles in terms of released mass accumulated by sample mass. Error bars: standard deviation (*n*=5). The smaller graph is an enlargement of the larger graph of the first 7h of release. 57
Figure 33 – Fraction of released DF in relation to that introduced in scaffold. Error bars: standard deviation (*n*=5). The smaller graph is an enlargement of the larger graph for the first 7h of release. The represented lines are only intended to facilitate the profiles identification. 58
Figure 34 - X-ray diffractogram representative of biphasic ceramic granules used in the manufacturing process of scaffolds. 61
Figure 35 - Distribution of the particle size of the biphasic granules used in the production of scaffolds in function of the sample volume through laser diffraction. 62
Figure 36 – Epoxy mold with spherical CaPs granules used in scaffolds. 63
Figure 37 - Water contact angle of samples with and without diclofenac and non-sterilized and sterilized. 63
Figure 38 - An air bubble sitting beneath a surface of specimens: a) non-sterilized without DF, b) sterilized at 15kGy without DF, c) sterilized at 25kGy without DF, d) non-sterilized with DF, e) sterilized at 15kGy with DF, f) sterilized at 25kGy with DF. 64
Figure 39 - Swelling profile as a function of time. 65
Figure 40 - SEM images from the scaffold surface. A) non-irradiated (bar indicates 400µm); B) irradiated at 15kGy (bar indicates 400µm); C) irradiated at 25kGy (bar indicates 400µm); D) 25kGy irradiated scaffold amplification (bar indicates 200µm); 66

Figure 41 - Distribution chart of the chemical elements present in the analysed scaffold. 67
Figure 42 – Comparation between raw material with scaffold, with DF and not irradiated. 68
Figure 43 - Comparation between scaffolds with DF, irradiated and not irradiated. 69
Figure 44 - A) Scaffold covering 1/10 of the well; B) Scaffold covering 1/20 of the well. 70
Figure 45 - Graphic representation of cell viability (%) values obtained for the different scaffolds tested with the different line cells. 71
Figure 46 - Graphic representation of cell viability. 72
Figure 47 – Comparative graphic of cell viability between different amounts of material introduced into the wells. 72
Figure 48 - FTIR spectra corresponding to DF. i
Figure 49 - FTIR spectra corresponding to CS. ii
Figure 50 - FTIR spectra corresponding to CaPs. iii

LIST OF TABLES

Table 1 - Commonly prescribed drugs with diclofenac, dose and the recommended dosage..... 19
Table 2 - Interpretation of diffusional release mechanisms from polymeric films, taking into account the exponent of the Korsmeyer-Peppas model. 28
Table 3 - Mixing optimization processes. 35
Table 4 - Determination coefficient (R^2) obtained through the application of the mathematical models to the DF release profiles of the different prepared samples. 60
Table 5 - Values of the parameter n obtained from the Korsmeyer-Peppas model. 60
Table 6 - Cell viability percentage of the samples tested with 1/10 area of cell monolayer. 70
Table 7 - Cell viability percentage of the samples tested with 1/20 area of cell monolayer. 72

ABREVIATIONS

CaP	Calcium Phosphate
CIFs	Crystallographic information files
COX	Cyclooxygenases
CS	Chitosan
DD	Deacetylation Degree
DF	Diclofenac Sodium
DMSO	Dimethyl sulfoxide
FTIR	Fourier-transform Infrared Spectroscopy
HAp	Hydroxyapatite
IL	Interleukin
IR	Infrared spectroscopy
ISO	International Standards Organization
MAUD	Materials Analysis Using Diffraction
MSCs	Mesenchymal Stem Cells
MTT	3-(4,5-dimethylthiazol-2-yl)-2,5-diphenyl-tetrazolium bromid
NSAID	Nonsteroidal Anti-Inflammatory Drug
PBS	Phosphate Buffered Saline
PDS	Polydioxanone
PEG	Polyethylene glycol
PGA	Polyglycolic acid
PLA	Polylactic Acid
SAL	Security assurance level
SEM/EDS	Scanning Electron Microscopy/ Energy Dispersive X-Ray Spectroscopy
TCP	Tricalcium Phosphate
TNF-α	Tumor necrosis factor – alfa
UV-VIS	Ultraviolet-Visible
XRD	X-ray powder diffraction
β-TCP	β-tricalcium phosphate

INTRODUCTION

Healthy bones are extremely important in overall health and in human life quality. They allow the mineral storage, essential for the proper body functioning, mobility, support and protection[1]. Due to congenital anomalies, traumas, diseases or even aging, the bone deteriorates, promoting pain and physical incapacity, thus compromising daily activities, sometimes even leading to the need of high medical costs treatments [2–4].

Since the mid-twentieth century, there has been a significant increase in the use of orthopedic and maxillofacial implants for bone replacement[5,6]. Generally, these implants need to be associated with drug shots that can reduce the inflammatory process, counteract rejection and promote a more efficient regeneration. However, many of these bone fixation and repair devices rely on the use of metals, such as stainless steel, titanium and its alloys[7]. These metal implants are not biodegradable and they frequently require more surgeries to remove them[8].

Due to a major boost in science, there are already several biodegradable bone substitutes that support the surrounding cells and tissues, in order to promote tissue regeneration and repair, providing mechanical support and simultaneously the implant's degradation by the body[9]. In order to mimic the bone structure, several composites of different ceramic types and biodegradable polymers have been developed. Recently, chitosan has played an important role in bone regeneration, and more attention has been paid to chitosan composites and their applications in bone tissue, due to their ability to reduce adverse reactions to a foreign body, both being biocompatible, biodegradable and because of their ability to be shaped into various geometries and shapes. These scaffolds degrade at a rate similar to bond tissue regeneration, are osteocunductors and possess an interconnected pore structure that allow bone in-growth.

Chitosan (CS) and calcium phosphates CaPs namely Hydroxyapatite (HAp) and β-tricalcium phosphate (β-TCP) composites scaffolds have revealed great potential in bone regeneration since CaPs are the main inorganic component in natural bone[10]. Bioceramics such as HAp and β-TCP allow the occurrence of osteogenesis and strongly bind to bone tissue[10]. HAp has been amply used as coating in orthopedical implants, due to its osteoconductivity, despite of presenting limitations by the fact that this is a fragile material[2].

Chitosan, a natural polymer, as mentioned above, has come to be studied as a scaffold material since it is nontoxic, it can be shaped into complex structures, promotes adhesion and cellular migration, improves wound cicatrization and is biodegradable at a rate that depends only of controllable material characteristics such as deacetylation degree, molecular weight and crystallinity[11,12].

The inflammatory process is associated to the occurrence of lesions and traumas and it can be divided in multiple steps: the acute phase, which is characterized by a localized vasodilatation and an increase off capillary permeability; a sub-acute phase, comprised of leukocytes and phagocytic cells infiltration; and a proliferative chronical phase, at which tissue degeneration and fibrosis occurs. Nonsteroidal anti-inflammatory drugs (NSAID) are generally used to reduce pain and inflammation resulting from several types of lesions. Thereby, the incorporation of NSAIDs in the scaffolds allows the reduction of the inflammatory process[1], avoid adverse gastrointestinal effects and offer the possibility to administer the drug in the absence of inactivation over the effect of first transition at a hepatic level, as that release happens in the oral area[13].

This work aims to gather a wide range of knowledge about the development and characterization of chitosan and calcium phosphates composite scaffolds based on the commercially available injectable bone substitute **k-IBS®** produced at **Ceramed- Cerâmicos para Aplicações Médicas S.A**. in which NSAID has incorporated.

Despite the diversity of commercially available products aimed at bone regeneration, they can have high costs. Therefore, one of the great challenges is to develop a biodegradable scaffold from low cost raw materials, with easy access and with the proper characteristics to accomplish the envisioned function.

In accordance with market demands, the pretension of this work is to obtain a composite scaffold product easy to manipulate, that can be cut to fit bone defects independent of their shape and that stimulates bone growth and tissue formation.

.

[1] (If the inflammatory process reaches the chronic phase, excessive phagocytic activity of the neutrophil is observed and the bone regeneration process will be impaired)

MOTIVATION AND GOALS

This project's main objective is to create a scaffold composed of CaPs and CS combined with an anti-inflammatory drug, sodium diclofenac, which can be used for bone regeneration and targetted treatment of the initial inflammation.
It is intended to study the composite (calcium phosphates/chitosan) influence and the irradiation process influence on drug release, mechanical strength, body fluid absorption capacity, stability and degradation level. More specifically, it is intended to:

- Improve scaffolds' properties through changes in k-IBS® composition;
- Prepare chitosan-calcium phosphates composite scaffolds with incorporated diclofenac;
- Understand the influence of diclofenac in the obtained scaffolds properties;
- Evaluate the kinetic release behavior for the application of diclofenac drug delivery;
- Optimize process parameters in order to obtain non-cytotoxic scaffolds and promote bone formation;
- Study the effects of different gamma radiations on the scaffolds properties.

Figure 1 - Example of scaffold application developed in this project. Adapted [14]

1. THEORETICAL FUNDAMENTS

1.1. Tissue Engineering

Like Rami Mhanna and Anwarul Hansan[15] said “the tissue engineering is an interdisciplinary field that utilizes cells, biomaterials, biochemical and physical signals, as well as their combinations to generate tissue-like structures”.

In order to promote cell growth and proliferation, tissue engineering utilizes biomaterial manipulation, from both artificial and natural biomaterials that supply the structural basis for the controlled tissue growth. Biomaterial is a material in contact with biological fluids or tissues and its objective is to constitute partially or as an whole living structure [16,17]. It can also be utilized as a drug transport through several formulation types (foams, hydrogels, fibers and microparticles)[18].

Tissue regeneration matrices, also designated as scaffolds, are three-dimensional structures that work as a support and have physical, chemical and mechanical properties appropriated for new tissues formation both *in vivo* or *in vitro*. These structures goals are to mimic the extracellular matrix, promote cellular migration and adhesion, provide biochemical factors that will allow nutrient diffusion, and to tridimensionaly orientate new tissue formation[17,19].

For this reason, the scaffold architecture and morphology are important factors in the development of these structures due to their impact in tissue regeneration (e.g. porosity level and pore size and distribution)[20]. Other factors must be taking into account when developing a scaffold for a specific application, namely the damaged tissue location and the size of the defect.

1.2. Contributing Factors to the Clinical Success of Bone Substitutes Scaffolds

To achieve clinical success, scaffolds must have a good osteointegration, adhesion, proliferation, and a good cellular differentiation and migration. Generally, the goal is to potentiate the mechanical, physical and chemical properties from a variety of materials that complement each other[21].

Usually it is required that a scaffold demonstrate the following properties:

- Mimic the native extracelular matrix;

- Biocompatibility – the material and it's degradation products should not promote an immune system response or not to possess an unacceptable level of toxic substances[22];
- Adequate degradation rate – the matrix should be bioabsorved or degraded in a very well determined time period. This period must be equivalent to the time needed for the previously occupied tissue space to be substituted by new tissue;
- Chemical properties that allow adhesion, proliferation and cellular differentiation;
- Controlled degradation – different tissues have different regeneration rates. Thus, the scaffold's regeneration rate must be adjusted to the injured tissue;
- Mechanical properties – the material should have mechanical resistance similar to the resistance of the implantation local tissue;
- Pore interconnectivity and scaffold porosity – the pore size and structure influence the nutrients transport. The pore interconnectivity is desired, since it elevates the diffusion rates from the scaffold's exterior to its interior, potentiating vascularization, residues elimination and oxygen transport. The microporosity facilitates the regulatory agents and drugs inclusion into the scaffold, aiding the tissue regeneration;
- Sterilization – before its implementation, the scaffold must be submitted to one of the following techniques, in order to eliminate microbiological contamination: high temperatures, gamma radiation or ethylene oxide vapor;
- Facility and versatility – the scaffold must be easy to process at different geometries and manufacture level[22,23].

1.3. Bone Tissue

Bone is a tissue that present several important properties in our organism, working as body support, internal organs protector and allowing the storage and exchange of ions with the extracellular liquid[24,25].

Bone is a living, vascularized and dynamic tissue, notable for its hardness and regenerative capacity. It remains active throughout the life of the organism, being responsible for several functionalities and the capacity of multiple response to stimuli[26–28].

It is the biggest reservoir of calcium and phosphorus in the human body. Calcium is particularly important in the regulation of homeostasis process, also in the process of intracellular signalization on the cytoplasmic membranes and in the control of the proteins extracellular function, namely the ones related with the coagulation cascade[1,29].

As indicated in figure 2 and according to the definitions of several authors[24,26,28,30–32], bone tissue is a highly specialized type of connective tissue composed of a mineral phase, formed by calcium phosphate crystals, in the form of hydroxyapatite [$Ca_{10}(PO_4)_6(OH)_2$], which confers rigidity and maintains some degree of elasticity, and by an organic matrix formed essentially (95%) of type I collagen fibers, figure 2.

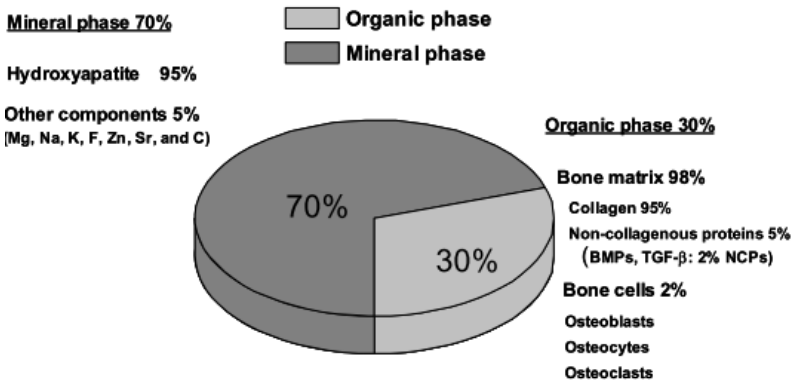

Figure 2 - Composition of bone tissue [24].

The bone matrix is primarily collagen which is responsible for the tensile strength. The mineral component of bone is calcium phosphate, which imparts compressive strength to the bone tissue. There are two types of bone tissue, as illustrated in figure 3: cortical (compact), and cancellous (trabecular)[4].

- Cortical bone is dense and the collagen matrix is organized in the form of concentric lamellae, usually around the central vascular canal constituted by the Havers system;
- Trabecular bone has a porous matrix, organized in trabeculae (100 to 150μm thick) in a three-dimensional network, which follows the lines of mechanical forces, giving bone a good resistance to loads transmitted by the articular surfaces. The trabeculae are composed of bony lamellae that delimit the intercommunicating cavities by bone marrow[26,32].

Compact bone has a Young's modulus of elasticity ranging from 17–20GPa and compressive strength in the range of 131–224MPa, while Young's modulus and compressive strength for trabecular bones are 50–100MPa and 5–10MPa respectively[4].

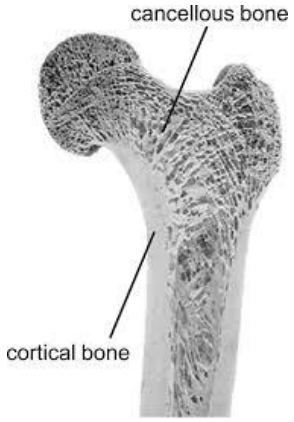

Figure 3 – Structure cortical and cancellous bone[33].

1.4. Mechanism of Bone Growth

Bone originates mainly in pluripotent mesenchymal cells during embryonic development. These cells, by definition, have the ability to autoregenerate and repopulate all appropriate cell lines, being able to differentiate into osteoblastic, myoblastic, adipogenesis, chondrogenic, neurogenic endothelials[26,27].

Formation of bone tissue occurs during embryonic development, but also during the growth phase, in the remodelling process, in the treatment of fractures and after the implantation of osteoinductive medical devices[27].

Figure 4 shows specialized cells found in bone tissue, responsible for all bone homeostasis: osteoblasts, osteoclasts and osteocytes.

- Osteoblasts are highly differentiated, non-migratory cells responsible for the synthesis (type I collagen, glycoproteins, cytokines and growth factors) and deposition of the organic component of the extracellular matrix, called osteoid, and its subsequent mineralization (inorganic component). After completing their biological activity, and with terminal differentiation, they suffer from one of three destinations: apoptosis, differentiation in coating cell, or differentiation in osteocytes[5].
- Osteocytes are mature osteoblasts that are trapped in the bone matrix and are responsible for bone maintenance and homeostasis. These are found within the bone matrix, located between the lamellae, which communicate between them through canaliculi to effect small molecules and ions exchanges.
- Osteoclasts are derived from hematopoietic stem cells that differentiate along the monocyte/macrophage lineage. Cells responsible for bone resorption through bone acidification promoting its dissolution and demineralization by the enzymatic degradation of the bone matrix[5].

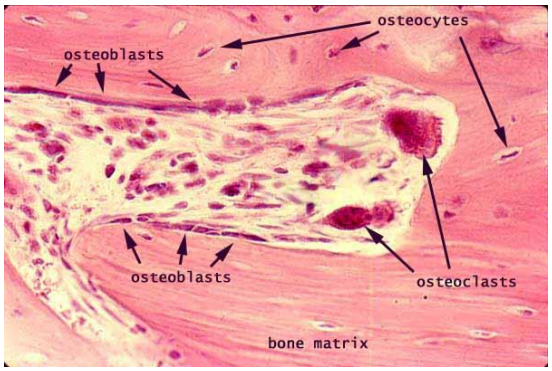

Figure 4 - Bone matrix and cells that constitute it [34].

1.5. Regeneration Process

When developing implants that will replace defective bone or even lack thereof, one must take into account factors that affect the growth of bone tissue, and it is therefore important to know the regeneration process

The regeneration of the bone tissue is a dynamic and complex process in which the repaired tissue is restored to its original function and anatomic structure. It does not occur the formation of conjunctive fibrous tissue, by opposition to what happens in soft tissues.

In the bone regeneration process, from the lesion to the final reshuffle, there are an enormous number of cellular phenotypes involved. They are responsible for the coordination of the proliferation, migration, cellular differentiation functions and the synthesis of the extracellular bone matrix. The development of those functions in a determinate and correct temporal sequence, by several cellule lines presents, or mobilized to the lesion local and in reply a specific stimuli, allows the success of this process [34,35].

However, there are situations where there is a total or partial loss of bone tissue by various pathological and traumatic processes, which then need prolonged and expensive treatments. In order to accelerate the postoperative, with the improvement of the patient's health status, the development of new therapies that promote and accelerate the process of bone regeneration has been increasing.

The regeneration process occurs without affecting the shape and density of the bone, through a sequence of events including osteoclastic activation, bone resorption, osteoblast activation and the formation of new bone[27]. However, the patterns of remodeling have changed dramatically depending on age and disease.

Generally, the regeneration process begins with an inflammatory response phase, immediately after the trauma, with the formation of a hematoma.

The inflammatory response is necessary for the healing process, causing the hematoma to coagulate between the ends of the lesion and within the medulla, forming a model for the formation of the bone callus[36]. The inflammatory response lasts for approximately 2/3 weeks, however, proinflammatory molecules continue to perform important functions at the end of regeneration[27].

The initial proinflammatory response involves the secretion of tumor necrosis factor-α (TNF-α), interleukins (IL), macrophages, inflammatory cells and mesenchymal cells. These factors recruit inflammatory cells and stimulate angiogenesis[27,36].

TNF-α, stimulates the function of osteoclasts and promotes the recruitment of mesenchymal stem cells (MSCs), inducing apoptosis of hypertrophic chondrocytes during endocondral bone formation[37].

After the cartilaginous matrix, which eventually mineralizes, the bone transition occurs, with the start of reabsorbing mineralized cartilage.

The formation of the primary bone after 12 weeks is followed by remodeling, in which the initial bone callus is modified by formation and secondary bone resorption to restore the anatomic structure that supports mechanical loads[27,36,38,39].

The expression of IL, mainly IL-1 and IL-6, increases in association with remodeling during secondary bone formation, whereas TNF-α expression increases in association with reabsorption of mineralized cartilage at the end of the endochondral repair phase of the fracture[36].

When implantation of a biomaterial occurs, the sequence of biological processes includes: is tissue regeneration in the presence of cells capable of forming new tissue (osteogenesis), which can adhere and proliferate throughout the material (osteoconduction) and the phenotypic differentiation of osteoblasts (osteoinduction)[5].

In order for bone regeneration to occur, when a biomaterial is implanted, it is strictly necessary that there is porosity on the material. The minimum diameter for cell growth to occur, and to form blood capillaries that infiltrate the biomaterial leading nutrients to the internal regions, should be 100-500μm. Smaller pores will only allow the passage of fibrous tissue, which will help the mechanical fixation of the matrix[40].

1.6. Bone Substitutes

Synthetic osseous grafts can be divided into metals, polymers, ceramics and composites[41,42]. Polymers are used in several situations, as bone fixation elements, suture materials, prostheses, dental material, tridimensional porous structures to bone filling, membranes and release pharmaceutical products systems[43]. Ceramics like calcium phosphates (HAp and β-TCP), calcium sulfate, coral derivates, alumina (aluminum oxide) and zirconium are inorganic

nonmetallic solids[42]. Ceramic materials can form biological interactions with bone, but they have weak biomechanical properties. Some of these materials, by having a chemical composition too similar to the osseous tissue and a good adherence to it, had created big expectations in the usage as substitutes of stiff tissues. However, the limitations of its mechanical properties reduces its range of applications. Tissues substitution in non-loads subject areas (osseous defects) and in the coating of metallic implants (for leverage its capacity of quickly accession to bone tissue) are the principal indications of these materials[42,44,45].

In the orthopedic biomaterials market CaPs have a big importance[21].

Bone substitutes are being increasingly used in medicine, especially in traumatology, spine surgery and revision prosthetic surgery. Applications include the fill of cavities or defects, the treatment of osseous cysts and tumors, union delays, articulations immobilization, column arthrodesis, fractures fixation, maxillofacial and periodontal surgeries, etc.[46]. More than two million bone grafting procedures are performed every year, which represents an estimated market of five billion euros that is increasing 10% every year[47,48]

In accordance with literature, Gutierres et al. (2006)[21] and Fernandez-Yague et al. (2014)[49], and with the final goal to mimic the properties of bone tissue and accelerate the bone regeneration, several synthetic bone substitutes present different combinations of materials in order to tailor the final mechanical and chemical characteristics. The most used are:

- Calcium phosphates;
- Calcium sulphates;
- Bioglass.

Nevertheless, due to its excellent biocompatibility and bioactivity, the CaPs are the ones that more stands out.

HAp is one of the more studied CaPs, due to its chemical similarity with the mineral component of the bone tissue.

HAp is known for its osteoconductive properties, but its clinical usage presents limitations due to its slowly biodegradation[50].

In the osseous reshuffle process, implants reabsorption rate should, ideally, be equal to the new bone formation rate, in a way that total implant substitution is enabled and in order not to affect bone mechanical, physical and chemical properties. Several mechanisms are involved in implants reabsorption as the dissolution caused by *in situ* pH modification, the physical disintegration in minor particles and biological factors as phagocytosis. The cellular component mainly performed by the osteoclasts, in these mechanisms, presents a central role in the implant's biodegradation. The osteoclasts degrade the implant by dissolution and its by product is CaP crystals, throughout a *in situ* pH decrease next to its membrane and by phagocytosis, originating CaP crystals degradation process in its cytoplasmic vacuoles. However, there are

other cells that are also responsible for the ceramic degradation by CaP crystals phagocytosis such as macrophages and giant cells. The implants surface characteristics have a huge role in the determination of which type of cellules will adhere to the implant. The rough surfaces are the ones that have evidenced a bigger osteoclastic accession if compared to smooth surfaces [51].

The most common combination of CaPs is HAp and β-TCP. This mixture allows a chemical stability (HAp role) and a quick reabsorption immediately after the implementation (TCP role). The TCP frequently used has a Ca/P ratio of 1.5,which allows the quickly reabsortion of the biomaterial without biocompatibility nor osteoconductive problems. However, it is known that Ca/P ratios of 1.5 are too much soluble and the degradation rate on the organism is too high, making this option inappropriate for some medical applications[42].

1.6.1. Biomaterials

Biomaterials development has proven itself fundamental in the improvement of our life quality. A biomaterial, according to Gutierres et al.[21], is a substance or combination of substances, pharmacologically inert, natural or synthetic in nature, to be implanted or incorporated, for any period of time, in a system that treats, augments or replaces any tissue, organ or function in the human body.

The selection criteria for a biomaterial to produce a matrix, for a given purpose, is one of the most important steps. The choice should be made taking into account similar characteristics, physical or chemical, that the material presents in comparison to the tissue to be replaced. For this analysis, there is a specific set of properties that become fundamental for the use of biomaterials in living tissue[21,52,53]: biocompatibility; structure and morphology; porosity; chemical composition; mechanical resistance; surface topography; superficial energy; corrosion resistance; absence of toxicity and degradation[53].

The most important characteristic is biocompatibility, since we can only consider a biomaterial adequate and biofunctional if it does not cause local or systemic damages (toxic, cancerous or radioactive) in the surrounding tissues, having the capacity to induce in the host a proper response to a specific application.

Biocompatibility of a material can only be assessed when all the mechanisms are understood, being those chemical, biochemical, physiological, physical or other that involve the interaction between the implant and the tissues of the human body. Depending on the application for the biomaterial, biodegradability might also be an important property, for instance in the support of tissue growth and drug release systems, in which the implanted matrices are not removed after the terminus of their function but rather degraded by the organism[52,54].

Biomaterials are classified in accordance to the reactions they cause in the biological tissues. They can be bioinert, biotolerable, bioactive and biodegradable. As for the interaction with the tissues, biomaterials can be classified according to their chemical nature: synthetic (PLA, PGA, PDS…) or natural (hyaluronic acid, silk, chitin, collagen, gelatin, chitosan, silk, polyhydroxyalkanoates,…)[55].

A bioinert material presents a minimal interfacial response that does not result in binding or rejection by the host tissue[43].

Bioactive materials potentiate the interaction in the implant site through the occurrence of osteo-integration, that arises without the presence of fibrous containers, in the replacement of bone tissue[53]. The bone tissues connect with the implant depending on the chemical similarity between the materials and the mineral part of the bone, allowing the osteoconductivity to happen over the surface of the material with bone cells. The main materials for this class are HAp and TCP.

HAp is the most chosen ceramic due it good biocompatibility and compression resistance. Although It has been widely used in bone repair, it is a material with high elasticity and density when compared to polymers. TCP is considered a ceramic with fast resorbance and exists in allotropic form α e β. Its actuation mechanism results of a high concentration of calcium and phosphorous at the surface. Its chemical formula is $Ca_3(PO_4)_2$ with molar ratio Ca/P=1.5, containing 39% calcium and 20% phosphorus. The high concentration of calcium and phosphorous improves its osteo-integration, initiating biomineralization, stimulating osteoclasts and influencing the phenotypical differentiation of osteogenic cells.

1.6.1.1. Synthetics Biphasic Bones Substitutes

The biphasic osseous substitutes, based on HAp and TCP, have the capacity to form chemical connections directly with the bone, allowing, that way, a strong bonding. Interface formations between implant and bone is the result of cellular interaction with the material surface and the carbonated hydroxyapatite formation, identical to the bone mineral phase, by dissolution processes and the CaP crystals precipitation[42,50].

The CaP crystals dissolution has the capacity to proportionate an increase of the calcium and phosphorus concentration *in loco*. As a consequence, the local breakthrough near to the implant takes to the occurrence of apatite crystals precipitation and the formation of carbonated hydroxyapatite, through incorporation of ions mostly carbonates obtained by corporal fluids. The osseous apatite crystal uses the material surface as local of nucleation, support and growing. Being chemically identical, the crystals are in perfect continuity with the implant crystalline net. This region of coalescence works as a matrix to the cellular adherence and the

osseous growing. During the extracellular matrix production and the collagen fibers mineralization occurs a crystals incorporation of carbonated hydroxyapatite recently formed.

The bioactivity of calcium phosphate biphasic osseous substitutes is important to reduce the micro-displacements between the bone and the implant, avoiding the formation of the fibrous capsule and accelerating the patient recovery process during post-surgery period. However, if the bone grafts objective is its quick substitution by new osseous tissue which requires an osteoconductive material to allow cellular colonization in all implant area. This property depends on the macroporosity (pores with dimensions superiors to 100µm) and microporosity (pores with dimensions lower to 10µm) of the bone substitute, allowing, this way, the nutrients and fluids diffusion thought the matrix [42,45].

1.6.1.2. Synthetic Biphasic Bones Substitutes with Chitosan Incorporation

In the biphasic osseous substitutes, their interconnected porosity and chemical similarity with the carbonated hydroxyapatite mimics the inorganic bone phase. To mimic the organic phase, polymer incorporation must be performed.

To accomplish this goal, several polymers, either of natural or synthetic origin, were tested by some authors[47,56]**. C**ombinations of ceramics and polymers (i.e. composites) have been developed to combine within a single bone substitute the advantageous properties of both materials. The advantages are the strength provided by the ceramic phase, and the toughness and plasticity provided by the polymer phase[57]. Due to their extracellular matrix-like properties, necessary for cell survival and function, and low toxicity, natural polymers are attractive materials in the development of ceramic-polymer composites[57]. Actually, in the market we can find a polymer of animal origin that possesses interesting properties - chitosan. This multifaceted biopolymer is obtained through the alkaline deacetylation of chitin.

Chitin is the second organic substance more abundant in the nature, after cellulose, present in all vegetables and also in some microorganisms, being chitin, very abundant in the invertebrates exoskeletons and in the cellular walls of some fungi and algae [58]. Chitin, illustrated in figure 5, is a polysaccharide very stable and linear, constituted by monomers of β-1,4-N-acetyl-glucosamine and β-1,4-glucosamine distributed in the polymer chain. When the number of N-acetyl-glucosamine is superior to 50%, the biopolymer is called chitin. In opposition when the number of N-acetyl-glucosamine is inferior to 50%, biopolymer is called chitosan [58]. The deacetylation degree (DD) is a parameter that defines the quantity of deacetylated units in the polymer chain and should be between 70% and 95% because of biological properties[54].

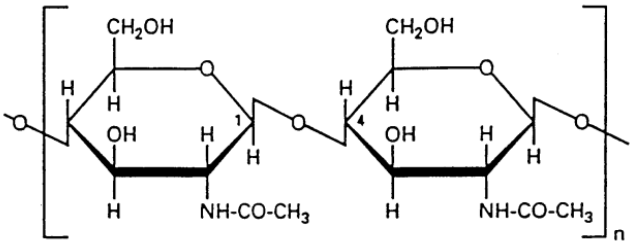

Figure 5 - Chemical structure of chitin.

1.6.1.2.1. Chitosan

Chitosan (figure 6) is a semi-crystalline co-polymer, that results from the partial deacetylation of chitin, the second most abundant natural polymer[12]. CS is studied in different investigation lines in the biomedical area, as for example, in the osseous regeneration, wounds healing and controlled pharmaceutical products release. It is a biodegradable, hemostatic, biocompatible, antimicrobial, osteoconductive, osteoinductive polymer, with low toxicity and immunogenicity and also with antioxidant capacity [49,55]. Due to its chemical and physic characteristics, namely its solubility in acid aqueous solutions, the chitosan is a biopolymer of relatively easy manipulation. Several of its properties are associated to its positive charge character and the connection that establishes with cellular components of negative charge. CS properties are influenced by its viscosity, crystallinity, deacetylation degree and molecular weight[12,54].

The degree of deacetylation influences properties, like biodegradability and immunological activity since it acts on the solubility, hydrophilicity, viscosity and cross-linking ability of the polymer[59].

The molecular mass is a parameter that determines the solubility of CS. Chitosan solution viscosity increase with the concentration of the polymer and the degree of deacetylation and decreases with temperature. The molecular mass also influences biological properties such as: cicatrization, osteogenesis, and biodegradation of the polymer by lysozyme[60].

Due to the protonation of (-NH2) groups of CS, the solubility is affected. The greater the degree of deacetylation, the greater the number of free amine groups in the chain and consequently the number of amine groups protonated in solution.

Ruel-Gariépy et al.[60], point out that chitosan with a low degree of deacetylation induces an inflammatory response, as it degrades more rapidly causing accumulation of amino-saccharides, while that of a high degree of deacetylation causes minimal response in adjacent

tissues due to low degradation rate. However, chitosan's with high degree of deacetylation have a positive effect in the adhesion and cellular proliferation. In other words, the bigger the deacetylation degree, the bigger will be the quantity of free amines groups (-NH2) which can form cations (-NH3+), making the surface positive. CS has chemical properties that helps to fix the proteins and enzymes[61]. Also, allows them to be incorporated in its matrix different therapeutically agents, growing factors or cells [62].

There are numerous studies and applications using CS as hemostatic material. The CS hemostatic mechanism is ruled by two different phenomena:

- The CS and the platelets adhere one to each other through the mediation proteins and, after that, the complex formed by chitosan/platelets, accelerates the fibrin monomers polymerization and forms clots;

- The CS induces the erythrocytes aggregation and stimulate the vasoconstriction.

Consequently, local thrombosis is formed and the wound is sealed.

It is believed that the ion interaction between the positively changed polymer chain of chitosan and the cellular membranes, negatively charged, of the erythrocytes is responsible for the clot formation.

This mechanism can act independently of the events cascade that occurs in the normal coagulation, which results in the fibrin formation. This way, chitosan can form a stable blood clot in the fibrins absence [63].

The hemostatic agents, available in the market, depend essentially of the fibrins formation. An agent that works in an independent way or inside the events cascade of the normal blood clot process, can be very utile in the cases where the fibrins formation is inhibited pharmaceutically (by heparin or anticoagulant therapy) or, in some cases, due to diseases that affects the normal coagulation process [63,64].

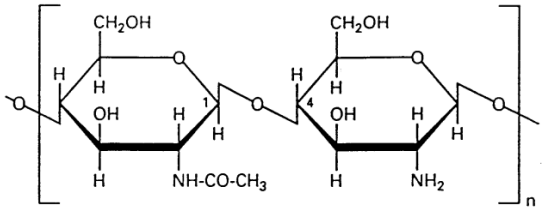

Figure 6 - Chemical structure of chitosan.

1.7. Nonsteroidal Anti-Inflammatory Drugs

Nonsteroidal Anti-inflammatory Drugs (NSAIDs) belongs to the pharmaceutical group of anti-inflammatory drugs, and they are amongst the most commonly prescribed drugs in medicine for the resolution of inflammatory pathologies[65].

There are a group of drugs with antipyretic, anti-inflammatory and analgesic action that aims to suppress pain and inflammation, but not cure. These drugs act as inhibitors of cyclooxygenases (COX) which are key enzymes responsible for the conversion of compounds involved in inflammation. They are usually used for long periods of time in the treatment of diseases such as rheumatoid arthritis, osteoarthritis, post-operative and postoperative pain[66].

The analgesic effect is related to the inhibition of the production of prostaglandins when a tissue aggression occurs. The anti-inflammatory effect is associated with the inhibitory effect of cyclooxygenase and consequently on the synthesis of prostaglandins. The antipyretic effect occurs from the inhibition of prostaglandins of the synthesis at hypothalamus level, mainly prostaglandin, which regulates body temperature. Sill, not all NSAIDs demonstrate the same analgesic, anti-inflammatory, and antipyretic activity[67].

The dose of NSAID that is required to provide the anti-inflammatory effect is greater than the dose required to promote the antipyretic and analgesic effect.

Pharmacological actions and adverse effects are closely related to the mechanism by which the drugs act, that is, the inactivation of cyclooxygenases, leading the production of prostaglandins decrease, which are responsible for several pathophysiological processes in the organism[67,68].

1.8. Mechanisms of Action of NSAIDs

Most NSAIDs inhibit the two COX isoforms, however there are anti-inflammatory drugs that selectively inhibit each of them. Its selectivity can be expressed on the basis of the COX Ic_{50}, i.e., the concentration required to inactivate 50% COX activity[69,70].

COX-1 is a constructive isoenzyme found in most tissues (blood vessels, platelets, stomach, intestines, and kidneys) in which its inhibition by NSAIDs is associated to adverse renal and gastric effects. COX-2 is induced during the inflammatory process and when inhibited it is related to anti-inflammatory actions[68].

In general, NSAIDs vary considerably in their selectivity for COX-1 or COX-2. NSAIDs can be divided into 3 distinct groups according to their enzymatic selectivity:

- Inhibitors without selectivity (without cyclooxygenases preference, similarly inhibit the two isoforms);
- Selective inhibitors (prefer one of the isoforms);
- Specific inhibitors (exclusively inhibit COX-2)[70].

According to the Ic_{50} COX-2 / Ic_{50} COX-1 ratio, diclofenac has a value of 0.7, indicating that it is a non-selective NSAID[69,70]. This explains the existence of more adverse effects than in NSAIDs selective for COX-2.

NSAIDs entering in the bloodstream bind to plasma proteins, demonstrating a variable plasma half-life. The diclofenac's half-life is short, since it is lower than 6 hours.

Figure 7 shows the pharmacological action of NSAIDs, in which the process starts after cell membrane damage, where the enzyme phospholipase A2 is activated by proinflammatory cytokines, such as interleukin-1 (IL-1). This promotes the degradation of phospholipids, from which results the formation of arachidonic acid. The acid to be metabolized, forms leukotrienes due to the action of the enzyme lipoxygenase, and through the action of the enzyme COX originates prostaglandins, prostacyclins and thromboxanes[68].

COX, by oxygenation, converts arachidonic acid into prostaglandin G2 and prostaglandin H2. These are subsequently transformed by isomerases into prostacyclin, thromboxane A2, and prostaglandins D2, F2α and E2.

COX 1 and COX 2 enzymes, although very similar at the level of protein structure, have distinct functions once they are encoded by different genes. COX 1 undergoes NSAID action, reduces gastric protection, platelet aggregation, vascular homeostasis, and maintenance of renal blood flow. In contrast, when COX 2 is expressed by cells involved in the inflammatory process and when it undergoes NSAIDs, it reduces the production of prostaglandin thus controlling inflammation, fever and pain sensitivity[68,71].

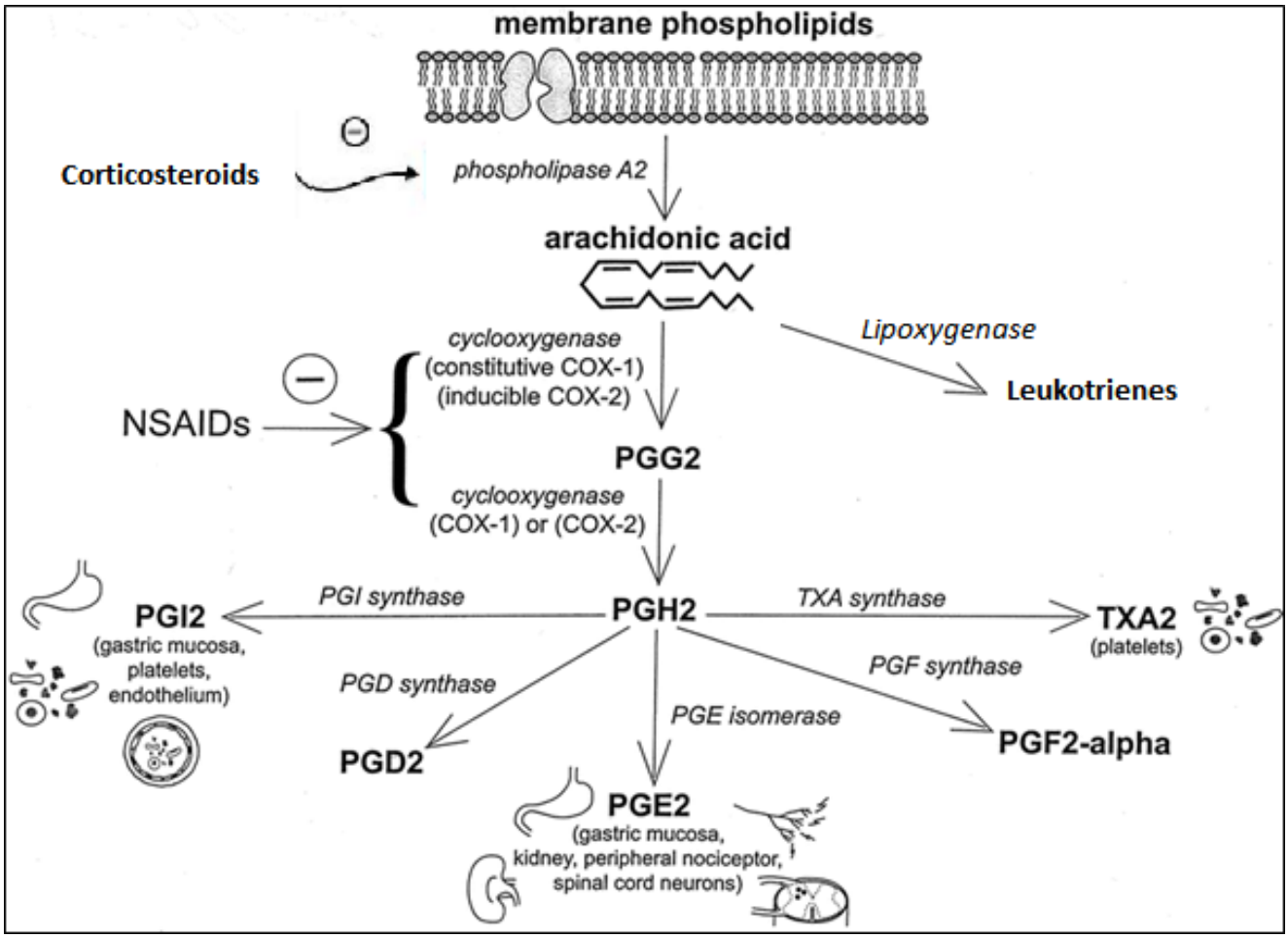

Figure 7 – Mechanism of action of non-steroidal anti-inflammatory drugs [Adapted 69].

1.8.1. Diclofenac Sodium – Structure and main properties

At the structural level, most NSAIDs present at the structural level an acidic group and a carboxyl group, which may be required for efficient drug binding to their site of action. The aromatic planar group and lateral chain, belonging to the same structure, allow to verify the good disposition of the drug by the hydrophilic and hydrophobic tissues of the organism[66].

Diclofenac (2(2,6-dichlorophenyl)amino) benzeneacetic acid, as shown in figure 8, is a sodium salt of an amino phenyl acetic acid that is quickly absorbed by the organism after oral administration, and it reaches peak plasma levels in 1 to 2 hours. DF has a short plasma half-life and it circulates in a bound-to-free equilibrium with plasma proteins.

This acetic acid is hydroxylated by the liver and undergoes enterohepatic recirculation. It can cause some side effects, such as gastritis, peptic ulcer and bleeding. However, diclofenac sodium appears to be an effective anti-inflammatory drug in the treatment of rheumatic arthritis with a good safety profile[72].

This sodium salt presents a solubility that varies with the pH, being more soluble in alkaline medium and little soluble in acid medium[73].

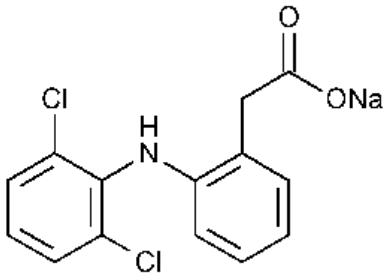

Figure 8 - Chemical structure of DF.

Table 1 shows some of the drugs marketed, as well as the dose and the dosage, where the active principle common to all is DF.

Table 1 - Commonly prescribed drugs with diclofenac, dose and the recommended dosage[74–79].

Active Substance	Medical Product's Name	Indication	Dosage Form	Posology
Diclofenac	Voltaren ®	Pain and oedema post-surgical; Inflammation	Tablet Suppositories	50-150mg/day (2 to 3 doses)
	Dorcalor ®			
	Flameril ®		Inject	75 mg/ 3ml
	Fenil-V ®		Gel	10-23mg/g
	Olfen ®		Eye drops	1 mg/ml

Most medications used to treat inflammation require several doses per day to maintain the concentration of the active ingredient at the recommended therapeutic level[80]. However, this thesis intends to develop a controlled release system of anti-inflammatory for direct and convenient application in the target site (*in loco*), allowing not only to eliminate the number of daily doses, but also maintain the therapeutic level appropriate thus avoiding hepatic metabolism. This system would increase the effectiveness of the drug and the patient's quality of life.

1.9. Incorporation of an Active Substance

For a bone medical device containing an active substance, it is essential to be able to target the drug to specific sites of the bone in order to be able to control its release, maintaining the desired concentrations for long periods without reaching the toxic levels or effective therapies below levels.

The choice of diclofenac for scaffolds is directly related to the fact that this is an anti-inflammatory, widely used in the treatment of diseases of bones and joints.

The treatment of bone diseases, inorganic materials, such as calcium phosphates, can be considered important in the transport of drugs to the tissue, since they present pores with approximate diameters of 10μm, in order to confine the active substance inside the ceramic[6]. According to studies carried out over time, the porosity of the ceramics allows to control, and to, some extent, adjust the rate of release of the drug[6].

The use of organic materials, such as chitosan, allows the creation of a hydrogel matrix which controls the release of the active substance by the degree of hydration and swelling[72].

1.10. Controlled Drug Delivery

Search and development of new controlled drug delivery systems has been decisive to establish more efficient and effective therapeutic alternatives that allow drugs administration in a safety way and with fewer adverse effects[81]. The drugs can be administered to humans and animals by different routes, however, only a small fraction of the dose reaches the target site, most of which is wasted due to its distribution to other tissues and to their metabolization or excretion before reaching the site of action[82].

The controlled release system is intended to maintain control over the release rate and duration of the drug in blood or target tissues. The administration of drugs optimally allows the reduction of toxic effects.

Release patterns can be divided into two classes, in patterns that release drug at a slow zero or first order rate, where the release rate remains constant over time; and in the release patterns with a rapid initial rate, in which thereafter will follow a slow zero or first order release[82].

In order to exert an effective control on the drug release rate, the controlled release systems usually start releasing a significant part of contained dose, so they can attain rapidly the effective therapeutic drug concentration. In a later stage the drug release is reduced in a

controlled manner until it becomes null. The whole process follows a well-defined behavior in which the desired drug concentration is always achieved.

The drug release kinetic can be described by a large number of models, based in different controlled release formulations. These models can be classified into three categories:

- Statistical Methods (exploratory data analysis method, etc.);
- Model independent methods (similarity factor, etc.);
- Model dependent methods (zero order, first order, Higuchi, Korsmeyer-Peppas, Hixson Crowell, etc.) [82].

Statistical methods depend on the exploratory data analysis method, which provides improved understanding about the dissolution data of the controlled release formulation, and the multivariate approach. These methods were based upon repeated measure designs, where time is the repeated factor and percent dissolved is the dependent variable[82].

Dependent methods model is based on different mathematical functions that allow a dissolution profile description. Once a suitable function has been selected, the dissolution profiles are evaluated depending on the derived model parameters[82].

The model independent methods use the difference factor (f1) and the similarity factor (f2) in order to compare the dissolution profiles. f1 is a measurement of the relative error between two curves, and f2 is a logarithmic reciprocal square root transformation of the sum of squared error. The similarity factor is a measurement of the similarity in the percent dissolution between the two curves[82].

1.10.1. Polymers in Drug Delivery Systems

One of the great challenges of controlled release systems is to ensure that the charged drug is delivered in the right place at the right time and in the exact amount. Low solubility, degradation, drug toxicity or rapid clearance of the organism may reduce the effectiveness of the systems. Natural and synthetic polymers are considered effective solutions for the release systems.

Polymers incorporated with therapeutics can be bioactive to provide their own therapeutic benefit or can be biodegradable to improve release kinetics and prevent carrier accumulation[83,84].

Polymer-based release systems can liberate the drug by different mechanisms:

- Diffusion-controlled – monolithic systems or reservoir system;

- Solvent-activated – swelling system or osmotically-controlled system;
- Chemically controlled – biodegradable (bioerodible) system or pendant-chain system[83].

Chemical-controlled systems may be divided into: monolithic systems where the drug is dispersed or dissolved in polymer matrix and liberates at the rate of bioerosion (biodegradation) of the matrix; or by pendant chain systems where the drug is chemically bound to the polymer chains, releasing as hydrolysis or enzymatic cleavage of the linkage occurs, figure 9[84,85].

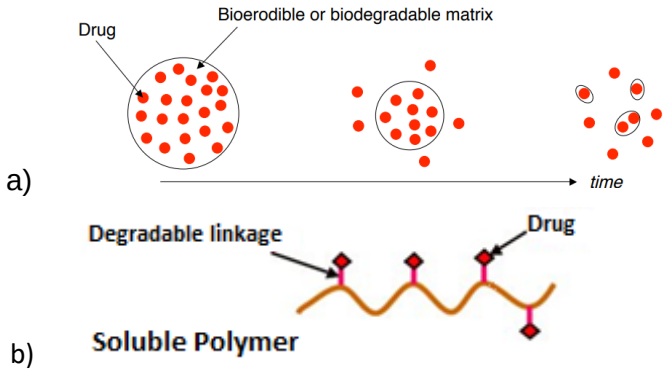

Figure 9 - Schematic representation of chemically controlled release. a) biodegradable system; b) pendant-chain system.

The solvent controlled systems can be controlled by osmotic pressure, where the constant volume reservoir, in which the drug is in the solid state, and a saturated drug solution, is coated by a semipermeable membrane, which allows solvent to pass through and not of the drug. The osmotic pressure causes a flow of water from the outside into the reservoir, causing the drug-saturated solution within the reservoir to escape through an orifice in the membrane, figure 10.

In swelling controlled systems, drug aggregates are homogeneously dispersed into a dry swellable polymeric network. When these systems are immersed in water or body fluid, the flow of water into the polymeric network will hydrate the systems. Therefore, the aqueous solvent content within the system and the network mesh size increase, resulting in the dissolution and diffusion of drugs throughout the hydrated polymeric network[85].

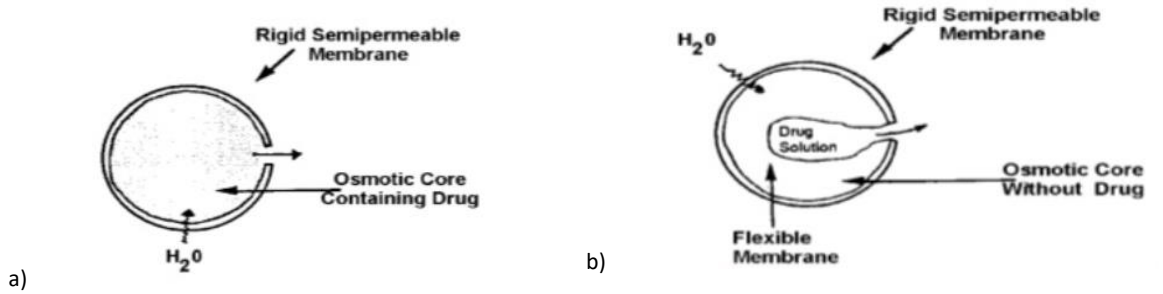

Figure 10 - Schematic representation of osmotically controlled release systems and swelling system. a) Type A contains an osmotic core with drugs; b) Type B contains a drug reservoir surrounded by osmotic core.

Diffusion-controlled systems are the mechanisms most used in drug control. They may be from reservoir where the bioactive agent is in liquid or solid form in a core coated by an inert polymeric membrane depending on the type of material and properties of the polymer and the drug the diffusion may be slower, figure 11. They may also be by monolithic system, where the bioactive agent is uniformly dispersed or dissolved in a polymer matrix, where the release of the drug is controlled by diffusion along the matrix[84].

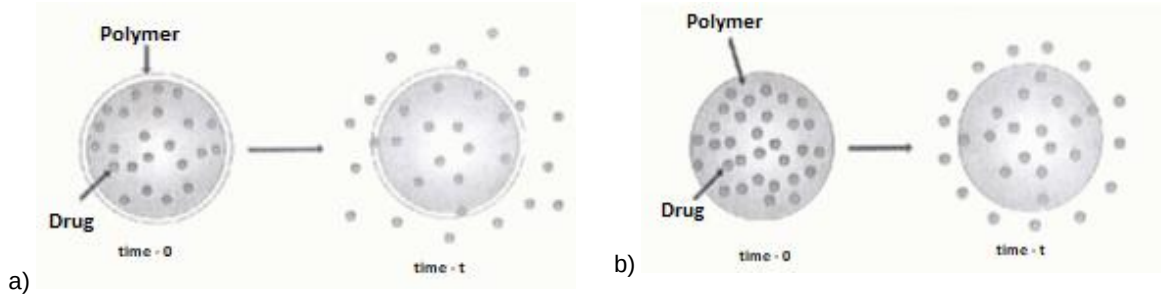

Figure 11 - Schematic representation: a) reservoir diffusion-controlled release systems, b) monolithic diffusion-controlled release systems[84].

1.10.2. Mathematical Description of the Drug Release Kinetics from the Scaffolds

Of the previously described models none applies directly to composite drug delivery systems. Thus, this design will be guided by release models from polymer systems, since the drug is uniformly distributed throughout the chitosan matrix. The developed scaffold is expected to exhibit a mechanism of controlled drug release by diffusion and biodegradation.

Diffusion is a mass transfer-based mechanism that occurs between two different systems due to the existence of a concentration gradient. It describes a substance's transfer from a medium with higher concentration to another with a lower concentration value[86].

The simplest description of diffusion is given by Fick's laws, which were developed by Adolf Fick in 1855.

Fick wrote the first law to describe the phenomenon of diffusion in a stationary state, where he did not consider the time in which the process occurs. That means that the particle flow in a one-dimensional system caused by a concentration gradient can be expressed as:

$$J = -D\frac{\partial \mathrm{C}}{\partial x} \qquad \textbf{Equation 1}$$

Where J is the flux per time unit, D is the diffusion coefficient, C is the drug concentration and x represents the distance between the place where the drug is accumulated and the release surface. The negative sign stems from the fact that diffusion occurs in the direction opposite to the increasing concentration gradient. In controlled drug release systems of the polymer matrix type, diffusion coefficient depends on drug concentration, cross-linking density, crystallinity degree and the size of crystalline areas.

Fick's first law cannot be used to estimate the diffusion coefficient of the components due to the absence of a time parameter. In this way, Fick proposed a second law that describes the phenomenon of mass transfer in non-stationary state.

$$\frac{dQ}{dt} = -D\frac{\mathrm{dC}}{dx} \qquad \textbf{Equation 2}$$

dQ/dt represents the drug mass change with respect to time, being Q the drug mass, t time, C concentration of drug, X the spatial coordinate normal to the section and D the diffusion coefficient[87].

Parameters such as the drug solubility in water or degradation of the carrier are crucial to infer about mechanism of release. The cumulative profiles of released drug are adjusted by mathematical equations that eventually relate various parameters, such as drug delivery system or the dissolution curve obtained.

These mathematical models by providing information on the type me release mechanism, allow the tailoring of the drug release system to improve its efficacy, having as major advantages the reduction of experimental optimization time and costs[88].

The empirical and semi-empirical existing models are only descriptive and not based on physical-chemical phenomena. The prediction capacity of these models is somehow limited. However, these models are based on mathematical description of the release profiles and can be useful for the sake of comparison between profiles obtained from different[87].

According to the geometry of the scaffold and the type of release, it was decided to select the following models of release profiles as being the most appropriate for this project: zero order, first order, Korsmeyer-Peppas, Higuchi and Hixson-Crowell.

Zero-order model

The zero-order model is based in an active substance slow release, at a constant rate, from diverse geometric forms that do not disaggregate. This model can be expressed by the following equation:

$$Q_t = Q_0 + K_0 t \qquad \textbf{Equation 3}$$

Where Q_t is the amount of drug dissolved in time t, Q_0 is the initial amount of drug in the solution (most times, $Q_0 = 0$) and K_0 is the zero order release constant expressed in units of concentration per unit time[82].

This model is generally used to describe the release by various types of controlled release pharmaceutical dosage forms. Ideally, preparations intended to deliver active substances upon prolonged release have a zero-order release profile, it being found that the diffusion rate of the drug from the inside to the outside of the matrix is less than the respective rate of dissolution,

forming a saturated solution, which allows the constant yield of the drug. This ideal release situation is very difficult to obtain in practice. The application of this model presents many limitations due to the few adjustment factors to the model[89].

First order model

This model has been used to describe absorption and/or elimination of some drugs, although it is difficult to conceptualise this mechanism in a theoretical basis. The rate of drug delivery decreases exponentially with time, being represented by Equation 4, where K is the first order rate constant, C is the drug concentration at time t. Equation 4 can be expressed in equation 5:

$$\frac{dC}{dt} = -Kc \qquad \textbf{Equation 4}$$

$$log\ C = log\ C_0\ - \frac{Kt}{2.303} \qquad \textbf{Equation 5}$$

where C_0 is the initial concentration of the drug, K is the first order rate constant and t is the time. This model can be used to describe the drug dissolution in pharmaceutical dosage forms such as those containing water-soluble drugs in porous matrices[82,89].

Higuchi model

In 1961, Higuchi described the drug release from a matrix planar geometry. Over the years, the proposed model suffered amendments so that it can be used in different geometric systems and porous. This model is based on the following hypotheses:

1) The initial drug concentration within the matrix is much higher than the solubility thereof outside the matrix;
2) The drug diffusion takes place only in one dimension;
3) The drug size is smaller than the thickness of the matrix in which it is contained;
4) Matrix swelling and dissolution are negligible;
5) Drug diffusivity is constant;
6) In the release medium, the condition of total submersion of the matrix is ensured.

The model expression is given by the equation:

$$f_t = Q = A\sqrt{D\,(2C - C_S)C_S\,t}$$ **Equation 6**

where Q is the amount of drug released in time t per unit area A, C is the drug initial concentration, C_s is the drug solubility in the matrix media and D is the diffusion coefficient.
In order to simplify the Higuchi model, we have the following equation, which serves to study the dissolution from a planar heterogeneous matrix system, where the drug concentration in the matrix is less than its solubility and the release occurs through pores in the matrix:

$$f_t = Q = K_H\,t^{1/2}$$ **Equation 7**

Where K_H is the Higuchi dissolution constant, which considers the porosity, tortuosity and free volume created by the interconnectivity of the matrix pores[82,89].

Hixson-Crowell model

In 1931, Hixson and Crowell recognizing that the particle regular area is proportional to the cubic root of its volume derived an equation that can be described in the following manner:

$$W_0^{1/3} - W_t^{1/3} = K_H\,t$$ **Equation 8**

Where W_0 is the initial amount of drug in the pharmaceutical dosage form, W_t is the retained in the matrix in time t and κ is a constant incorporating the surface-volume relation.
Above equation describes the drug's release from a system which undergoes changes in area and diameter during drug release, but maintaining the initial geometry.
The model applies to dosage forms with disk and spherical geometry, if their dimensions decrease proportionally, i.e., not changing their initial geometric shape[89].

Korsmeyer-Peppas model

The model developed by Korsmeyer et al in 1983 is one of the more general models that can be used to describe the release of a drug taking into account mechanisms involving diffusion control and polymer relaxation.

This model is used to polymeric release systems with various geometries previously described, and therefore different constants are employed dependent on the studied geometry. This equation is only applicable to the first 60% of the release profile[90].

$$Q_t = \mathrm{K}t^n \qquad \textbf{Equation 9}$$

Where K is a constant incorporating structural and geometric characteristics of the drug dosage form, *n* is the release exponent, indicative of the drug release mechanism, and the function of *t* is M_t/M_∞

Accordingly to the n value, it is possible to identify the predominant release mechanism. For n=0,5 the mechanism is considered purely Fickian; for 0,45 < n < 0,89 the diffusion is considered anomalous with a diffusion rate similar to the polymer matrix relaxation; for n = 0.89 the diffusion rate is higher than the process of polymer matrix relaxation (Case II transport); for n > 0,89 the mechanism is considered to fall on the Super Case II transport; finally, for n < 0,45 the diffusion rate is lower than the process of polymer matrix relaxation (Case I transport)[91].

Table 2 - Interpretation of diffusional release mechanisms from polymeric films, taking into account the exponent of the Korsmeyer-Peppas model.

Release exponent (n)	Drug transport mechanism
n < 0,45	Case I
0,45 < n < 0,89	Case Anomalous
n = 0,5	Fickian
n = 0,89	Case II
n > 0.89	Super Case II

In this project, the model's choice that best fits the release profiles will be made considering the highest coefficient of determination (R^2)[92].

1.11. Sterilization

Sterilization consists of a chemical or physical process that allows the elimination of the microbial load. This process is critical in the medical device industry where pharmaceuticals and devices must meet to ensure high safety and performance levels and will not cause damage when contacted with body fluids[93].

There are several types of sterilization methods that can be used in tissue regeneration devices, however, care must be taken with the type of material in medical device and type of microorganisms involved.

The methods of sterilization are classified into physical and chemical, within each one we can choose:

- Physical: Filtration, heat (dry or moist-steam) and radiation (ionizing or non-ionizing);
- Chemical: Liquid (ethanol) and gaseous (ethylene oxide, plasma, ozone and supercritical gases)[94].

However, the types of sterilization most used in materials that use polymer compounds in their structure are: heat, radiation and ethylene oxide.

1.11.1. Gamma Radiation

Gamma radiation is an ionizing radiation that has enough energy to ionize atoms and molecules. It is one of the most used sterilization processes in the industry where gamma rays used for sterile processing are formed with the self disintegration of Cobalt-60 (^{60}Co). Among thousands of gamma emitters only Cobalt-60 is indicated for sterilization processing[94].
Cobalt-60 is specifically manufactured with the intent to be used in irradiation process, being housed in chambers that are specially designed and operate under very strict regulations and standards. It is a known fact that the sterilization through gamma irradiation process does not involve sufficient energy promote radioactivity by the treated products, it will only harm the microorganisms present in the products[94].
This type of radiation allows the energy of the gamma rays to break down the bacterial DNA, inhibiting the division of the bacteria. In this way, changes at the molecular level cause the death of the contaminating organisms or render them incapable of reproducing.
This process leaves no residue or allows radioactivity to be transmitted to the products. Gamma rays have a high penetration power so materials can be sterilized after filling them in

the final container. The method is suitable for all types of materials such as dry, moist and even frozen items[94,95].
However, this method may be associated with some changes in the molecular structure of the polymers since the formation of radicals leading to cleavage or cross-linking may occur[95].
To ensure that the radiation obtained by the products is uniform and within the specified limits (maximum and minimum dose), dosimeters are placed together with the products in order to monitorize the acquired radiation during the process[96]. The radiation dose limits are determined through a validation process that follows the International Standard ISO 11137.

The sterilization process utilized at the industrial level is realized accordingly to a previous validation, as mentioned above, where the product's dose limits are determined. The dose is defined by the product's biological component, its radiation resistance and the sterility assurance level (SAL).

According to the ISO 11137-2, the sterilized product's SAL must be 10^{-6}. In order to assure that SAL value, the radiation dose must be selected accordingly to the product's tolerance, and it can sometimes be equal or lower than 25kGy[97].

In this project it was used gamma radiation to sterilize the scaffolds that contained an inorganic phase, a polymeric phase and an incorporated drug.

1.11.2. Gamma sterilization influence in drug release

One of the most critical controlled drug release systems parameters is the sterilization[98].

The gamma radiation can lead to loss of activity of some drugs. It can also occur several disturbances at physicochemical polymer properties which can lead to changes in the system's release profiles.
When the drugs are in an aqueous solution radiolytic products formation occurs due to the chemical reactions between species generated by water radiolysis and the drug solute. However, the solid state drugs show a lower loss of activity after exposure to ionizing radiation[98,99].

The drug degradation can be minimized through a gamma radiation and sterilization conditions optimization.

2. PROCESS, MATERIALS AND METHODS

With the aim of satisfying the necessary requirements of this project, the developed scaffolds combine CS dissolved in lactic acid solution and mixed with CaPs spherical granules, to enhance osteoconductivity, accelerate the tissue regeneration time and promote cell adhesion and proliferation, and with DF to promote the inflammation treatment. All materials are biocompatible and suitable to substitute the tissues that are meant to be repaired.
The scaffold manufacture requires a high knowledge of the material characteristics, as well as the tissue and scaffold interactions, as mentioned above.
The manufacture process used in this project is based in the freeze-drying process.

2.1. Freeze Drying Process

There are a variety of dehydration methods, but the freeze drying (lyophilization) is the most suitable for heat sensitive substances. Freeze drying is a process where the water or other solvent is removed from frozen material, directly converted to steam without any intermediate formation of liquid. The freeze drying process may be divided into three stages: freezing, primary drying, and secondary drying[100,101].

The process begins with the product freezing. Then, by sublimation, the water is removed from the sample, occurring the primary drying and then freezing water is removed by desorption (secondary drying). Thus, freeze drying is the process of removing moisture from a frozen product using vacuum[101].

The main principle involved in this technique is a sublimation, where water passes directly from its solid to the vapor state. Water sublimation can take place at pressures and temperature below triple point (i.e. 4.579 mm of Hg and 0.0099 degree Celsius)[101]. The material subjected to freeze-drying is firstly frozen and then subjected to a high vacuum in order to heat, so that frozen liquid sublimes leaving the solid and dried components of the original material[102].
At atmospheric pressure, approximately 1.0 atm, water can have three physical states: solid, liquid and gaseous. Below its triple-point only the solid and the gaseous states exist, as seen in the below figure.

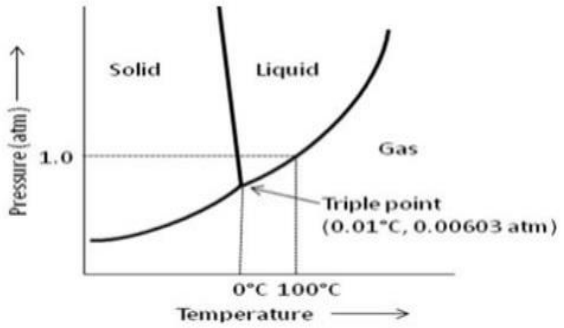

Figure 12 - Water's phase diagram[101].

The concentration gradient of the water vapor between the drying front and condenser is the driving force for removal of water during lyophilization.

During the primary drying, the increase in temperature causes the water's vapor pressure to increase. Thus, it is important to keep the temperature during the primary drying as high as possible, below the critical process temperature, in order to avoid structure loss. It also important to refer that the collapse temperature for amorphous substance or eutectic melt for the crystalline substance is defined as the critical process temperature[101]. During the freezing the solution becomes maximally concentrated while the ice crystals start separating out, and on further cooling the phase separation of the solute and ice takes place[102].
The entire process described above allows the dried material constituents to remain homogeneously dispersed and also allows long conservation periods due to 95 to 99.5% water removal[101].

2.2. Scaffolds Preparations

In the scaffold production all the reagents were provided by Ceramed S.A. The company also revealed the method and the quantity of reagents necessary for the kIBS® production, being the composition of this product the starting point for the production of scaffolds. Since the technical information of kIBS® is confidential, its main production stages are summarized below:

1) High molecular weight chitosan with 79% deacetylation degree (Chitopharm® L, Chitinor AS, Norway), is dissolved in a lactic acid (Fagron, Spain) solution at room temperature with continuous mechanic stirring system, until completely dissolution of chitosan.
2) PEG with a molecular weight of 380-420g/mol (Panreac, Spain) is added to create the polymeric gel.

3) The calcium phosphate granules with a ratio of 75% Hap and 25% β-TCP (Neobone®, Ceramed, Portugal) and with a circular grain size of 125-355μm of diameter are mixed. The final mixture is obtained when all the components are uniformly distributed.

To prepare the scaffold it was necessary to fulfill two basic steps: firstly, the mixture between the drug and the polymeric mixture; secondly, the calcium phosphates addition and respective mixture molding to lyophilization (figure 13). Therefore, the diclofenac was added to the kIBS® production process before the stage 3.

The addition of diclofenac, with purity degree over 98%, (Alfa Aesar, Germany), was made through dissolution in apyrogenic water (Fresenius Kabi, Portugal). The dissolved diclofenac was posteriorly introduced in the lactic acid and chitosan mixture, and then stirred for four hours. To select the way to introduce diclofenac into the existing production process, it was necessary to carry out an optimization study, as explained in section 2.2.1 (Table 3). For each gram of kIBS® paste was added 1100 μg of diclofenac.

The final mixture was then placed into two different circular molds and it was freezed at -30ºC, for at least 24 hours. The scaffold obtained from the mold of approximately 5 mm diameter and 65 mm length was cut to sample sizes of 3 mm diameter and 20 mm length (small scaffold diameter). On the other hand, the scaffold obtained from the mold of 12 mm diameter and 40 mm length was cut to sample sizes of 3 mm diameter and 20 mm length (large scaffold diameter).
After this process, and without unfreezing the samples, they were placed in the freeze drier (Christ Alpha 1-2 / LDplus, Germany) at -45ºC and 0,02mbar of pressure during 24 hours. At the end of the freeze-drying cycle the samples are removed from the mold and present a visual appearance similar to a stiff sponge.

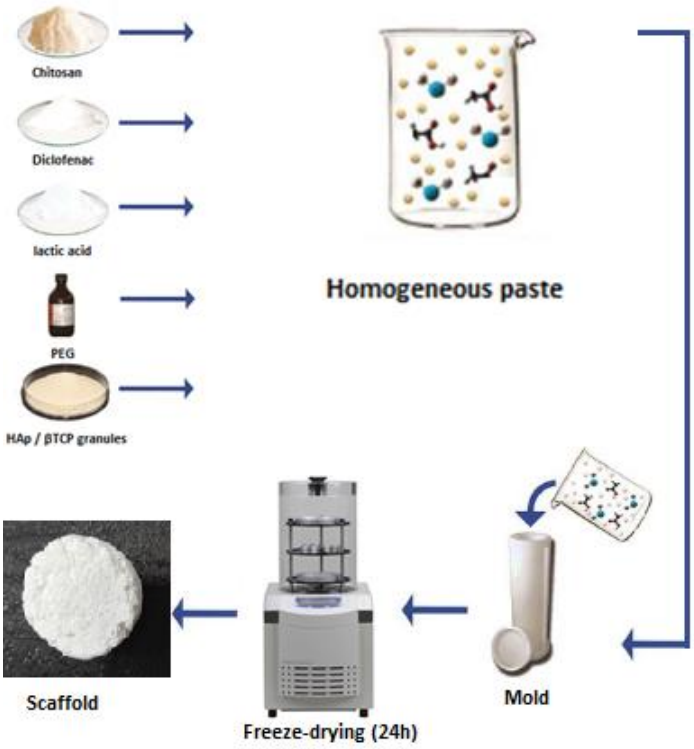

Figure 13- Schematic illustration of scaffolds production (adapted Asadian-Ardakani et al.)[103].

2.2.1. Optimization Process

The sodium diclofenac utilized in this project is a sodic powder salt with a yellow coloration, slightly hygroscopic and it has a greater solubility in alkaline mediums[104]. Since chitosan only dissolves in an acid medium, the objective is to introduce the diclofenac directly into the polymeric matrix, without resorting to the drug's encapsulation. In order to do this, it was necessary to test several components combinations that did not lead to diclofenac's emulsion. The following table demonstrates the various components mixture attempts, up to the final formula. Despite the different mixing possibilities, the original weight proportions of the kIBS® components were maintained.

Table 3 - Mixing optimization processes.

Compounds mixing order	Processes	Result	
Lactic A. Sol. + DF	Direct mix of both compounds	DF emulsion FAIL	
Lactic A. Sol. + CS + DF Sol.	DF's dissolution in ($^1/_3$) H_2O, then added to the CS dissolution in Lactic Acid ($^2/_3$) H_2O	DF emulsion FAIL	
Lactic A. Sol. + CS + DF Sol.	DF's dissolution in ($^1/_3$) H_2O, then added through a dropper into the Latic A. dissolution ($^2/_3$ H_2O)	DF emulsion FAIL	
Lactic A. Sol. + CS + DF Sol. + PEG	CS's dissolution in Lactic A.($^2/_3$)H_2O, then added through a dropper into DF ($^1/_3$ H_2O) mixing with PEG.	DF emulsion FAIL	
Lactic A. Sol. + DF Sol. + PEG + CS	CS is dissolved into the Lactic A. solution ($^2/_3$ H_2O). PEG's addiction followed by DF ($^1/_3$ H_2O) dissolution's mix.	Homogenous Mixture PASS	

In accordance with this project's intended objectives, the last mixture was the one that allowed to obtain a uniform mixture between drug, polymeric matrix and calcium phosphates.

2.2.2. Sterilization Process

Gamma radiation was the only sterilization method used, in order to assure the microbiological activity total elimination, and to access the influence of the sterilization process in the controlled drug release.

The sterilization process occurred in Aragogamma S.L. facilities, in Barcelona, by a ^{60}Co radiation source, during 7 and 10 hours to achieve 15kGy and 25kGy doses, respectively.

The Red Perspex 4034 dosimeter (Harwell, range 5 – 50kGy) was used to monitor and validate the absorbed dose.

After the irradiation samples did not change its appearance, that remained yellow and dry. According to the authors, R.Galante, A.Oliveira et al.,2018, the radiation does not alter the dry diclofenac sodium when it is gamma irradiated[105].

Figure 14 - Example of irradiated scaffolds. These were inserted in Tyvek bags with yellow gamma indicator and sent to Aragogamma. After the radiation, the indicator gets red, as a sign that the radiation occurred.

2.3. Diclofenac Controlled Release Experiments

To determine sample release profiles human body conditions were mimic using saline PBS at 36ºC with pH 7.4 prepared with MiliQ water as the release medium. This solution is widely used in tests due to a set of reasons: its pH is similar to the physiological one and it presents saline concentrations and osmotic pressure similar to the biological fluid ones[106]. The same procedures were performed for all the release assays.

Scaffold samples of small diameter were prepared as reported in section 2.2. Considering the weight of the samples, the amount of water lost during the freeze drying process and supposing a uniform distribution of the diclofenac in the polymeric matrix, it was assumed that each sample was loaded with 500 µg of diclofenac.

The samples used in this test were:

- 5 samples - Without DF and not irradiated;
- 5 samples - With DF and not irradiated;

- 5 samples - With DF and irradiated at 15kGy;
- 5 samples - With DF and irradiated at 25kGy.

The samples were placed in falcon tubes with 5mL of PBS, at 36ºC, and mixed at 180rpm on a stirrer (Incubating Mini Shaker from VWR). Over defined times and in order to assure sink conditions, aliquots of 2,5mL were withdraw from each tube, being replenished by 2,5mL of fresh PBS in order to maintain the release volume constant. The released drug concentration over the time was determined by UV-Vis spectroscopy (Multiskan™ GO Microplate Spectrophotometer of Thermo™ Scientific) based on the Beer's law principles. The used wavelength for the DF was 275nm. The absorbance values were converted to concentrations using the DF in PBS calibration curve, in the 1,0 – 50,0µg/mL range.

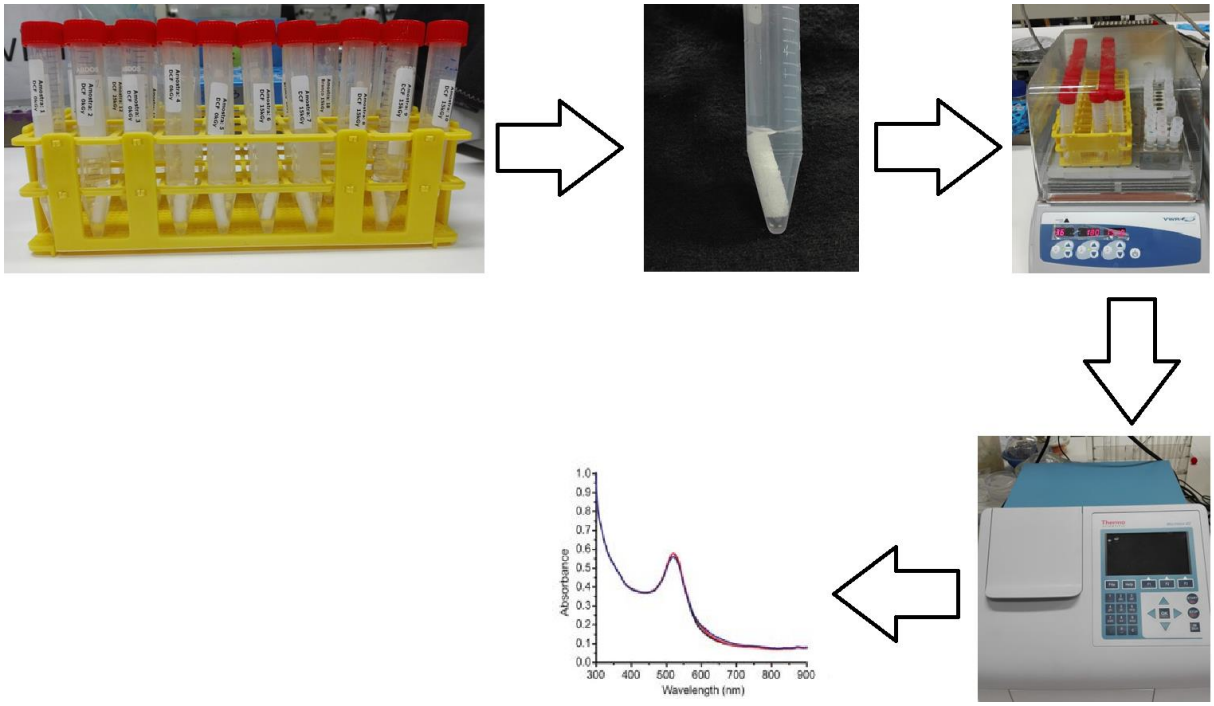

Figure 15 - Preparation of the irradiated and non-irradiated samples with and without diclofenac, to the release assay and subsequent spectrophotometer analysis.

Drug Amount Determination

To determine the total amount of DF incorporated into composites scaffolds used in the release assay were dissolved in 2,5mL of PBS, being added another 8mL of fresh PBS in order to promote the drug's total release from the matrix. Samples were then stirred overnight, as shown in figure 16. Centrifugation (2078 x g for 30min at 5ºC) was used and the resulting supernatant was collected. Samples' absorbance was subsequently determined at 275nm,

using UV-Vis spectroscopy and converted to concentration values through a calibration curve.

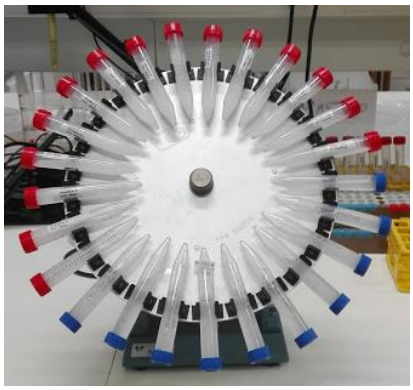

Figure 16 - Overnight shaking of the tubes that contains scaffolds emerged in PBS.

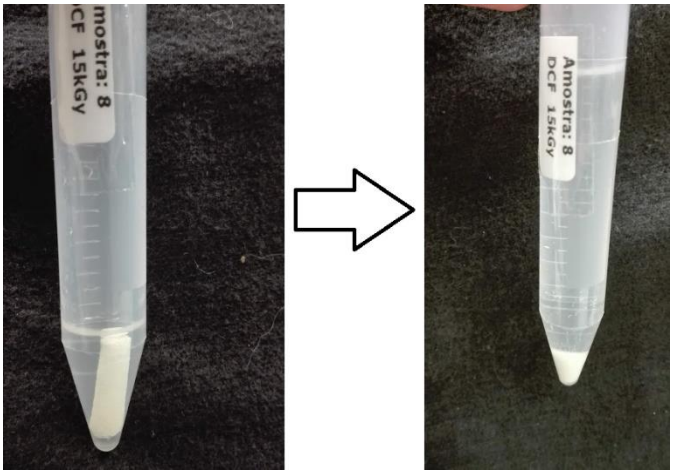

Figure 17 –a) Scaffold emerged in PBS before the shaking. b) Scaffold destroyed after the centrifugation.

2.4. Chemical and Structural Scaffold Characterization

Chemical, physical, mechanical and biological characterization of the composite scaffolds will allow the assessment of intrinsic material properties and the implications of its use.

The scaffolds were characterized through a set of techniques and methods, such as: FTIR, SEM/EDS, XRD, swelling, particle size and captive bubble. The scaffold samples used in these studies were prepared as explained in section 2.2.

Below is a description of the characterization methods used and their operation principles in the studies carried out for the scaffold with diclofenac's characterization.

2.4.1. Microscopy

There are several methods available for measuring particle size and porosity. One of these methods is microscopy which when using the microscope and small amounts of samples, allows to obtain enlarged images of the objects, allowing the observation of structures invisible to the naked eye[107].

In this work, two types of microscope methods were used for the structural evaluation and chemical composition of the scaffolds: Optical microscopy and scanning electron microscopy.

Optical microscopy provides a wealth of information on this project study material. This technique allows to observe, evaluate and obtain, in this work, the particles' size and shape measurements.

For the microscope observation, larger diameter scaffolds were embedded in epoxy resin, with a curing time of 2h at room temperature. The granules of the scaffold formulation were also analysed. Sample polishing was carried out with several different sandpaper (320, 600, 1200 and 4000µm) in order to be able to wear out the mold until the samples inside were reached, for later visualization.

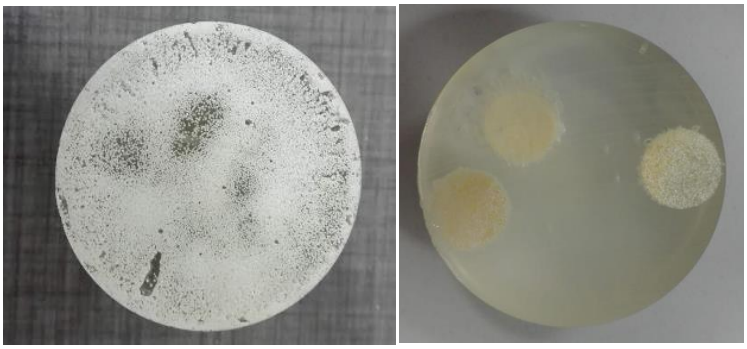

Figure 18 - Epoxy formers with granules of calcium phosphates, on the left and with scaffolds on the right.

2.4.1.1. Scanning Electron Microscopy / Energy Dispersive X-Ray Spectroscopy

Scanning electron microscopy is one of the most widely used techniques for the observation of surfaces from various types of materials. Besides morphological information, it also gives topographic information, chemical composition and microstructure. Therefore, in this study, this technique allows to analyse calcium phosphate granules' surface; to verify how the

polymer matrix changes with gamma radiation; to observe the presence of porosity in the sample and to obtain information on the drug distribution.

It uses a beam of electrons with a certain energy to bombard the sample's surface, thus allowing to obtain high resolution two-dimensional images with magnifications ranging from 5x to 300.000x[108].

The operating principle consists of an electron beam that strikes a point on the material's surface. Samples are scanned by a small diameter beam, focused through a system of electromagnetic lenses. The interaction of the electron beam with the sample results in the emission of several types of radiation and electrons, among which the secondary electrons and the backscattered electrons[109].

Morphological and topographic images are formed by secondary electrons released by the sample, which are collected by a detector. Since the electron beam does not pass through the entire sample – it only hits the surface – it is not possible to obtain information about the sample's internal structure. The backscattered electrons have more energy, therefore they allow to obtain information about the contrast and composition[109].

Energy dispersive X-ray spectroscopy (EDS) allows the determination of sample surface elemental composition and to obtain qualitative information. The electron beam strikes the sample and promotes the electrons excitation in the inner layers of the sample. Subsequently, they return to their fundamental state, emitting X-rays. Since X-rays energy depends on the chemical element present in the sample, it is possible to quantify its composition by measuring the energies emitted by the electrons[108].

One of this method's requirements is that the samples are conductive of electrons. If this does not happen it is necessary to previously coat samples with a thin metal film (Au, Au-Pd or Pt)[109].

Experimental Procedure

The SEM analysis was performed at IST. Specimens of each sample to be analysed (granules, drug, large diameter scaffolds with and without DF) were placed in a metallic support and then coated with a thin layer of gold-palladium, which made them electrically conductive, as shown in figure 20.

Specimens were then observed in Scanning Electron Microscope from HITACHI, model S-2400, (figure 19) using a beam energy of 20kV.

In order to obtain information on the drug's distribution in the samples, EDS analysis was performed. Since DF contains sodium and chloride in its molecular structure, EDS allows, through different colour maps, to detect and identify areas of the sample where certain chemical elements are present.

Figure 19 - Scanning Electron Microscope from HITACHI, model S-2400 by IST.

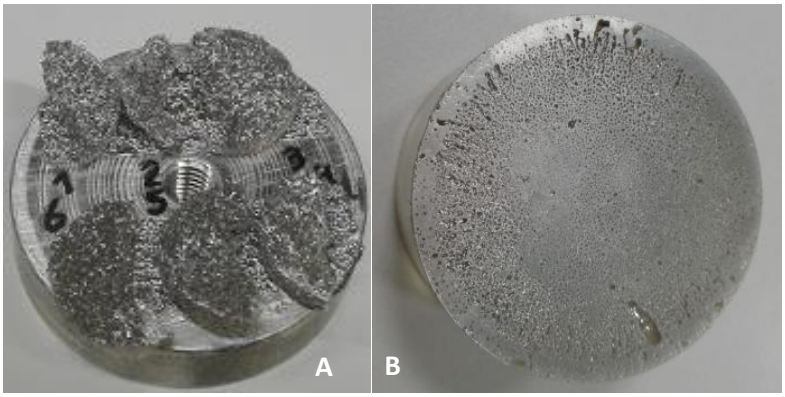

Figure 20 – A) Scaffolds half's without DF (1, 2 and 3) and with DF (4, 5 and 6) on the SEM support; B) Epoxy former of the CaPs granules overlayed with gold-palladium.

2.4.2. X-ray Diffraction Method

X-Ray diffraction is a non-destructive experimental technique. The X-rays are electromagnetic radiation with very small wavelengths, in the range of 0.1-10Å. This radiation arises from a beam of accelerated electrons, originated by a potential differential of the order of 35KV between an cathode and an anode, in which the whole process is kept in vacuum[110].

X-rays are diffracted by atoms on different atomics planes of a crystal, separated by a certain distance. Part of the incident radiation is reflected by the first plane of atoms, but the remaining radiation penetrates the structure, being reflected by inner atomic planes. The paths traveled by the rays reflected by the inner atomics planes are superior to those of the outer atomics planes. Whenever the difference in the path between the diffracted rays (2dsenϴ) equals an integer multiple (n) of the wavelength (λ) of the incident radiation, constructive interference occurs, with the Bragg law[111]:

$$n \lambda = 2d \text{ sen } ɵ \qquad \textbf{Equation 10}$$

where ɵ is the angle of incidence, d is the distance between the successive planes in the crystal lattice and n is the order of the diffracted beams.

A typical X-ray diffraction spectrum consists of a peaks sequence, characterized by their positions, intensities and widths. There are factors that promote the broadening of diffraction patterns, such as the particle size and stresses. The diffraction peak's width is influenced by the number of atoms, i.e. by the crystal's volume. The non-uniform stresses in a crystal give rise to non-homogeneous deformations that vary throughout the volume of the material, resulting in the diffraction peaks' widening. Uniform compressive stresses in the parallel direction to the surface cause a decrease in the d spacing between the planes, promoting a contraction of the unit cell and a shift of the diffraction peaks[112,113].

Experimental Procedure

The chemical composition and crystallographic structure of calcium phosphate granules were analyzed by an X-ray diffraction apparatus at the Universidade Nova de Lisboa, using a diffractometer model Rigaku Miniflex II goniometer, with the CuKα source. This apparatus has coupled a ϴ/2ϴ system, in which the sample rotates at an angle ϴ and the detector rotates simultaneously at an angle 2ϴ. The applied voltage was 30kV and the current intensity was 15mA.

A continuous scan was performed at 2Θ between 20°and 55° with a step size of 0,01 2Θ s^{-1}. Samples to be analyzed were transferred to a sample holder and pressed, obtaining a regular surface.

The spectra-fitting software called MAUD (Materials Analysis Using Diffraction)[114] was used to quantify the percentages of crystalline phases. MAUD software requires crystallographic information files (CIFs) to fit and quantify each specific phase within the XRD spectrum. CIFs used in the powders evaluation were HAp (COD: ICSD-22060) and β-TCP (COD: ICSD-6191).

2.4.3. Particle Size Analyser

Different methods can be used to analyze the particle size distribution including the laser beam diffraction. This technique is based on the Fraunhofer diffraction principle, which allows to evaluate the particle size as a function of the diffraction angle that a laser beam suffers when crossing a set of particles[115]. The signal from the detectors is then converted to the particle size distribution by mathematical algorithms.

The most common method of describing the granulometry of the powders are D values. The D10, D50 and D90 are commonly used to represent the midpoint and range of the particle sizes of a sample. Particle size distributions are normally determined based on a S-curve of cumulative mass/volume and calculating the intercepts for 10%, 50% and 90% mass/volume.

Experimental Procedure

Particle size distribution was obtained using a Coulter™ LS230 equipment at the Aveiro University. The granules samples submitted to the analysis were initially separated in 125μm and 355μm sieves, since it is the desired range for incorporation into the scaffolds.

Subsequently, 0.40g of sample was suspended in 40ml of water. To facilitate granules dispersion, a few drops of Reotan deflocculant were added. The suspension was placed in the specimen compartment of the equipment.

The sample was then crossed by a laser, which was diffracted by the particles, creating a pattern of diffracted light dependent on the particles size.

2.4.4. Wettability – Contact Angle (Captive bubble)

Surface properties of scaffolds directly influence its biological response. The interaction between the scaffold and the surrounding tissue is essential for implant's success or failure. Currently, implanted devices need to have a surface that is capable of reducing adverse reactions from the body to the implant.

Wettability is a method used to describe a fluid's tendency to spread or adhere to a solid surface, being defined thermodynamically by the contact angle created between the fluid and the solid[116,117].

The contact angle (θ) is described as the angle that is created between the surface of the solid and the tangent to the liquid / gas surface at the triple point of contact with the surface of the solid, respectively.

The triple point formed between solids, gas and liquid, changes until the forces imposed by the three interfacial tensions (solid/liquid (γ_{sl}), liquid/vapour (γ_{lv}) and solid/vapour (γ_{sv})) reach equilibrium. Young's equation describes this balance.

$$\mathrm{Cos}\,\theta = \frac{\gamma_{sv} - \gamma_{sl}}{\gamma_{lv}} \qquad \textbf{Equation 11}$$

There are two methods for measuring the contact angle: by sessile drop or captive bubble. The sessile drop is based on the profile analysis of a drop of a liquid placed on the surface of the solid, as showed in figure 21. In the captive bubble process, the gas bubble is placed on the material's surface that is immersed in a liquid, as illustrated in figure 21[117]. In both methods the contact angle is measured with a goniometer.

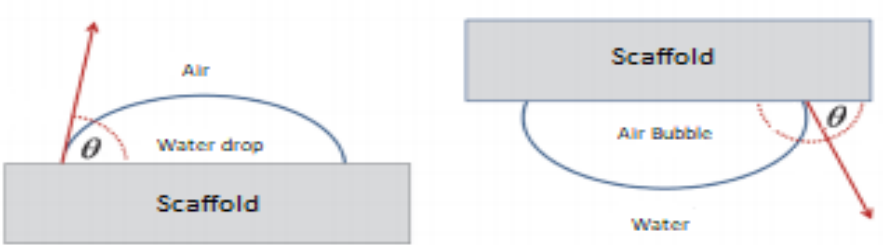

Figure 21 - Sessile drop (left image); Captive bubble (right image). Adapted 118

The wettability allows to determine whether an implant's surface is hydrophobic or hydrophilic. If the surface has a hydrophilic character, interactions with biological fluids and cells are favored. If hydrophobic, the absorbed proteins will be subject to conformational changes which will limit cell adhesion and cell function[119,120].

According to figure 22, the surface that has a high contact angle shows a hydrophobic behavior, since the surface is composed of non-polar groups that have a low affinity. However, if the surface is composed of polar groups, which allow a greater water adhesion, the contact angle is smaller, demonstrating a hydrophilic behaviour[121].

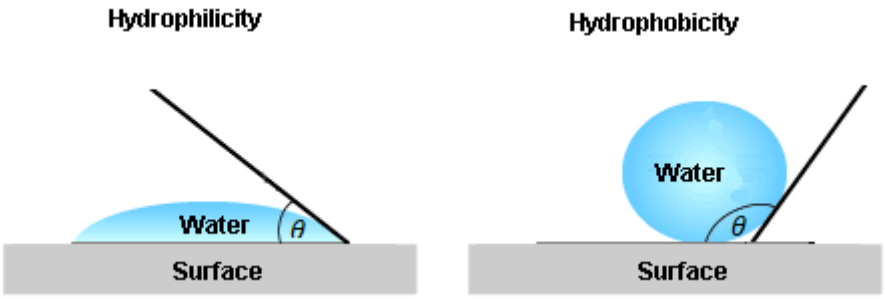

Figure 22 - The water contact angle (θ) on a hydrophilic surface and a hydrophobic surface. Adapted 122

Contact angle measurement can easily be influenced by chemical or mechanical heterogeneities that the substrate surface may contain. According to Ferguson & Jianmin Qu[123], if the obtained angle is lower than 90º, it indicates a solid surface with high wettability (hydrophilic), that is, the liquid is spread on the surface occurring its absorption. In the case of a complete or perfect absorption the θ equals zero. If the angle has a value higher than 90º, it indicates low wettability of the material (hydrophobic), evidencing the inability of the fluid to wet the surface.

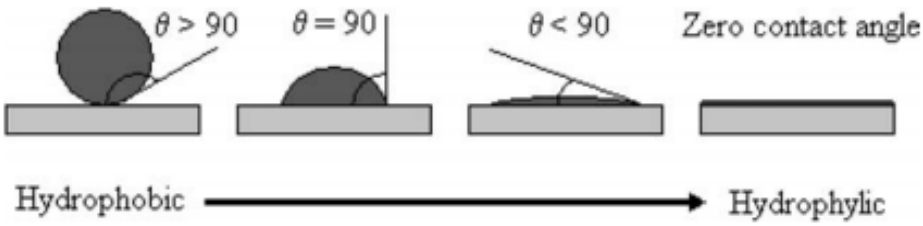

Figure 23 - Hydrophobic and hydrophilic water contact angle[123].

Experimental Procedure

In this work the captive bubble method was used to analyze the wettability of large diameter scaffold samples. Before contact angle measurements, all samples were dried. They were hydrated in distilled and deionized water for 10 minutes. The hydrated sample was individually fixed in a quartz test cell immersed in distilled and deionized water.

Using a micrometer syringe with an appropriate needle, air bubbles (3-4µl) were deposited on

the underside of the sample surface.

Figure 24 - Micrometer syringe with a needle inverted in the edge and the liquid cell.

Several images were obtained during a certain period of time in order to evaluate the contact angle evolution over time.

This angle was analyzed from the images acquired by a JAI CV-A50 camcorder, installed on a WildM3Z microscope and connected to a Data Translation DR3155 frame grabber, at room temperature. The apparatus is illustrated in figure 25. In each sample, of disk-like geometry, three air bubbles were made at different sites. Seventeen images were recorded for each air bubble over 1 minute.

Figure 25 – Goniometer: 1) Light source 2) Micrometer syringe 3) Liquid cell 4) Video camera.

The contact angles obtained in the images were analyzed by the Axisymmetric Drop Shape Analysis Profile (ADSA-P), which uses the Laplace capillarity equation (Equation 12)[122] to relate the surface tension of the liquid and the drop profile.

$$\Delta P = \gamma \left(\frac{1}{R_1} + \frac{1}{R_2}\right)$$ **Equation 12**

In this equation, ΔP represents the pressure difference at the liquid / vapor interface, R1 and R2 define the main curvature radii of the bubble, γ is the liquid surface tension[122].

2.4.5. Swelling

The developed scaffolds were subjected to swelling assays in order to be study the absorption behavior. The study of water absorption capacity is an important factor in determining the space occupied by the scaffold and the drug´s diffusion velocity.

Experimental procedure

These swelling tests were performed on large diameter scaffold samples, as shown in figure 26. These samples were duly weighed to obtain its dry weight. Subsequently they were immersed in PBS solution of pH 7.4 at room temperature.

Figure 26 - Scaffold dried used in swelling assay.

At each time set, until the values stabilized and for reproducibility purposes, each sample was withdrawn from the PBS and the excess solution on the scaffold's surface was removed with the aid of a filter paper. Subsequently the sample was weighed, obtaining the wf value. The procedure was done in triplicate and ended when the weights were constant over time.
The swelling was determined based on the following equation:

$$\text{Swelling (\%)} = \frac{Wf - Wo}{Wo} \text{ x } 100$$ **Equation 13**

Where Wf is the weight measured at a certain time and $W0$ is the dried scaffold weight[124].

2.4.6. FTIR - Fourier-transform Infrared Spectroscopy

Infrared spectroscopy (IR) is a rather useful technique to identify and analyze chemical bonds and functional groups, in a sample. It can be applied to a variety of samples either organic or inorganic. In this work, this technique was used to observe the connection types existing in scaffolds, as well as try to understand if and how the drug is bonded and the effect of radiation on those bonds.

Chemical functional groups vibrate at characteristic frequencies of radiation, thus IR spectra are obtained by detecting changes in absorption (or transmittance) intensity as a function of frequency[125].

Vibration frequencies of the molecular bonds are specific for the bonds between the atoms that constitute them, undergoing slight changes conditioned by the molecular environment around that bond. It is the energy absorption at a specific wavelength that allows the identification of the chemical bond present in the molecule and, through the obtained information crossing with known reference values, to identify the molecule[107].
In the FTIR the light source provides infrared radiation across the entire wavelength range. This light passes through an interferometer, at which output the two formed beams are combined: one fixed optical beam and the other with a wavelengths combination that vary over time. However, the required information for sample analysis is the spectrum for the entire wavelength range, in which each wavelength corresponds to a certain absorption. Thus, the intensity of light reaching the detector is subjected to a Fourier transform to obtain the absorbance at each wavelength[107,125]. This technique allows to obtain information as if the sample were illuminated by monochromatic light, although it is always illuminated by polychromatic light.

Experimental Procedure

FTIR was performed at FFUL, with the IRAffinity-1 Shimadzu spectrometer equipment, figure 27. The used software in data collection, processing and results generation was the LabSolutions IR software.

Figure 27 - IRAffinity-1 Shimadzu equipment.

The preparation of solid state samples had to be carried out in potassium bromide tablets (KBr). The sample chips and KBr were prepared in a ratio of approximately 2mg powder sample to 180mg of KBr, figure 28. The following samples were analysed:

- Sample – Without DF and not irradiated;
- Sample – Without DF and irradiated at 15kGy;
- Sample – Without DF and irradiated at 25kGy;
- Sample – With DF and not irradiated;
- Sample – With DF and irradiated at 15kGy;
- Sample – With DF and irradiated at 25kGy;
- Sample – DF;
- Sample – CS;
- Sample – CaP.

Standard samples of DF, CS and CaPs were prepared in order to be possible to identify its presence in the FTIR spectra of the scaffolds. The scaffolds used in this assay were those of large diameter.

After mixing and grinding in a mortar, the blends were transferred into a metallic mold and pressed.

The spectrum was obtained in transmittance in a scan of 4000 to 300 cm^{-1}.

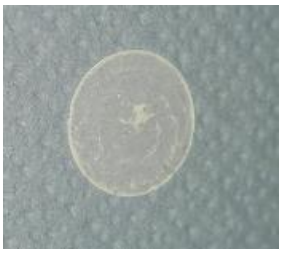

Figure 28 – Example of KBr tablet with scaffold powder blend.

2.5. Biological Analysis

2.5.1. *In Vitro* cytotoxicity test

Cytotoxic effect's detection is the first test to evaluate the biocompatibility of any material for use in medical devices, through the study of the *in vitro* biological response, with mammal's cells. After proven its non-cytotoxicity the work can be continued by conducting *in vivo* tests[126].
Cytotoxicity studies are mandatory to prove a good performance and the safety of the biomaterial. Although biocompatibility and the consequent non cytotoxic effect of calcium is largely documented, along with chitosan's biocompatibility and the good *in vitro* performance of both components, the specificity of the scaffolds and the DF concentration, force that cytotoxicity tests are conducted to prove biocompatibility[2].
Toxicity promotes disturbances and changes in cellular homeostasis, promoting negative effects on cell functions. This phenomenon can be evaluated through proliferation and cell death and reduction of cell adhesion, reduced biosynthetic activity and altered cellular morphology[126].
The aim of this work is to verify the scaffolds cytotoxicity effects in a human osteoblast-like cell line (MG63 cells) and the mouse fibroblast cell line (L929). For this sterile scaffolds samples with and without DF will be used.
According to the International Standard ISO 10993-5, we can determine the biological response of mammalian cells *in vitro* using appropriate biological parameters. For this, the standard provides three categories of tests (extract test, tests by direct contact and tests by indirect contact)[127].
In this work, only the tests by direct contact were used, because it allows qualitative and quantitative assessment of cytotoxicity.

The MTT test is a quantitative colorimetric method used to evaluate the metabolic activity of cells. In viable cells, yellow water-soluble MTT *3-(4,5-dimethylthiazol-2-yl)-2-5 diphenyltetrazoliumbromid)* is reduced to a dark purple colored formazan precipitate.
The MTT-formazan production is then proportional to the number of metabolically viable cells[128].

Experimental Procedure

The evaluation of the cytotoxic response was performed on the following scaffolds (triplicates), composed of CaP granules suspended in a polymer matrix based on CS, and:

- Without DF and not irradiated;

- Without DF and irradiated at 15kGy;
- Without DF and irradiated at 25kGy;
- With DF and not irradiated;
- With DF and irradiated at 15kGy;
- With DF and irradiated at 25kGy.

Cytotoxic tests were performed according to International Standard ISO 10993-5[127] and Matos et al. 2014[129], at FFUL.

The method is initiated with cell cultures that were removed from culture flasks by enzymatic digestion (trypsin/EDTA). The cells are then resuspended in culture medium (RPMI 1640 culture medium supplemented with 10% Fetal bovine serum (FBS), 100 units of penicillin G (sodium salt) and 100µg of streptomycin sulfate and 2mM L-glutamine) and the cell suspension was adjusted at a density of $1x10^5$ cells/mL, 500 µL of this suspension was used to inoculate a 24 well tissue culture plates.

To perform the cytotoxicity tests, according to direct-contact tests, L929 (Mouse fibroblast cell line, ATCC® CCL-1™) and MG63 cells (MG63 a human osteoblast-like cell line, ATCC CRL-1427™) were seeded ($1.5x10^5$cells/well) in 24-well plates (Greiner, Germany) and cultured for 24h (5 % CO_2, 37 °C, >90% humidity) in order to form a subconfluency monolayer. After the incubation time, the culture medium was replaced by fresh culture medium. In each well were carefully placed, on the top of the cell monolayer, individual specimens of the tests samples on the center of the cell layer, covering approximately one tenth of the cell layer surface in both cell lines, and a twentieth with L929 cells.

Subsequently, two set of control samples were created: positive control and negative control. For these samples two different actions were performed:

- To the negative control was added culture medium.
- To the positive control, medium with 1mg/mL of sodium dodecyl sulfate (SDS) was added. This material promotes a cytotoxic response on the cell cultures.

The well plates were again incubated in the same conditions, for the same period of time.

After 24 h treatment, the culture medium from the plates was removed and replaced with medium containing 0.5mg/mL of MTT and the plates were further incubated for 3h in the incubator at 37 °C. Then the MTT solution was discharged and 500 µL of DMSO was added in each well. 200 µL from each sample were transferred to a 96 well plate and the absorbance at 570 nm wavelength was measured in a microplate reader (FLUOstar Omega, BMG LABTECH, Germany).

The formazan formation was determined for each well and compared to that determined in control cultures. For each treatment the percentage of cell viability was calculated.

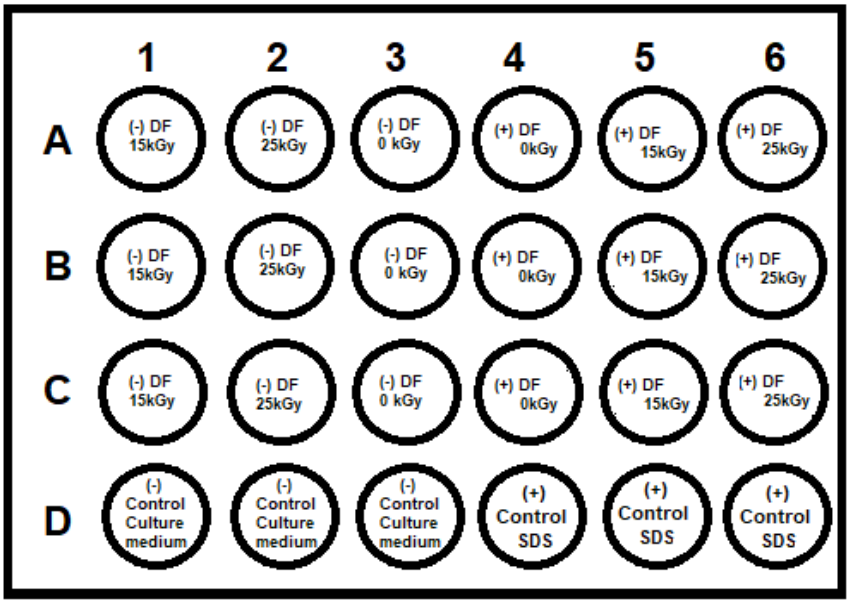

Figure 29 – 24-well plate real and layout for the MTT cytotoxicity test, accounting for the 6 different samples of scaffolds and respective positive and negative controls.

A decrease in the number of viable cells as a result of a cytotoxic response results in a decrease of the metabolic activity of the samples. This decrease directly correlates to the amount of blue-violet formazan formed that is monitored density measurements at 570nm (OD_{570nm}). Cell viability (%) of the different conditions tested was calculated using as reference the negative control and the following equation[127]:

$$Cell\ Viability(\%) = \frac{100\ x\ OD_{570nm\ samples}}{OD_{570nm\ control}} \qquad \textbf{Equation 15}$$

Where, $OD_{570nm\ samples}$ is the mean value of the optical density for the 100% extract from the test sample or from the positive control and $OD_{570nm\ control}$ is the mean value of the optical density for the negative control.

According to the ISO standards, if the viability is reduced to values lower than 70% of the ones obtained for the negative control, the sample tested presents a cytotoxic potential[127].

Statistical analysis

All data sets are presented as mean ± SD (result of at least three determinations) and were examined by one-way analysis of variance (ANOVA) for cytotoxic assay to other methods, using GraphPad PRISM software (version 6, GraphPad Software Inc.). The level of statistical difference was defined at a $p < 0.05$ level.

3. RESULTS AND DISCUSSION

3.1. Diclofenac Release System on CaPs and CS Scaffolds

As noted in section 2.2., scaffolds were prepared using different component adding sequences with the main aim of introducing the anti-inflammatory drug without its emulsion.
After several attempts, the chosen mixture was the one that allowed to dissolve all DF in 1/3 of water and lactic acid in 2/3 of water. Since DF contains N, O, Cl and Na heteroatoms, it causes high polarizability of the molecule, and thus there are specific interactions with solvents that subsequently strongly affect the drug's solubility. Due to the presence of the NH group, that can act either as the proton donor or proton acceptor toward the solvents, and the presence of the carboxylic group, the drug possesses a Lewis acid-base character[130]. The solubility of the drug strongly depends on the solvent used and, thus, on the intermolecular forces between sodium diclofenac and the solvent. The sodium presence in sodium diclofenac reduces the Lewis-acid properties of the drug[130].

For the scaffolds production it was found that the mixture of substances referred above was the one with the highest homogeneity. After mixing all components, lyophilization was used in order to obtain a spongy structure that was easy for medical application and did not alter DF after exposure to gamma radiation.
The mold used in the freeze-drying process allowed the cylinders formation, which needed to be cut after the process. In figure 30, a SEM image of the lyophilized scaffold can be observed.

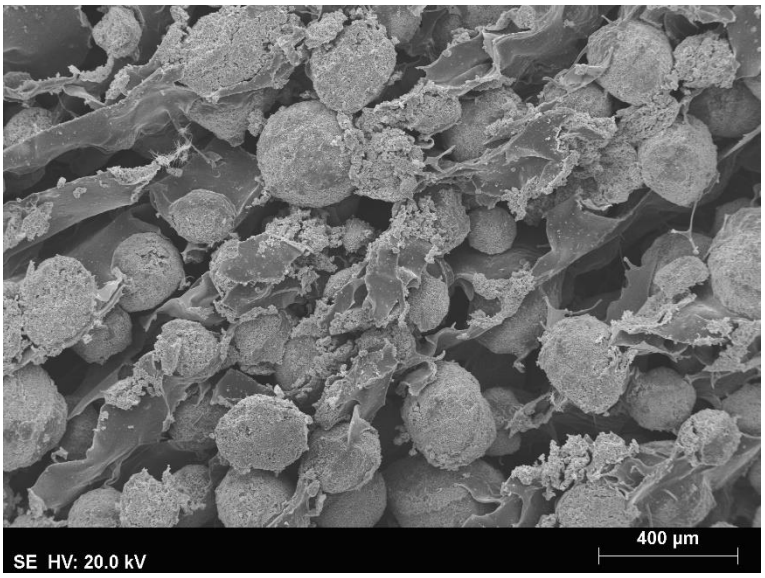

Figure 30 - SEM image of the lyophilized scaffold, obtained from the dissolution of DF in 1/3 of water and lactic acid in 2/3 of water. Resolution of 20.0kV and magnification of 60x.

The porosity of the scaffold (microporosity) allows the drug's inclusion in the material and promotes better proliferation, diffusion and cell adhesion in the scaffold, causing subsequent growth of new tissue. Microporosity also has a great influence on the material's degradation rate, which is an important parameter in *in vivo* regeneration[131]. Although the presence of high porosity in the scaffold is biologically beneficial, it impairs the mechanical behavior of the structure.

Through SEM images with several magnifications, it was possible to observe that both the scaffolds and the CaPs granules have porosity.

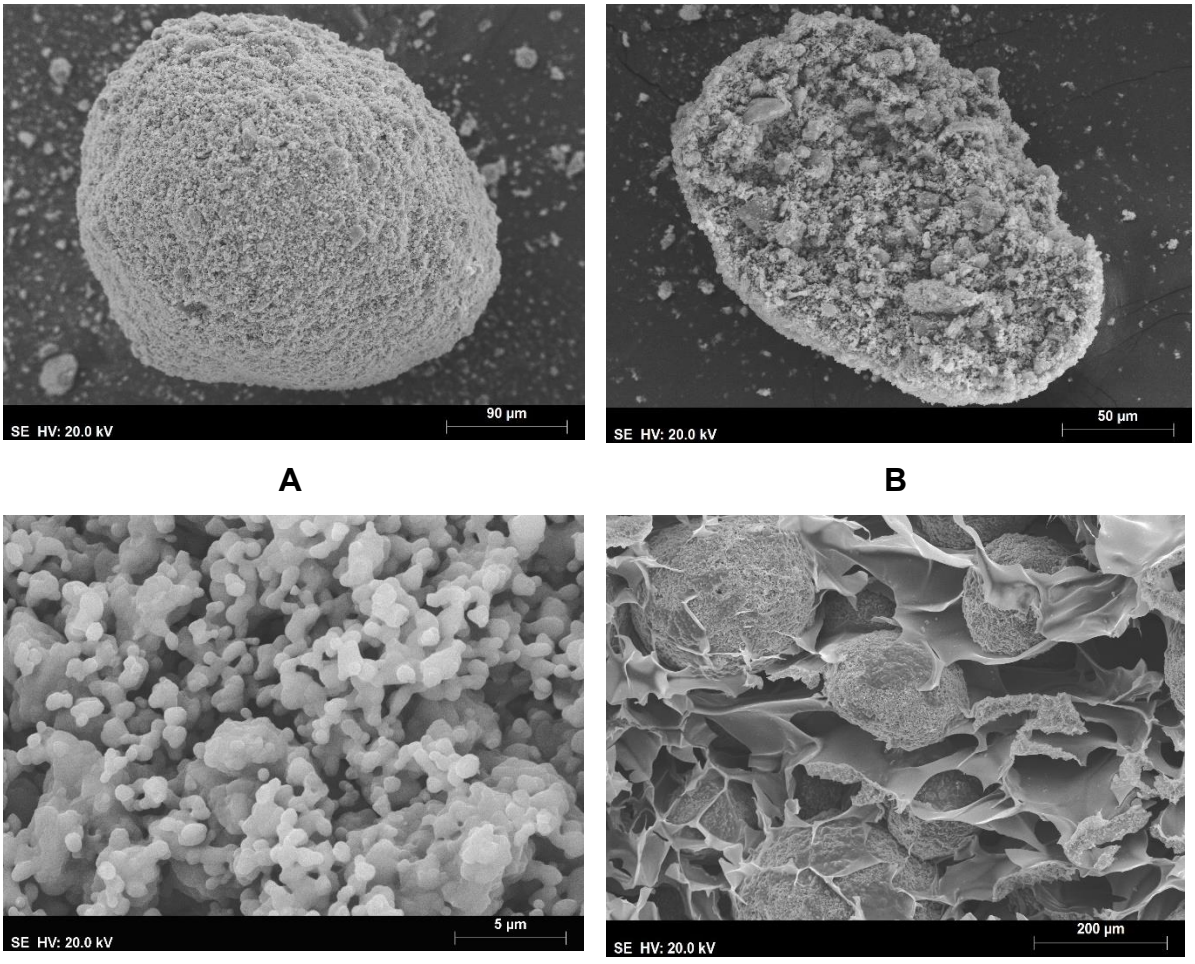

Figure 31 – A – CaPs granule exterior; B,C-CaPs granule interior with different amplifications; D – scaffold's porosity.

It can be verified that the pore size values inside the CaPs granules is less that 5µm, being smaller than 200µm in the scaffold.

Release Profile

According to a leaflet pill where the active substance is DF, the drug's dose for inflammatory treatments should be 100-150mg per day given in 2-3 doses[132]. However, since this work's aim is to place DF directly at the inflammation site, and based on the information from Sidney et al.[133], in which it is reported that scaffolds loaded with 300-650µg of DF demonstrate good results in terms of cell viability, calculations were made so that the amount of drug incorporated into the 2cm length and 3mm diameter scaffolds evaluated in the release assays was approximately 500µg.

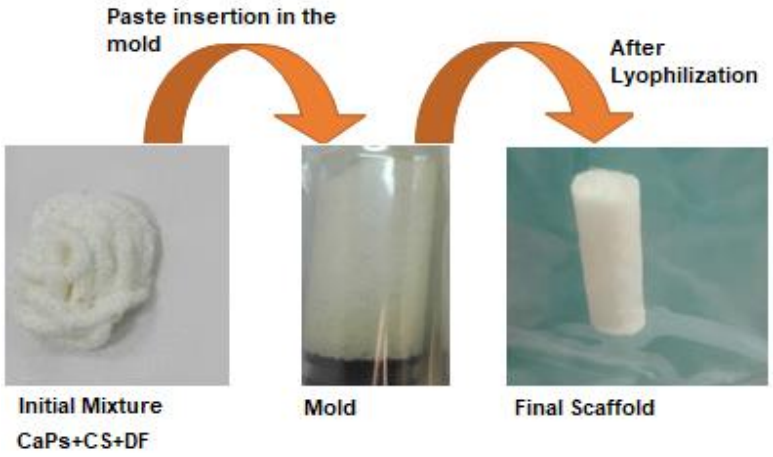

This study allowed to evaluate the sterilization effect on DF release. Figure 32 shows the release profiles of DF scaffolds under different conditions: unsterilized and sterilized by gamma radiation at 15kGy and 25kGy.

The graphical representations were made considering the ratio between the mass of accumulated released diclofenac and the sample's mass, as a function of time and in terms of the released diclofenac percentage. The profile relative to the scaffolds without DF represents a blank. It was studied in order to verify if there was any matrix component that was detected by spectrophotometry in the same DF wavelength range. From the graph of Figure 32 and from UV-Vis spectroscopy it can be concluded that there is no other scaffold compound to be released at 275nm

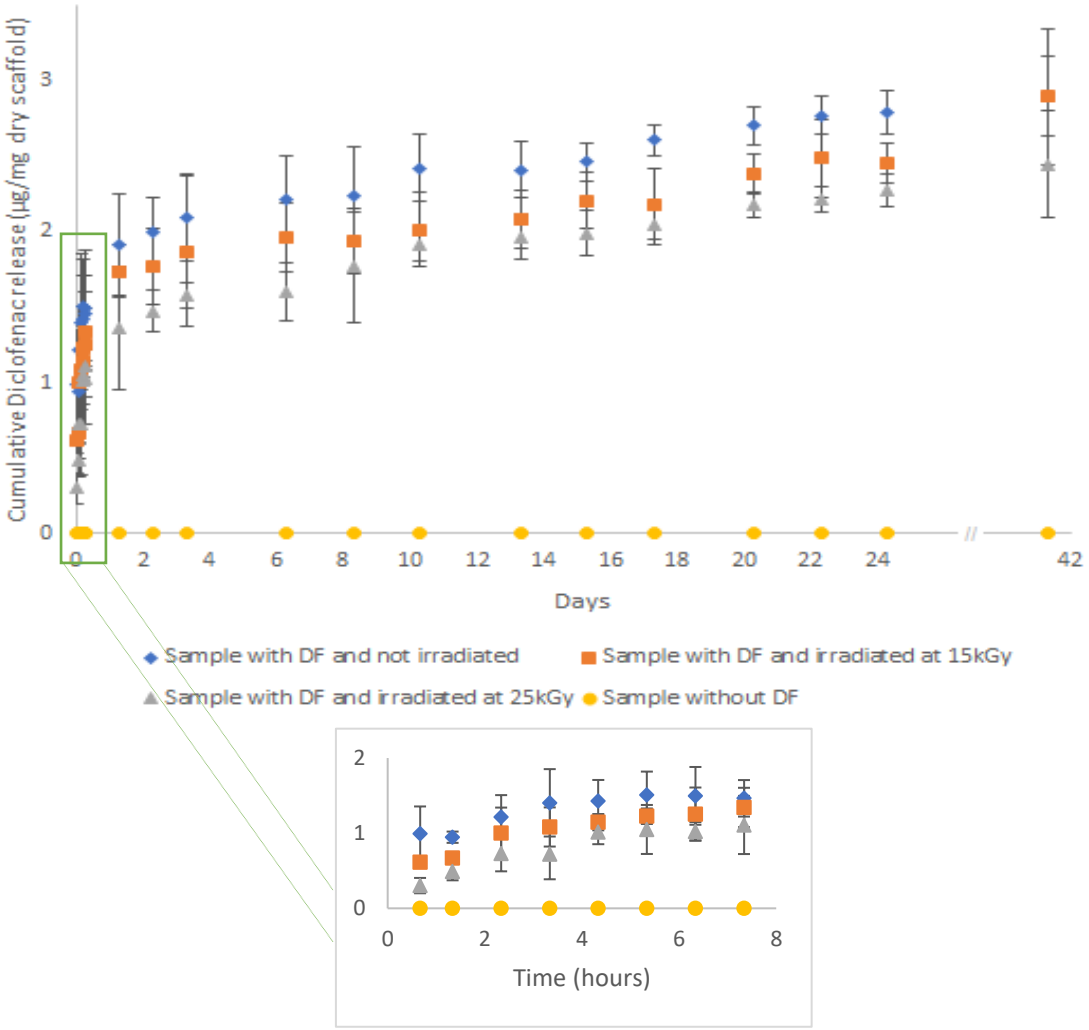

Figure 32 - DF release profiles in terms of released mass accumulated by sample mass. Error bars: standard deviation (*n*=5). The smaller graph is an enlargement of the larger graph of the first 7h of release.

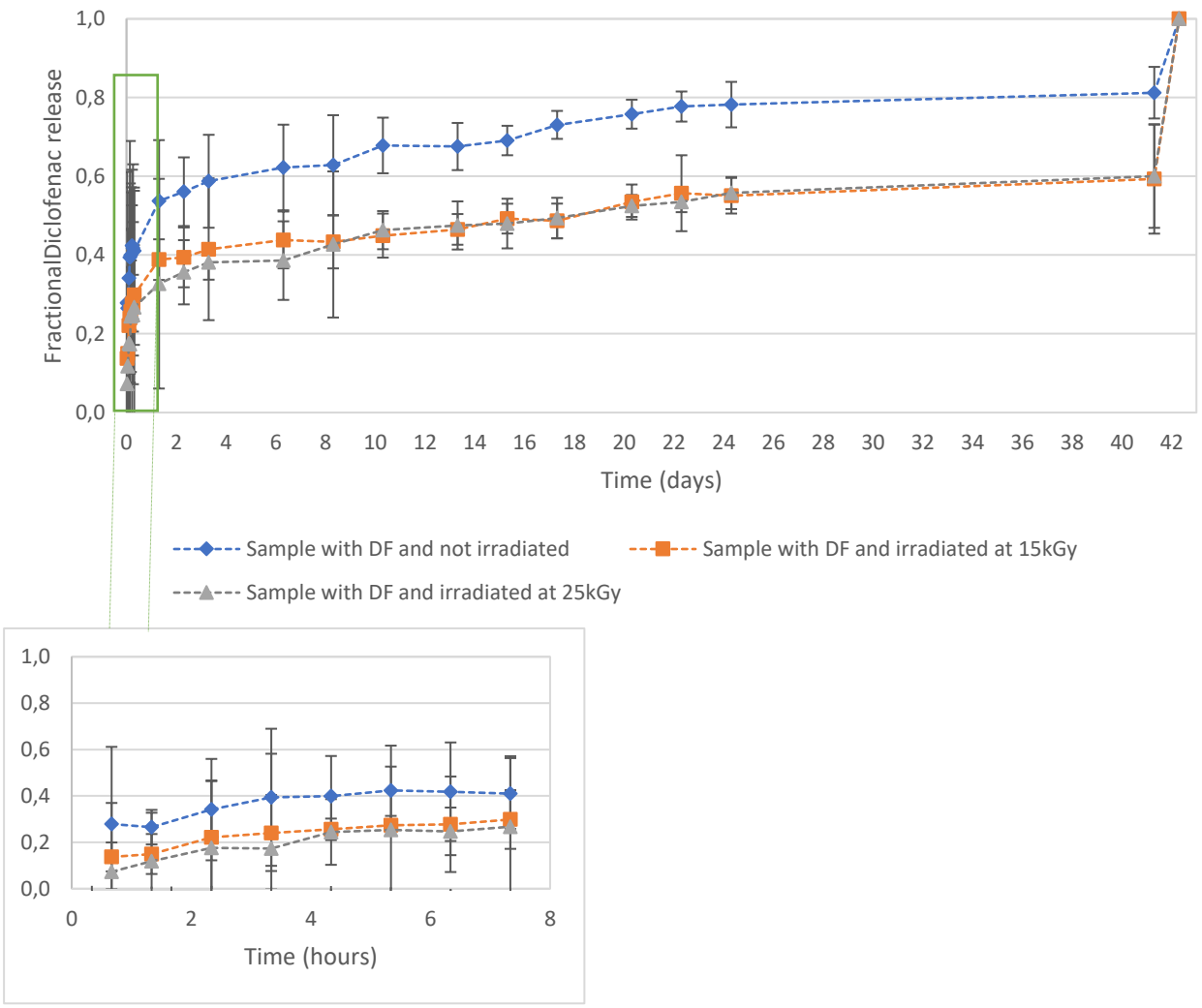

Figure 33 – Fraction of released DF in relation to that introduced in scaffold. Error bars: standard deviation (*n*=5). The smaller graph is an enlargement of the larger graph for the first 7h of release. The represented lines are only intended to facilitate the profiles identification.

Generally, the drug release profile is characterized by a drug burst in the first hours, followed by a near zero order release. The scaffolds irradiated at 25kGy present a release profile below the scaffolds irradiated at 15kGy and non-irradiated, which indicate lower amounts of DF are being released (figure 32). In fact when the fractional release profiles of the 3 scaffolds are compared (figure 33) it is possible to observe that all present similar release kinetics, but the non-irradiated scaffold releases higher amounts (mass) of diclofenac for the same time period of the other scaffolds (figure 33).

The non-irradiated samples profile indicate that at the end of 3 days of release, approximately 60% of the total incorporated drug has been released. At the same time point, irradiated samples released 40% of the total diclofenac present on the scaffold.

Although all scaffolds were cut and weighed to ensure the presence of 500µg of drug, the sterilization process may have led interactions in the chitosan matrix, which allowed some slow release of the irradiated samples. In all cases the initial DF release burst is well evidenced.
After 41 days of release experiments, the non-irradiated scaffolds were found to have released 2.79µg/mg of dry scaffold, in a total of approximately 400µg DF. The 15kGy irradiated scaffolds released 2.46µg/mg of dry scaffold, in a total approximately 370µg DF, and the 25kGy irradiated scaffolds released 2.27µg/mg of dry scaffold, in total approximately 330µg DF.
At 41 days of release the drug profiles had reach an equilibrium, with no drug being released. Nonetheless, and as referred above, 500µg of drug were expected to be present in each sample. To verify the presence of non-released DF inside the scaffolds, the samples were destroyed as described in section 2.3.1..
After analysing the absorbance readings, it was confirmed that there was approximately 20% of DF trapped the non-irradiated scaffolds and 40% in the irradiated ones. With these results, it was verified that although all samples were cut with approximately the same sizes and weights, the amount of drug in the samples varies between 590µg and 600µg.

Kinetic Release Analysis

As referred in section 1.10.2, the drug release kinetics were study through the application of empirical models. The aim of this study was to verify which model best described the DF release curves obtained for the 3 different scaffolds and, therefore, determined the mechanism that regulated DF release.

The selection of the best model was achieved by evaluation of the correlation coefficient (R^2), in which the model with higher R^2 was the model that better characterized the release mechanism.

For the studied scaffolds (with DF non-irradiated, irradiated either with 15kGy or 25kGy) the empirical models used were: zero-order, first order, Higuchi, Hixson-Crowell and Korsmeyer-Peppas.

In the following table, the R^2 values are presented for each type of scaffold and the five applied models.

Table 4 - Determination coefficient (R^2) obtained through the application of the mathematical models to the DF release profiles of the different prepared samples.

Samples	R^2 value for the different models				
	Zero Order	First Order	Higuchi	Hixson-Crowell	Korsmeyer-Peppas
With DF and not irradiated	0,723	0,610	0,867	0,723	**0,932**
With DF and irradiated at 15kGy	0,708	0,549	0,838	0,708	**0,916**
With DF and irradiated at 25kGy	0,731	0,509	0,788	0,731	**0,837**

Based on R^2 values listed in table 4 and taking into consideration the assumptions for each model, the Korsmeye-Peppas model is the best to describe the mechanism of release, for all scaffolds (with DF non-irradiated, irradiated either with 15kGy and 25kGy) since it presents the higher values of R^2.

It is possible to obtain the model related parameters through the graphical representation and the linear and non-linear fittings. For the release profiles analyzed, the *n* values for the Korsmeye-Peppas model were obtain considering the first 60% of the release profile. As described in the literature, the *n* value can vary from 0,43 to 1 accordingly to the system geometry and with the release mechanisms present. The cylindric geometry of the scaffolds was, therefore, considered. In the following table, the obtained *n* values are presented.

Table 5 - Values of the parameter n obtained from the Korsmeyer-Peppas model.

Samples	Release mechanism exponent - *n*
With DF and not irradiated	0,17
With DF and irradiated at 15kGy	0,23
With DF and irradiated at 25kGy	0,30

Since n < 0,45, the diffusion rate is lower than the process of polymer matrix relaxation (case I transport).

3.2. Scaffolds and Components Characterization Analysis

3.2.1. XRD Analysis

The XRD technique was used.to analyze the purity of the Hap and β-TCP crystalline phases. Through the diffractogram obtained from the biphasic granules (figure 34), it was possible to identify the Hap and the β-TCP phases and also the absence of other crystallographic phases. The hydroxyapatite and beta-tricalcium phosphate characteristic peaks were identified according to ISO 13779-3.

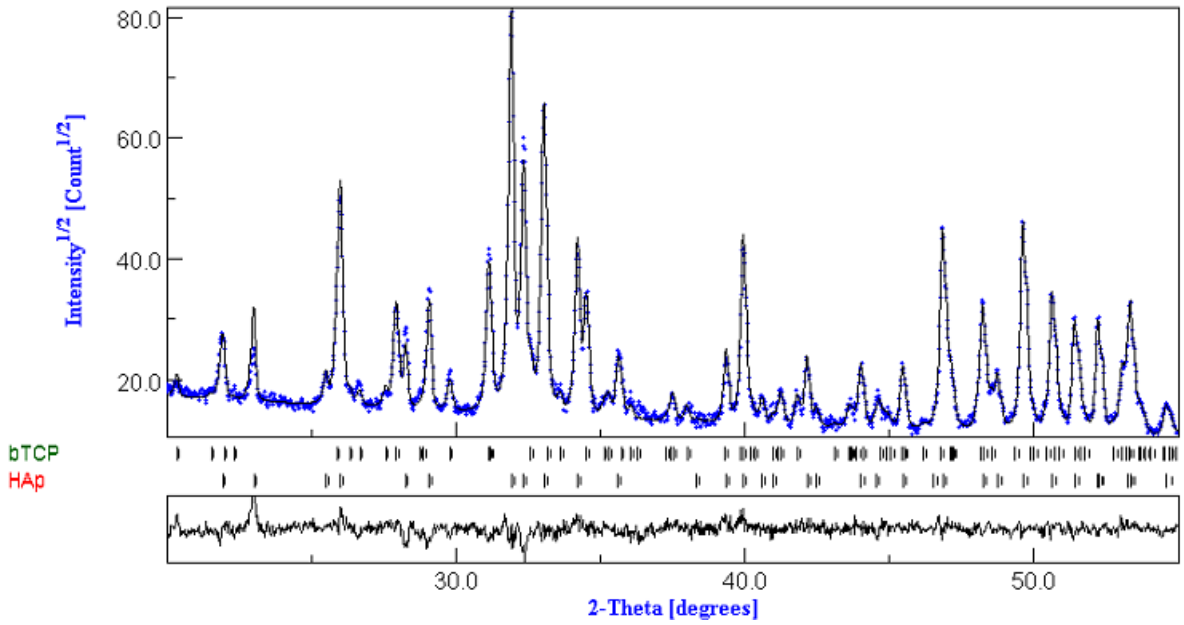

Figure 34 - X-ray diffractogram representative of biphasic ceramic granules used in the manufacturing process of scaffolds.

Using the respective calibration curve, the presence of 77,02% Hap and 22.98% β-TCP was verified, confirming the Hap / β-TCP ratio of 75/25% (±5%).

The calibration curve was obtained through the preparation of different Hap and β-TCP samples of high purity, with progressive addition of β-TCP mass. The diffractograms were analyzed in MAUD. Patterns confirmed the Hap formation with the most intense XRD peak in the diffraction plane of 200 and for the β-TCP phase in the diffraction plane of 296.

3.2.2. Particle Size Distributions

The particle size and size distribution knowledge are important in the scaffolds production process. These parameters influence the mechanical resistance, density and occupied volume in a significant way.

The scaffold's biphasic granules particle size analysis results (figure 35), showed a ceramic particle size distribution as a sample volume function of d(10) equal to 187µm, d(50) equal to 257µm and d(90) equal to 294µm.

.

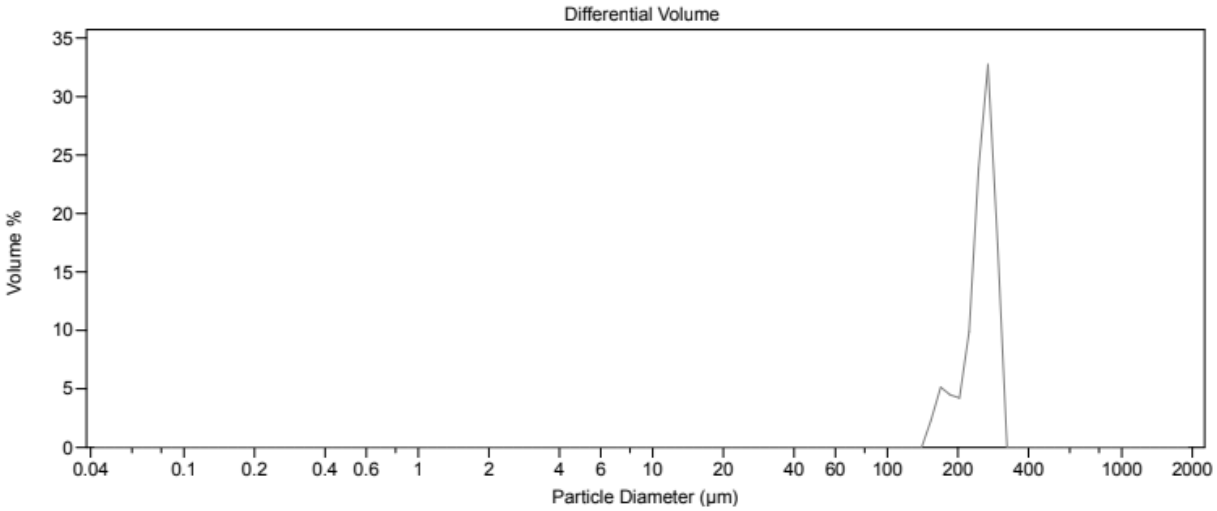

Figure 35 - Distribution of the particle size of the biphasic granules used in the production of scaffolds in function of the sample volume through laser diffraction.

In this way, it was verified that the particle size used in the scaffolds varies between 125 - 355µm and does not present smaller size granules. Thus, as described in the literature, acute inflammation processes due to granules with particle sizes smaller than 20µm, which in a certain way promote cellular damage through the membranes rupture mechanism, are avoided.

This was also verified with optical microscopy, in which was possible to visualize the size of granules incorporated in the epoxy support.

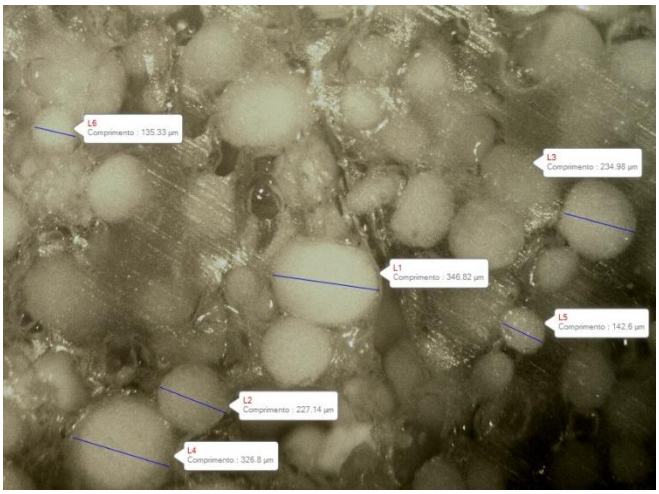

Figure 36 – Epoxy mold with spherical CaPs granules used in scaffolds.

3.2.3. Wettability

Samples hydrophilicity was evaluated by the contact angle with water, using the captive bubble method described previously.

The aim of this technique was to evaluate the changes in surfaces of the various samples subjected to different gamma radiations and with the drug's addition, in order to understand if those changes would compromise biological interactions.

The following bar graph shows the contact angles mean values obtained in the various sample types: irradiated and non-irradiated samples with diclofenac and irradiated and non-irradiated samples without diclofenac.

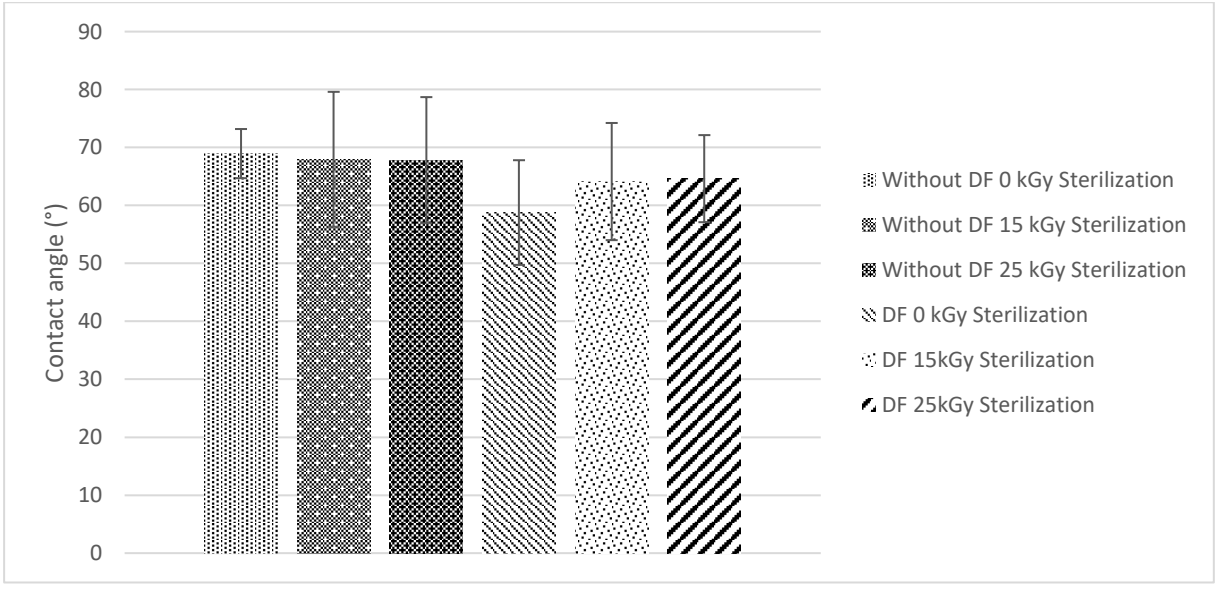

Figure 37 - Water contact angle of samples with and without diclofenac and non-sterilized and sterilized.

According to the obtained values, it is possible to verify that the contact angles are slightly lower in the samples containing diclofenac.

In general, results indicate that both the sterilized and non-sterilized samples with and without drug have contact angles with values lower than 90º, as can be inferred in figure 38, thus presenting a hydrophilic surface, which is an indicator of good biological interactions.

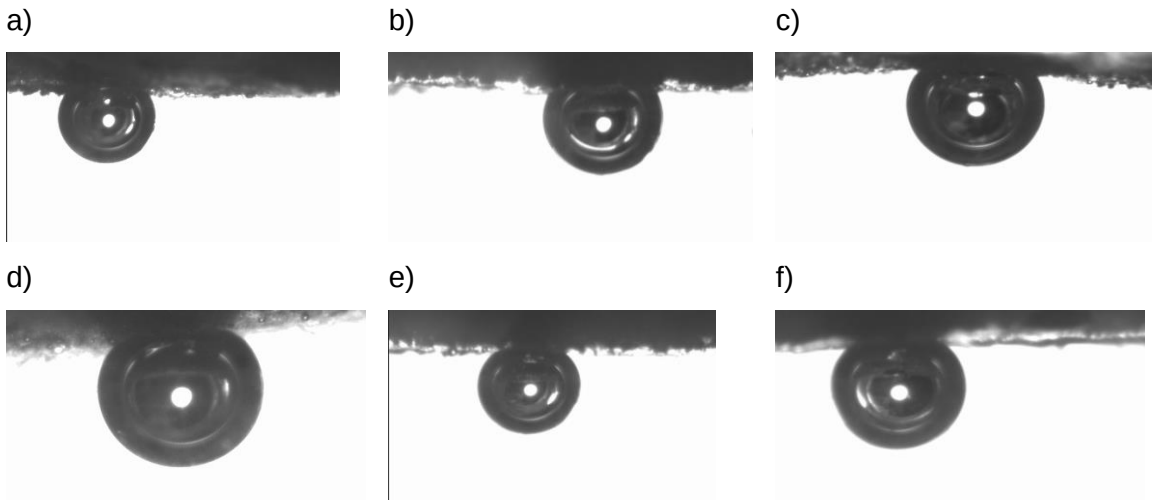

Figure 38 - An air bubble sitting beneath a surface of specimens: a) non-sterilized without DF, b) sterilized at 15kGy without DF, c) sterilized at 25kGy without DF, d) non-sterilized with DF, e) sterilized at 15kGy with DF, f) sterilized at 25kGy with DF.

3.2.4. Swelling

The absorption capacity of the medium is an important factor that must be taken into account when developing a composite for bone regeneration, since these materials play decisive roles in the osteoblasts adhesion. For this purpose, it is necessary to proceed with the scaffolds' swelling coefficients determination.

The swelling is directly related to the hydrophilicity of the polymer, being possible to determine if the scaffolds polymer matrix is of hydrophilic or hydrophobic character.

In this work, the swelling was evaluated during 57 hours, through the equation 13 mentioned in section 2.4.5., for the following samples:

- without DF, non-irradiated;
- irradiated at 15kGy;
- irradiated at 25kGy.

Triplicate assays were performed for each type of scaffold, and the vertical bars in the graph of figure 39 indicate the standard deviation between them.

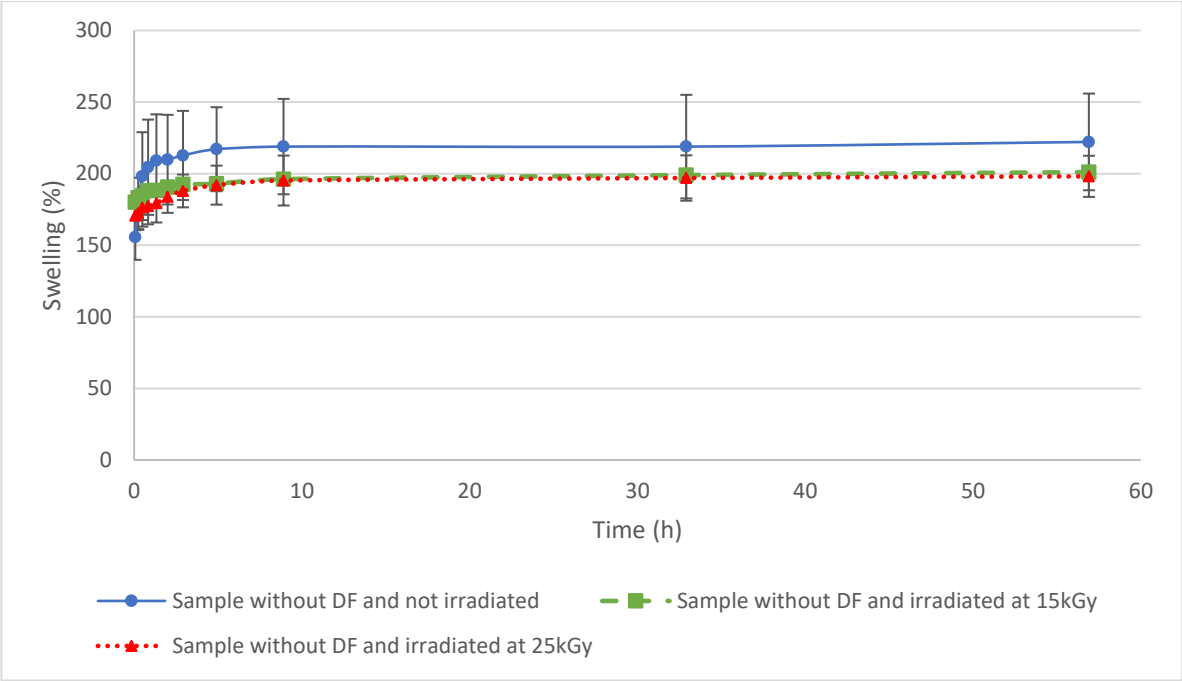

Figure 39 - Swelling profile as a function of time.

A high swelling capacity of the scaffold is proof that the scaffold material could absorb large volume of water than its original weight.

From the graph's observation it is possible to verify that all types of scaffolds have high absorption values. In this way, swelling promotes the increase of scaffolds' pore size, causing the internal surface area of the structure to increase as well, facilitating cells infiltration and adhesion, as well as the occurrence of ionic exchanges. However, the structure's mechanical strength weakens[134].

The swelling curves evolution shows that the absorption capacity increases over time, until the equilibrium is reached. It reaches equilibrium 5 hours after the test's beginning, and at this point the swelling rate is around 192% for scaffolds irradiated at 25kGy, 211% for scaffolds irradiated at 15kGy and 217% for the non-irradiated scaffolds.

Comparing the three curves, it is possible to observe that the largest amount of liquid retained in the pores was reached after 2 hours, indicating a reduction of the hydrophilic groups available to interact with the water molecules, after which a gradual evolution occurs until the equilibrium is reached. According to the obtained values, the absorption rate stabilization was reached approximately 5 hours after the test's beginning.

All three scaffolds have similar high absorption capacity percentage, resulting in an identical drug release profile between all these scaffolds.

3.2.5. Scanning Electron Microscopy / Energy Dispersive X-Ray Spectroscopy

Calcium phosphates granules surfaces and the gamma radiation sterilized scaffolds were observed and analysed by SEM. Figure 39 shows surfaces of the scaffolds which contained DF embedded in the matrix, subjected to different radiations.

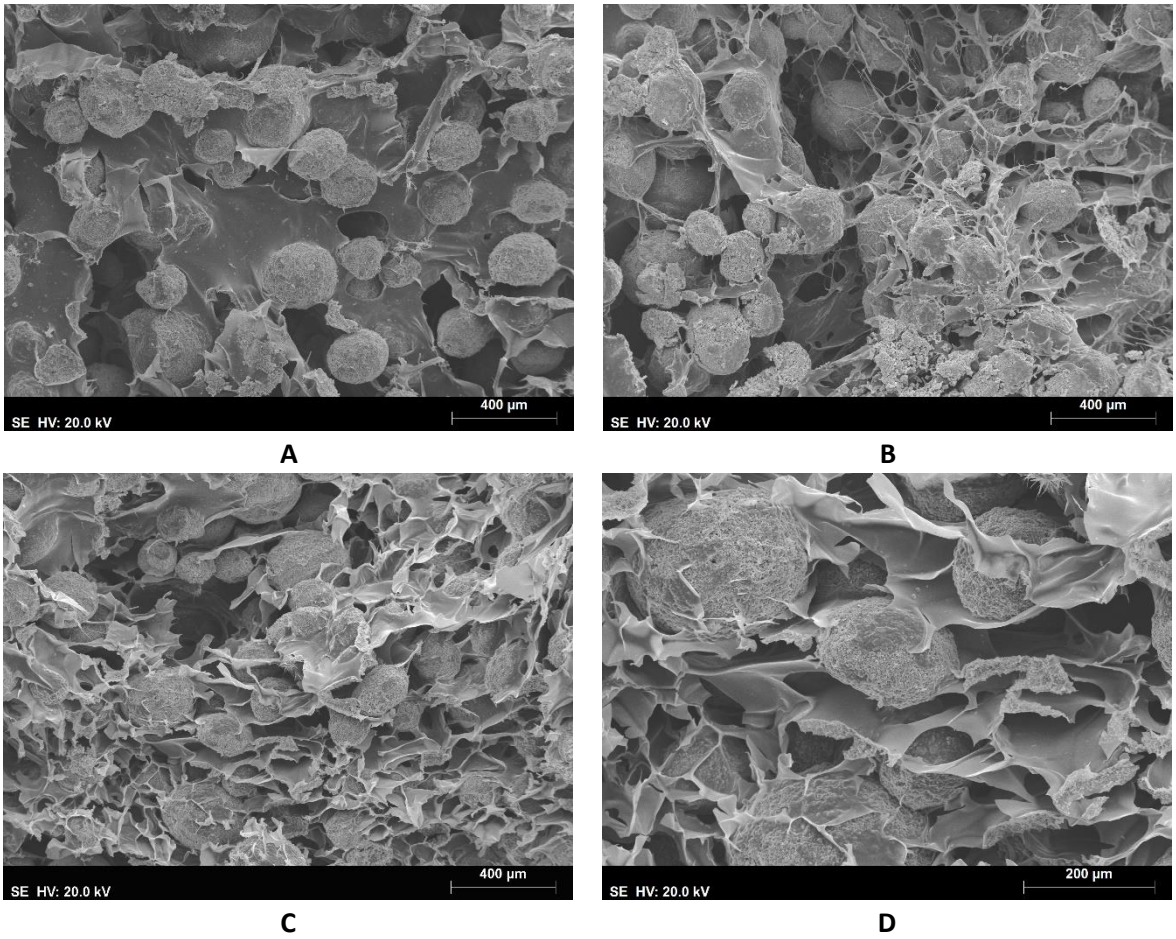

Figure 40 - SEM images from the scaffold surface. A) non-irradiated (bar indicates 400µm); B) irradiated at 15kGy (bar indicates 400µm); C) irradiated at 25kGy (bar indicates 400µm); D) 25kGy irradiated scaffold amplification (bar indicates 200µm);

SEM images show that there are differences between surfaces. In the non-irradiated scaffold, the CS matrix appears as a binder of the CaPs granules, whereas in the B image the polymer matrix, irradiated at 15kGy, appears to be fibrous. In the C image, where the scaffold was subjected to 25kGy of gamma radiation, the matrix is more reticulated.

Comparing images A and B, it is possible to visualize larger pores and at the same time lower porosity in the non-irradiated scaffold, while in the 25kGy irradiated sample a larger number of pores of smaller dimensions, with less than 200µm can be observed image D, that corresponds to the enlargement of image C.

Regarding the drug's distribution in the scaffolds it was not possible to visualize by SEM its presence. However, by EDS it was possible to analyse the scaffolds chemical composition and verify the presence of CaPs elements.

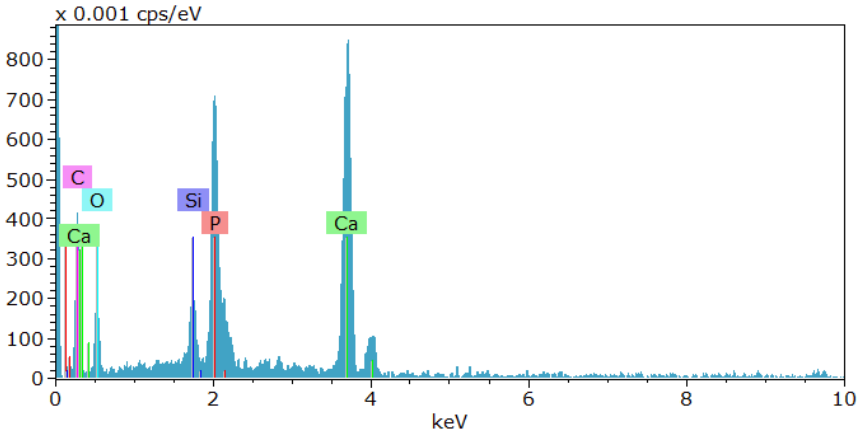

Figure 41 - Distribution chart of the chemical elements present in the analysed scaffold.

In figure 41 it is possible to visualize the characteristic elements from the scaffolds inorganic phase (calcium phosphates) and from the organic one (chitosan). However, the DF characteristic elements are not present.

3.2.6. FTIR

FTIR tests were performed to chemically characterize the freeze-dried scaffolds. The purpose of this analysis was to confirm the scaffold's composition, verify the DF presence in the scaffolds and understand if gamma radiation had any influence.

Gamma radiation is the most widely used sterilization method in medical devices. However, it is a non-innocuous process promoting changes in chemical structure and sometimes in mechanical properties as well. The spectra of this study are shown in the following figures.

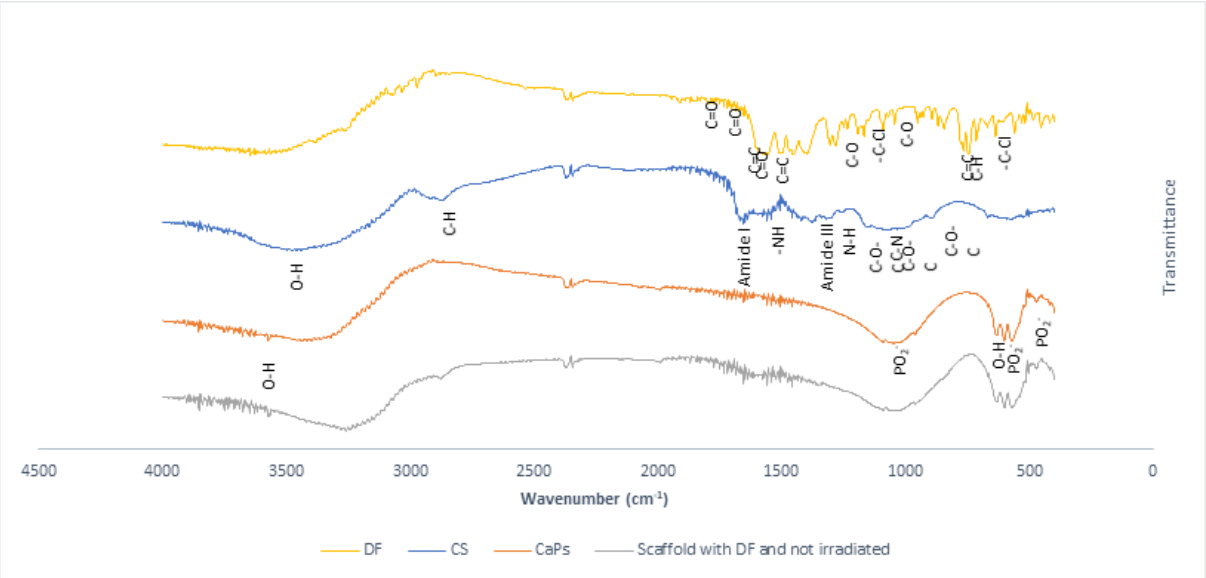

Figure 42 – Comparation between raw material with scaffold, with DF and not irradiated.

The IR spectrum of DF showed characteristic peaks at 1167 and 682cm^{-1} for aromatic -C-Cl. The stretches between 800 and 600cm^{-1} also support the presence of -C-Cl group. The strong peaks in the region of 1600–1700–1800cm^{-1} indicate the presence of -C=O. Moreover, the presence of peaks in the region of 1250, 1283, and 1044cm^{-1} confirms the -C-O- group. The peaks at 1603, 1507, and 869 – 716cm^{-1} confirm the presence of an aromatic ring[135].

The IR spectrum of CS showed that the band between 3400-3500cm^{-1} corresponds to the elongation of the O-H bond, while the band that occurs at 2874cm^{-1} is due to the elongation of the C-H bond. At around 1655cm^{-1} and 1325cm^{-1} the typical amide band I and III occurs, respectively. The bands related to the C-O-C bridges are located at 1150cm^{-1} and 892cm^{-1} (elongation od the glycosidic bond). At 1064cm^{-1} the vibratory band attributed to the C-N elongation occurs[131].

The IR spectrum of CaPs shows bands typical of HAp functional groups, namely at 3572cm^{-1} and 631cm^{-1}, due to the O-H group, and at 1089, 1046, 962, 601, 571 and 474cm^{-1} due to the phosphate group[136].

When comparing the FTIR spectra of the non-irradiated scaffold with the raw material spectra (figure 42), only the characteristic peaks of the calcium phosphates and the chitosan C-H peak could be visualized, since the remaining elements peaks could be superimposed.
The raw materials individual spectra can be observed in this work's Annex A.

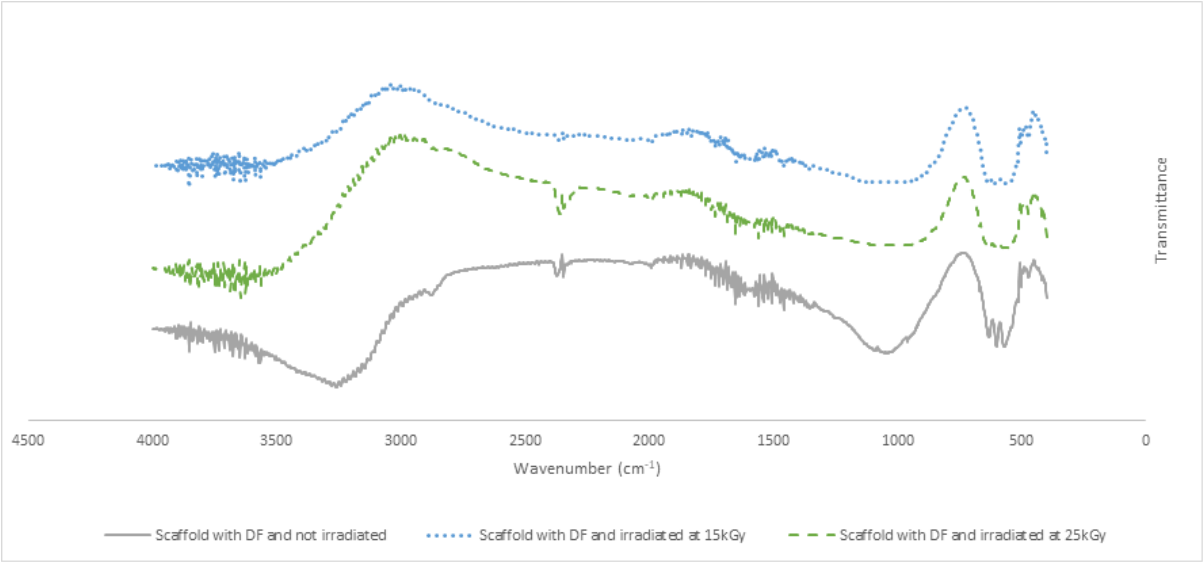

Figure 43 - Comparation between scaffolds with DF, irradiated and not irradiated.

When comparing the irradiated to the non-irradiated scaffolds, calcium phosphates are predominant in the spectrum, as previously mentioned. It is found that in the C-H 2874cm^{-1} chitosan band there is a depression in the spectrum of the non-irradiated sample, that is not observable in the irradiated samples spectra. Considering this factor, it is possible that a partial alteration of the chitosan structure occurred after sterilization.

3.2.7. *In Vitro* cytotoxicity test

The objective of this study was the evaluation of the cytotoxic response of six different samples of scaffolds, like described in section 2.5..

The cytotoxic response is evaluated by the incubation of cultured cells in contact with the device. The cytotoxicity effects can be determined though quantitative means.

The percentage of viable cells after the contact with the extract product is measured and quantified by the reduction of a dye compound named MTT. The test was based on the measurement of the viability of cells via metabolic activity.

The cytotoxicity tests were performed according to the ISO 10993-5 and ISO 10993-12.

In a general way, to perform the cytotoxicity tests, L929 fibroblasts and MG-63 are seeded in 24-well plates and cultured 24 hours to obtain a confluent monolayer (80%-90% confluence), the materials were placed on top of the culture for 24 hours. Afterwards, the cultures were evaluated

The four scaffolds tested were already sterile and were handled aseptically without any modification. The other two were not sterilized. To the negative control was added culture medium. To the positive control was medium with 1mg/mL of sodium dodecyl sulfate (SDS).

A decrease in the number of viable cells as a result of a cytotoxicity response results in a decrease of the metabolic activity of the samples. According to the ISO standards, if the viability lower than 70% of the ones obtained for the negative control, the sample tested presents a cytotoxic potential.

Since the scaffolds are absorbent, they were soaked in culture medium prior to the start of the test, in order to avoid absorption of the well culture medium. Triplicates of the samples to be tested and the controls were used in the assays.
In the first assay, the scaffolds were carefully placed on the L929 and MG63 cell monolayer, to cover approximately one tenth of the well, figure 42 A.

A  B 

Figure 44 - A) Scaffold covering 1/10 of the well; B) Scaffold covering 1/20 of the well.

The following tables show the cell viability results, with the mean and standard deviation values for the three replicates.

Table 6 - Cell viability percentage of the samples tested with 1/10 area of cell monolayer.

Sample name	Cell viability ± SD (%)
Negative control (L929 cells)	100 ± 4.3%
Positive Control (SDS)	12,3 ± 2.2%
Scaffold without DF and not irradiated	58.5 ± 8.5%
Scaffold without DF and irradiated at 15kGy	60.5 ± 4.9%
Scaffold without DF and irradiated at 25kGy	68.5 ± 3.4%
Scaffold with DF and not irradiated	43.0 ± 2.5%
Scaffold with DF and irradiated at 15kGy	40.0 ± 5.0%
Scaffold with DF and irradiated at 25kGy	36.0 ± 5.6%

Sample name	Cell viability ± SD (%)
Negative control (MG63 cells)	100 ± 6.0%
Positive Control (SDS)	15.5 ± 0.2%
Scaffold without DF and not irradiated	56.0 ± 3.2%
Scaffold without DF and irradiated at 15kGy	65.7 ± 6.0%
Scaffold without DF and irradiated at 25kGy	67.8 ± 4.4%
Scaffold with DF and not irradiated	49,8 ± 2.8%
Scaffold with DF and irradiated at 15kGy	41.5 ± 7.0%
Scaffold with DF and irradiated at 25kGy	43.9 ± 1.6%

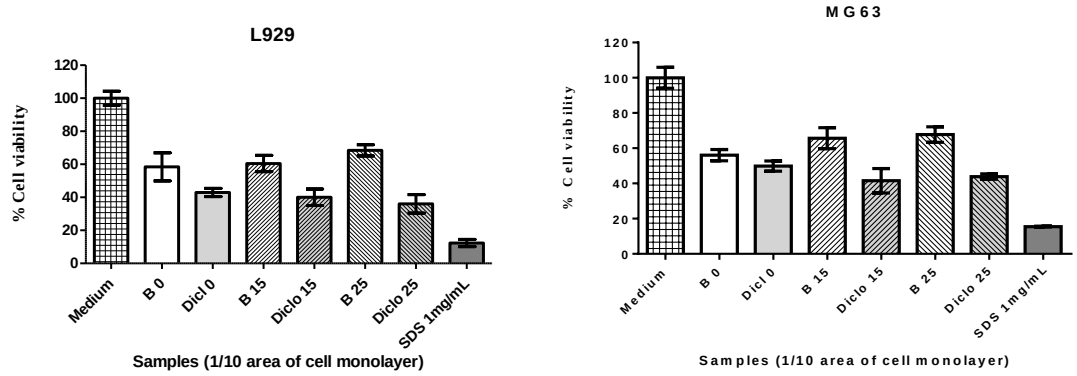

Figure 45 - Graphic representation of cell viability (%) values obtained for the different scaffolds tested with the different line cells.

All results concerning the cell viability of the scaffolds under study were obtained comparing with the cells' control values. For scaffolds with DF and irradiated at 25kGy in the L929 cell line assay, viability was found to be less than 40% and thus considered to be severely cytotoxic. The remaining samples showed values higher than 40% and less than 70%, being considered cytotoxic.

In both cell lines the difference in cell viability values between the samples with and without DF is quite visible. It has been observed that in scaffolds without DF the viability values increase depending on the radiation applied. The same does not happen when DF is present in the sample.

Literature[137], indicates that the radiation does not cause changes in DF when it is in the solid state. However, if it is sterilized in solution, more than 40% degradation will occur. Since in the scaffolds under study the DF was dissolved in solution into the matrix and subsequently lyophilized, its structure may possibly not be equal to its original structure as powder. In the FTIR analysis it was not possible to verify drug binding to the matrix, due to the presence of a large amount of CaPs, it can be assumed that the new DF structure, although dry, is different, and when sterilized at 15kGy and 25kGy may originate products that render the scaffolds unfeasible, making it cytotoxic. However, the pH of medium is acid due to lactic acid and DF, this can be another contributed factor for cytotoxicity.

A new assay was performed only with L929 fibroblast cells, in which the material was placed to 1/20 of the well. The following table shows the obtained results from cell viability.

Table 7 - Cell viability percentage of the samples tested with 1/20 area of cell monolayer.

Sample name	Cell viability ± SD (%)
Negative control (L929 cells)	100 ± 4.8%
Positive Control (SDS)	7.0 ± 0.2%
Scaffold without DF and not irradiated	81.5 ± 4.6%
Scaffold without DF and irradiated at 15kGy	70.1 ± 2.0%
Scaffold without DF and irradiated at 25kGy	78.0 ± 6.2%
Scaffold with DF and not irradiated	74.5 ± 5.5%
Scaffold with DF and irradiated at 15kGy	70.3 ± 3.0%
Scaffold with DF and irradiated at 25kGy	65.9 ± 4.5%

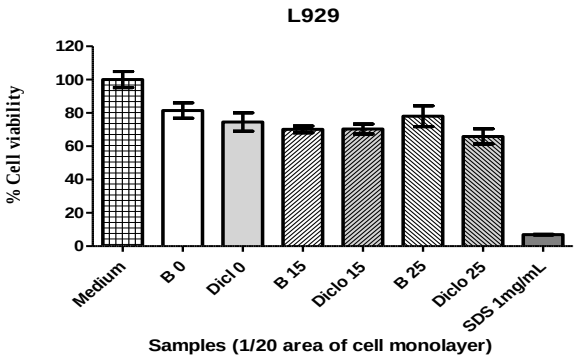

Figure 46 - Graphic representation of cell viability.

When comparing the results obtained with the control values, it was verified that almost all scaffolds present cell viability (values higher than 70%), demonstrating the biocompatibility existence. However, scaffolds with DF sterilized at 25kGy presented values of 66%, indicating moderate cytotoxicity.

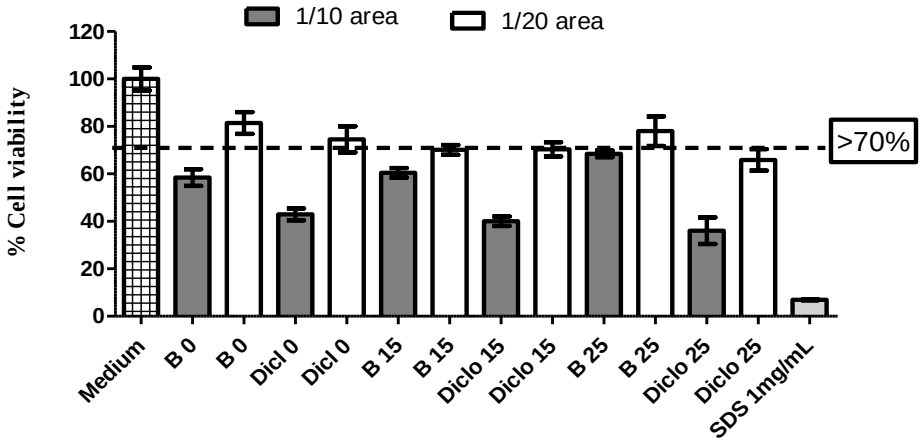

Figure 47 – Comparative graphic of cell viability between different amounts of material introduced into the wells.

Comparing the viability values of L929 cells, obtained in 1/10 and 1/20 of the well, it can be concluded that less material makes the viability values have no cytotoxic effect. The medium pH is another factor that contributes to cell viability. The lactic acid and DF concentration present in the sample may decrease the medium pH, promoting the cytotoxic effect.

4. CONCLUSION AND FUTURE WORK

Initially, the proposed objective was to create a new bone substitute capable of being molded to the bone defect in a simple way, which allowed the reabsorption and growing of bone with the particularity of decrease the inflammatory process after it is implementation.

In order to do that, the DF was chosen, as being the non-steroidal anti-inflammatory more suitable to the scaffold future application, since it still presents an analgesic, anti-inflammatory and antipyretic pharmacology activity.

As it was intended to obtain a solid matrix that could be cut and molded to the bone defect, it was used a product that already existed in market - k-IBS®. The matrix k-IBS® displays a yellowish and pasty appearance and it is composed by a ceramic part (inorganic) and a polymeric part (organic).

In order to mimic the original bone composition, the matrix in the inorganic part uses HAp and β-TCP. In the organic part, it uses PEG, the lactic acid and the natural polymer CS.

First, it was studied the incorporation of the anti-inflammatory in the chitosan and calcium phosphates k-IBS® matrix. In order that emulsion of the drug did not occur, it was necessary to dissolve it in a determined water percentage and simultaneously create the lactic acid solution, apart, which would dissolve all percentage of existing CS. With the aid of the stirring process, by joining the components it was verified that the drug was homogeneously dispersed in the mixture. After the incorporation drug success, it was added approximately 71% of CaPs granules, in which the existing microporosity facilitates the adhesion, cellular proliferation and nutrients distribution.

Through the freeze-drying process it was possible to remove all water existing in the mixture and to transform the pasty matrix in a porous solid. However, when it was proceeded to the cut in discs and cylinders it was verified that it can occur some material degradation.

As in actual industry of medical devices, it exists a complex and rigorous normative basis, one of the goals of this work was to meet these regulations and submit the created scaffolds to sterilization processes with gamma radiation at 15kGy and 25kGy, ensuring, this way, the usage of decontaminated materials. However, the different radiations promote changes in scaffolds matrix components.

Through controlled diclofenac release trials, it was concluded that all the samples that contained the drug, both irradiated (at 15 and 25kGy) and non-irradiated, released 60% and 80%, respectively, of diclofenac in the first 7 hours, as expected. However, it was noted that the irradiated samples (15 and 25kGy) had a slower release behaviour.

At the end of 7h it was already released 2.79µg/mg of dry scaffold, in total approximately 400µg DF in the non-irradiated samples, 2.46µg/mg of dry scaffold, in total approximately 370µg in the irradiated samples at 15kGy and only 2.27µg/mg of dry scaffold, in total approximately 330µg DF in the samples irradiated at 25kGy. However, the incorporated DF was not totally released in the 10 to 15 expectable days, since at the end of 41 days the samples still released the drug. It was through the destructive methods performed on scaffolds, that it was verified that there was still drug trapped in the structures. From the mathematical models tested, Korsmeye-Peppas was the best fit for the different release systems. The n value that was obtained through the graph's line slope was less than 0.45, indicating Case I as the transport mechanism.

Regarding the amount of existing drug in each scaffold, at beginning of the release assays, it can be concluded that despite the samples have been cut with same dimension and present similar weight, not all exactly represented the intended 500µg. It was found that the drug variation between irradiated and non-irradiated samples could vary between 50µg to 100µg.

It was not possible to observe through SEM images, from SEM-EDS mappings, neither the FTIR trials how DF was incorporated / bonded to the material. This is because the amount of drug used is only 0,35% of the scaffold mass.

According to the results obtained in the release assays, it was concluded that the scaffolds irradiated at 15 and 25kGy represents a slightly controlled release. However, it should be taken into account that the obtained results presents the errors associated to the technique and the operator.

In relation to images obtained through SEM, it was possible to observe the irradiated and non-irradiated scaffolds morphology and the calcium phosphate granules. It was verified that the spherical granules present porosity and an irregular structure propitious to cell adhesion. This morphology can also to a certain extent, be able to retain DF, delaying its release. The scaffolds analysed through mentioned technique, allowed to observe the random granules distribution, its involvement in the polymer matrix and to verify the existence of porosity.

The swelling trials allowed to conclude that the radiation leads to a higher reticulation, taunting a decrease on absorption capacity. In this way, it can be argued that the drug released is slower in these scaffolds, since for that to occur it is mandatory to have structure degradation and expansion.

In relation to wettability tests, it was proved that all samples presented a hydrophilic structure, propitious to biological interactions, due to the contact angles that presented values lower to a 90º.

As currently it is essential to evaluate the cytotoxic effect of the biomaterial due to all legal and normative requirements of the medical devices directive, the scaffolds were submitted to in vitro tests. Cytotoxicity involves the disturbance of the cellular homeostasis that consequently affects the cellular function, leading to the loss of viability. In the orthopaedics and dental medicine, the osteointegration is mandatory to the success of the medical device and of is dependent of the viability and cell proliferation and differentiation. In order to evaluate cultures cellular viability, it was applied the MTT method by the direct contact assay.

It was verified that by using a tenth of the well, both cellular line MG63 as fibroblasts L929 presents cytotoxicity, obtaining viability values below 70%.

Therefore, it was decided to only use the cell line L929 for one-twentieth of the well. In this way, the reduction of the MTT to the purple colour was observed, evidencing the presence of viable cells. Almost all scaffolds had cell viability greater than 70%, except scaffolds irradiated at 25kGy.

The cytotoxicity study indicated a good performance and safety of the developed product when it is not subject to 25kGy radiation.

By compiling and analysing all the obtained results, it can be concluded that the scaffolds that best fit the proposed initial objectives are the irradiated ones (both at 15 and 25kGy), because both materials have a similar behaviour.

As an economic matter, 25kGy irradiated scaffolds would be the chosen ones, since the industry would have more expenses with carrying out more biological tests for the medical devices irradiated at 15kGy.

As a suggestion of future work, it would be interesting to understand better what happens to scaffolds loaded with DF after sterilization, their mechanical and structural properties and the effect of sterilization if the drug is incorporated into a controlled release system such as fibres or particles. Further properties should be studied and optimizations to the lyophilization process should be performed, since through this it is possible to control, in a certain way, the scaffolds porosity.

It is suggested that cell adhesion and proliferation be evaluated in vitro, and the in vivo study, because there are no in vitro models capable of completely mimicking the complexity of the organism.

It would also be interesting to associate growth factors to the matrix under study and to the anti-inflammatory.

It would be relevant to assess the structure and interactions that occur when diclofenac, in its powder state, is irradiated, after it has been previously dissolved in water and lyophilized.

In order to be able to evaluate the chemical bonds between the DF and the remaining matrix composition, Raman spectroscopy could be an alternative to FTIR, since it is a more precise technique.

The development of a mathematical model more appropriate to the material and its final application would give, with greater certainty, a release profile even closer to reality.

Since this work aimed at designing and developing a medical device, it would be interesting to introduce it in the market. This would require a conformity assessment procedure under the relevant Directive.

The Medical Devices Directive 93/42/CEE (as amended by Directive 2007/47/CE) establishes a set of essential requirements for the manufacture, marketing, labelling, rework and use of medical devices, which ensures the safety and performance of the device. Demonstration of compliance with essential requirements shall include: clinical evaluation of material performance; biological safety under normal conditions of use; evaluation of side effects and benefit / risk ratio.

5. BIBLIOGRAPHY

1. US Department of Health and Human Services. Bone health and osteoporosis: a report of the Surgeon General. *US Heal. Hum. Serv.* 437 (2004). doi:10.2165/00002018-200932030-00004

2. Chesnutt, B. M. *et al.* Design and characterization of a novel chitosan/nanocrystalline calcium phosphate composite scaffold for bone regeneration. *J. Biomed. Mater. Res. - Part A* **88,** 491–502 (2009).

3. Cummings, S. R. & Melton, L. J. Osteoporosis I: Epidemiology and outcomes of osteoporotic fractures. *Lancet* **359,** 1761–1767 (2002).

4. Sheikh, Z. *et al.* Biodegradable materials for bone repair and tissue engineering applications. *Materials (Basel).* **8,** 5744–5794 (2015).

5. Barrère, F., Mahmood, T. A., de Groot, K. & van Blitterswijk, C. A. Advanced biomaterials for skeletal tissue regeneration: Instructive and smart functions. *Mater. Sci. Eng. R Reports* **59,** 38–71 (2008).

6. Chevalier, E. *et al.* Ibuprofen-loaded calcium phosphate granules: Combination of innovative characterization methods to relate mechanical strength to drug location. *Acta Biomater.* **6,** 266–274 (2010).

7. Goodrich, J. T., Sandler, A. L. & Tepper, O. A review of reconstructive materials for use in craniofacial surgery bone fixation materials, bone substitutes, and distractors. *Child's Nerv. Syst.* **28,** 1577–1588 (2012).

8. Christensen, F. B., Dalstra, M., Sejling, F., Overgaard, S. & Bünger, C. Titanium-alloy enhances bone-pedicle screw fixation: mechanical and histomorphometrical results of titanium-alloy versus stainless steel. *Eur. Spine J.* **9,** 97–103 (2000).

9. Sheikh, Z., Javaid, M. A., Hamdan, N. & Hashmi, R. Bone Regeneration Using Bone Morphogenetic Proteins and Various Biomaterial Carriers. *Mater.* **8,** 1778–1816 (2015).

10. Ramay, H. R. R. & Zhang, M. Biphasic calcium phosphate nanocomposite porous scaffolds for load-bearing bone tissue engineering. *Biomaterials* **25,** 5171–5180 (2004).

11. Siddiqui, N., Pramanik, K. & Jabbari, E. Osteogenic differentiation of human mesenchymal stem cells in freeze-gelled chitosan/nano β-tricalcium phosphate porous scaffolds crosslinked with genipin. *Mater. Sci. Eng. C* **54,** 76–83 (2015).

12. Venkatesan, J. & Kim, S. K. Chitosan composites for bone tissue engineering - An

overview. *Mar. Drugs* **8,** 2252–2266 (2010).

13. Dias, S., Figueiras, A., Barata, P., Oliveira, R. & Veiga, F. A administração na mucosa bucal como uma estratégia alternativa à via oral. (2007).

14. Fialkoff, D. B. Extractions, Bone Grafts & Guided Bone Regeneration. Available at: http://www.baysidedentist.com/procedures/extractions-bone-grafts-guided-bone-regeneration/. (Accessed: 13th June 2018)

15. Mhanna, R. & Hasan, A. 1 . 2 Clinical Need for Tissue Engineering. 3–34 (2017).

16. Williams, D. F. On the nature of biomaterials. *Biomaterials* **30,** 5897–5909 (2009).

17. Nainar, S. M., Vicki, W. V., Begum, S. & Ansari, M. N. M. Review Article A review on bioscaffolds for tissue engineering application. **2,** 184–192 (2014).

18. Chaudhari, A. A. *et al.* Future prospects for scaffolding methods and biomaterials in skin tissue engineering: A review. *Int. J. Mol. Sci.* **17,** (2016).

19. Moreno, M., Amaral, M. H., Lobo, J. M. S. & Silva, A. C. Scaffolds for Bone Regeneration: State of the Art. *Curr. Pharm. Des.* **22,** 2726–36 (2016).

20. I, D. & LT, K. Design and characterization of calcium phosphate ceramic scaffolds for bone tissue engineering. *Acad. Dent. Mater.* **131,** 1796–1803 (2016).

21. Gutierres, M., Lopes, M. A., Hussain, N. S., Cabral, A. T. & Almeida, L. Substitutos Ósseos Conceitos Gerais e Estado Actual. *Arq. Med.* 19(4): 153-162 (2006).

22. Thomson, R. C., Yaszemski, M. J., Powers, J. M. & Mikos, A. G. Fabrication of biodegradable polymer scaffolds to engineer trabecular bone. *J. Biomater. Sci. Polym. Ed.* **7,** 23–38 (1995).

23. O'Brien, F. J. Biomaterials & scaffolds for tissue engineering. *Mater. Today* **14,** 88–95 (2011).

24. Alvarez, K. & Nakajima, H. Metallic scaffolds for bone regeneration. *Materials (Basel).* **2,** 790–832 (2009).

25. Florencio-Silva, R., Sasso, G. R. D. S., Sasso-Cerri, E., Simões, M. J. & Cerri, P. S. Biology of Bone Tissue: Structure, Function, and Factors That Influence Bone Cells. *Biomed Res. Int.* **2015,** (2015).

26. Judas, F., Palma, P. & Figueiredo, H. Estrutura e dinâmica do tecido ósseo. 1–51 (2012).

27. Kanczler, J. M. & Oreffo, R. O. C. Osteogenesis and angiogenesis: The potential for engineering bone. *Eur. Cells Mater.* **15,** 100–114 (2008).

28. Amini, A. R., Laurencin, C. T. & Nukavarapu, S. P. Bone Tissue Engineering: Recent Advances and Challenges. *Crit. Rev. Biomed. Eng.* **40,** 363–408 (2012).

29. Tan, S. *et al.* Deregulation of bone forming cells in bone diseases and anabolic effects of strontium-containing agents and biomaterials. *Biomed Res. Int.* **2014,** (2014).

30. Jones, J. R. & Hench, L. L. Regeneration of trabecular bone using porous ceramics. *Curr. Opin. Solid State Mater. Sci.* **7,** 301–307 (2003).

31. Salgado, A. J., Coutinho, O. P. & Reis, R. L. Bone tissue engineering: State of the art and future trends. *Macromol. Biosci.* **4,** 743–765 (2004).

32. Betti, L. V. Luciana viti betti. (2004).

33. Willems, N. M. B. K., Langenbach, G. E. J., Everts, V. & Zentner, A. The microstructural and biomechanical development of the condylar bone: A review. *Eur. J. Orthod.* **36,** 479–485 (2014).

34. King, D. Bone, Remodelling. *November 3* (2004). Available at: http://www.siumed.edu/~dking2/ssb/remodel.htm. (Accessed: 13th June 2018)

35. Viegas, C. A. A. *et al.* The platelet rich plasma utilization in regeneration of alveolar and cortical bone tissue. *Rev. Port. Ciências Veterinárias* **101,** 193–213 (2006).

36. Gerstenfeld, L. C., Cullinane, D. M., Barnes, G. L., Graves, D. T. & Einhorn, T. A. Fracture Healing as a Post-Natal Developmental Process : Molecular , Spatial , and Temporal Aspects of Its Regulation. **884,** 873–884 (2003).

37. Kayal, R. A. *et al.* No Title. doi:10.1359/JBMR.070115

38. Einhorn, T. A., Gerstenfeld, L. C., Surgery, O., Avenue, H. & Surgery, O. Fracture healing : mechanisms and interventions. **11,** 45–54 (2015).

39. Wagh, M. & Ravalia, D. Bone Regeneration and Repair: Current and Future Aspects. *Ijsr.Net* **4,** 351–355 (2015).

40. Karageorgiou, V. & Ã, D. K. Porosity of 3D biomaterial scaffolds and osteogenesis. **26,** 5474–5491 (2005).

41. Bohner, M. Resorbable biomaterials as bone graft substitutes. *Mater. Today* **13,** 24–30 (2010).

42. Dorozhkin, S. Calcium Orthophosphate-Based Bioceramics. *Materials (Basel).* **6,** 3840–3942 (2013).

43. Parida, P., Behera, A., Mishra, S. C. & Info, A. Classification of Biomaterials used in Medicine. **1,** 31–35 (2012).

44. Bauer, T. W. Bone graft substitutes. *Skeletal Radiol.* **36,** 1105–7 (2007).

45. Afonso, S. Interacção entre biomateriais e tecido ósseo. (1998).

46. Hing, K. A., Wilson, L. F. & Buckland, T. Comparative performance of three ceramic bone graft substitutes. *Spine J.* **7,** 475–490 (2007).

47. Campana, V. *et al.* Bone substitutes in orthopaedic surgery: from basic science to clinical practice. *J. Mater. Sci. Mater. Med.* **25,** 2445–2461 (2014).

48. Ghayor, C. & Weber, F. E. Osteoconductive microarchitecture of bone substitutes for bone regeneration revisited. *Front. Physiol.* **9,** 1–10 (2018).

49. Fernandez-Yague, M. a. *et al.* Biomimetic Approaches in Bone Tissue Engineering: Integrating Biological and Physicomechanical Strategies. *Adv. Drug Deliv. Rev.* (2014). doi:10.1016/j.addr.2014.09.005

50. Nandi, S. K., Roy, S., Mukherjee, P., Kundu, B. & Basu, D. Orthopaedic applications of bone graft & graft substitutes : a review. 15–30 (2010).

51. Rumpel, E. *et al.* The biodegradation of hydroxyapatite bone graft substitutes in vivo. **65,** 43–48 (2006).

52. Barbanti, S. H., Zavaglia, C. a. C. & Duek, E. a. R. Polímeros bioreabsorvíveis na engenharia de tecidos. *Polímeros* **15,** 13–21 (2005).

53. Williams, D. F. On the mechanisms of biocompatibility. *Biomaterials* **29,** 2941–2953 (2008).

54. Szymańska, E. & Winnicka, K. Stability of Chitosan—A Challenge for Pharmaceutical and Biomedical Applications. *Mar. Drugs* **13,** 1819–1846 (2015).

55. Bhat, S. & Kumar, A. Biomaterials and bioengineering tomorrow ' s healthcare. *Landes Biosci.* **3,** 1–12 (2013).

56. Neumann, M. & Epple, M. Composites of calcium phosphate and polymers as bone substitution materials. *Eur. J. Trauma* **32,** 125–131 (2006).

57. Bongio, M., Van Den Beucken, J. J. J. P., Leeuwenburgh, S. C. G. & Jansen, J. A.

Development of bone substitute materials: From 'biocompatible' to 'instructive'. *J. Mater. Chem.* **20,** 8747–8759 (2010).

58. Mathias, J.-D., Tessier-Doyen, N. & Michaud, P. Development of a chitosan-based biofoam: application to the processing of a porous ceramic material. *Int. J. Mol. Sci.* **12,** 1175–86 (2011).

59. Dash, M., Chiellini, F., Ottenbrite, R. M. & Chiellini, E. Chitosan - A versatile semi-synthetic polymer in biomedical applications. *Prog. Polym. Sci.* **36,** 981–1014 (2011).

60. Ruel-Gariépy, E. & Leroux, J. C. In situ-forming hydrogels - Review of temperature-sensitive systems. *Eur. J. Pharm. Biopharm.* **58,** 409–426 (2004).

61. Fakhry, A., Schneider, G. B., Zaharias, R. & Şenel, S. Chitosan supports the initial attachment and spreading of osteoblasts preferentially over fibroblasts. *Biomaterials* **25,** 2075–2079 (2004).

62. Baishakhi, M. A. D. Chitosan microspheres in novel drug delivery systems Methods of Chitosan Microspheres Preparation. *Indian J. Pharm. Sci.* **73,** 355–366 (2011).

63. Zhang, W., Sun, Y.-L. & Chen, D.-H. Effects of chitin and sepia ink hybrid hemostatic sponge on the blood parameters of mice. *Mar. Drugs* **12,** 2269–81 (2014).

64. Pusateri, A. E. *et al.* Effect of a chitosan-based hemostatic dressing on blood loss and survival in a model of severe venous hemorrhage and hepatic injury in swine. *J. Trauma* **54,** 177–82 (2003).

65. Boursinos, L. a, Karachalios, T., Poultsides, L. & Malizos, K. N. Do steroids, conventional non-steroidal anti-inflammatory drugs and selective Cox-2 inhibitors adversely affect fracture healing? *J. Musculoskelet. Neuronal Interact.* **9,** 44–52 (2009).

66. DeRuiter, J. *et al.* Central mechanisms of pain modulation. *Princ. Drug Action* **9,** 436–441 (2013).

67. Jesús Florez. *Farmacología Humana*. *Masson, S.a.* (1997). doi:10.1017/CBO9781107415324.004

68. Hilário, M. O. E., Terreri, M. T. & Len, C. A. Nonsteroidal anti-inflammatory drugs: cyclooxygenase 2 inhibitors. *J. Pediatr. (Rio. J).* **82,** 206–212 (2006).

69. Gilron, I., Millne, B. & Hong, M. Cyclooxygenase-2 inhibitors in postoperative pain management. *Anesthesiology* **99,** 1198–1208 (2003).

70. Carvalho, W. A., Carvalho, R. D. S. & Rios-Santos, F. Analgésicos inibidores

específicos da ciclooxigenase-2: avanços terapêuticos. *Rev. Bras. Anestesiol.* **54,** 448–464 (2004).

71. Vane JR & Botting RM. Mechanism of Action of Nonsteroidal Anti-inflammatory Drugs. *Am. J. Med.* **104 (3A),** (1998).

72. Ac, M. & Hincalt, A. A. Chitosan microspheres of diclofenac sodium: **13,** (1996).

73. Company, C. C., Arbor, A. & Company, C. C. Diclofenac sodium salt, Material Safety DATA, Product informations by Cayman Chemical Company, 2012. (2014).

74. SA, T. E. Indice Toda a Saude. (2017). Available at: https://www.indice.eu/pt/medicamentos/medicamentos/voltaren-solucao-injetavel/saber-mais. (Accessed: 16th August 2018)

75. Infarmed. Folheto informativo Dorcalor. (2016).

76. Infarmed. Folheto informativo Voltaren. (2016).

77. Infarmed. Folheto informativo Flameril. (2016).

78. Infarmed. Folheto informativo Olfen. (2016).

79. Infarmed. Folheto informativo Fenil-V. (2017).

80. Medicines, V. Committee for Veterinary Medicinal Products. *Distribution* (2004).

81. Laranjeira, M. C. M. & De Fávere, V. T. Quitosana: biopolimero funcional com potencial industrial biomedico. *Quim. Nova* **32,** 672–678 (2009).

82. Dash, S., Murthy, P. N., Nath, L. & Chowdhury, P. Review Kinetic modeling on drug release from controlled drug delivery systems. *Acta Pol. Pharm. - Drug Res.* **67,** 217–223 (2010).

83. Liechty, W. B., Kryscio, D.R., Slaughter, B. V. and Peppas, N. A. Polymers for drug delivery systems. *Annu. Rev. Chem. Biomol. Eng.* **1,** 149–173 (2010).

84. Blagoeva, R. & Nedev, A. Monolithic Controlled Delivery Systems: Part I. Basic Characteristics and Mechanisms. *Int. J.* 80–88 (2006).

85. Huynh, C. T. & Lee, D. Encyclopedia of Polymeric Nanomaterials. (2017). doi:10.1007/978-3-642-36199-9

86. Coelho, P. Desenvolvimento de formulações de libertação modificada de ranitidina. *Fac. Farmácia Univ. do Porto* 264 (2007).

87. Siepmann, J. & Siepmann, F. Mathematical modeling of drug dissolution. *Int. J. Pharm.*

453, 12–24 (2013).

88. Siepmann, J. & Göpferich, A. Mathematical modeling of bioerodible, polymeric drug delivery systems. *Adv. Drug Deliv. Rev.* **48,** 229–247 (2001).

89. Costa, P., & Lobo, J. M. S. Modeling and Comparison of Dissolution Profiles. *Eur. J. Pharm. Sci.* **13,** 123–133 (2001).

90. Korsmeyer, R. W., Gurny, R., Doelker, E., Buri, P. & Peppas, N. A. Mechanisms of solute release from porous hydrophilic polymers. *Int. J. Pharm.* **15,** 25–35 (1983).

91. Ritger, P. & Peppas, N. A SIMPLE EQUATION FOR DESCRIPTION OF SOLUTE RELEASE II. FICKIAN AND ANOMALOUS RELEASE FROM SWELLABLE DEVICES. *J. Control. Release* **5,** 37–42 (1987).

92. Costa, P. J. C. da. Avaliação in vitro da lioequivalência de formulações farmacêuticas. *Rev. Bras. Ciências Farm.* **38,** 141–153 (2002).

93. Baume, A. S., Coleman, N. V. & Boughton, P. C. Methods for Achieving Soft Tissue Scaffold Sterility. *J. Biomim. Biomater. Tissue Eng.* **4,** 59–69 (2009).

94. Team, T. Sterilization Methods Summary. (2017). Available at: https://tuttnauer.com/blog/sterilization-methods-summary. (Accessed: 16th August 2018)

95. Kanjickal, D., Lopina, S., Evancho-Chapman, M. M., Schmidt, S. & Donovan, D. Effects of sterilization on poly(ethylene glycol) hydrogels. *J. Biomed. Mater. Res. - Part A* **87,** 608–617 (2008).

96. IAEA. Trends in Radiation Sterilization of Health Care Products. *Int. At. Energy Agency* 261 (2008).

97. Standard, I. ISO 13485:2003 - INTERNATIONAL STANDARD - Medical devices - Quality management systems - Requirements for regulatoty purposes. **2,** 1–64 (2003).

98. Özer, A. *et al.* The effects of gamma irradiation on diclofenac sodium, liposome and niosome ingredients for rheumatoid arthritis. *Interv. Med. Appl. Sci.* **5,** 122–130 (2013).

99. Of, E., Irradiation, G. & Radioprotectorsi, T. O. Effect of gamma irradiation on drugs. **21,** 91–94 (1984).

100. Pikal, M. J., Shah, S., Roy, M. L. & Putman, R. The secondary drying stage of freeze drying: drying kinetics as a function of temperature and chamber pressure. *Int. J. Pharm.* **60,** 203–207 (1990).

101. Nireesha, G. R. *et al.* Lyophilization / Freeze Drying - An Review. **3,** 87–98 (2013).

102. Adams, G. D. J. & Irons, L. I. Some implications of structural collapse during freeze-drying using Erwinia caratovoraL-asparaginase as a model. *J. Chem. Technol. Biotechnol.* **58,** 71–76 (1993).

103. Asadian-Ardakani, V., Saber-Samandari, S. & Saber-Samandari, S. The effect of hydroxyapatite in biopolymer-based scaffolds on release of naproxen sodium. *J. Biomed. Mater. Res. - Part A* **104,** 2992–3003 (2016).

104. Pobudkowska, A. & Domańska, U. Study of pH-dependent drugs solubility in water. *Chem. Ind. Chem. Eng. Q.* **20,** 115–126 (2014).

105. Galante, R. *et al.* Drug-eluting silicone hydrogel for therapeutic contact lenses: Impact of sterilization methods on the system performance. *Colloids Surfaces B Biointerfaces* **161,** 537–546 (2018).

106. Biotech, C. Phosphate buffered saline. *Cube Biotech* (2010). doi:10.1101/pdb.rec11705

107. Dogra, S. A Chitosan–Polymer Hydrogel Bead System For A Metformin HCl Controlled Release Oral Dosage Form. *J. Chem. Inf. Model.* **53,** 1689–1699 (2011).

108. Inc., L. T. Scanning Electron Microscopy. *January 1* (2017). Available at: https://www.labtesting.com/services/materials-testing/metallurgical-testing/sem-analysis/. (Accessed: 12th June 2018)

109. Dedavid, B. A., Gomes, C. I. & Machado, G. Microscopia Eletronica de Varredura. Aplicação e preparação de amostras. 60 (2007).

110. Scintag. *Basics of X-ray Diffraction*. *Solutions* (1999).

111. Takashi, I. Bragg ' s law. *Grad. Sch. Eng. Nagoya Inst. Technol.* 1–8 (2013).

112. Birkholz, M. *Thin Film Analysis by X-Ray Scattering*. (2006).

113. Speakman, S. A. Basics of X-Ray Powder Diffraction. *Massachusetts Inst. Technol.* 1–97

114. Wenk;, H.-R., Matthies, S. & Lutterotti, L. Materials Analysis Using Diffraction (MAUD). Available at: http://maud.radiographema.eu/.

115. Shimadzu. Fraunhofer Diffraction Theory and Mie Scattering Theory. (2016). Available at: https://www.shimadzu.com/an/powder/support/practice/p01/lesson13.html.

116. Read, M. L., Morgan, P. B. & Maldonado-Codina, C. Measurement errors related to

contact angle analysis of hydrogel and silicone hydrogel contact lenses. *J. Biomed. Mater. Res. - Part B Appl. Biomater.* **91,** 662–668 (2009).

117. Lotfi, M., Nejib, M. & Naceur, M. Cell Adhesion to Biomaterials: Concept of Biocompatibility. *Adv. Biomater. Sci. Biomed. Appl.* (2013). doi:10.5772/53542

118. Montes Ruiz-Cabello, F. J., Rodríguez-Valverde, M. A., Marmur, A. & Cabrerizo-Viźlchez, M. A. Comparison of sessile drop and captive bubble methods on rough homogeneous surfaces: A numerical study. *Langmuir* **27,** 9638–9643 (2011).

119. Novaes, A. B. *et al.* Influence of implant surfaces on osseointegration. *Braz. Dent. J.* **21,** 471–481 (2010).

120. Bosco, R., Van Den Beucken, J., Leeuwenburgh, S. & Jansen, J. Surface Engineering for Bone Implants: A Trend from Passive to Active Surfaces. *Coatings* **2,** 95–119 (2012).

121. Ramos, J. A. Estudo experimental para transporte de microgotas por atuação electrostática Bioengenharia e Nanossistemas. *Diss. Mestr. em Bioengenharia e Nanossistemas, Tec. Lisboa, Univ. Lisboa* (2014).

122. Seth Lindblom, Emylee Ratzlaff, Morgan Hoos, M. S. Materials in neature. (2017). Available at: https://materialsinneature.wordpress.com/2017/02/04/superhydophobicity-conquering-our-fear-of-water/. (Accessed: 29th July 2018)

123. Ferguson, T. P. & Jianmin Qu. Moisture and temperature effects on the reliability of interfacial adhesion of a polymer/metal interface. *2004 Proceedings. 54th Electron. Components Technol. Conf. (IEEE Cat. No.04CH37546)* 1752–1758 (2004). doi:10.1109/ECTC.2004.1320355

124. Felinto, M. C. F. C. *et al.* The swelling behavior of chitosan hydrogels membranes obtained by UV- and γ-radiation. *Nucl. Instruments Methods Phys. Res. Sect. B Beam Interact. with Mater. Atoms* **265,** 418–424 (2007).

125. Ganzoury, M. A., Allam, N. K., Nicolet, T. & All, C. Introduction to Fourier Transform Infrared Spectrometry. *Renew. Sustain. Energy Rev.* **50,** 1–8 (2015).

126. Kirkpatrick, C. J. & Mittermayer, C. Theoretical and practical aspects of testing potential biomaterials in vitro. *J. Mater. Sci. Mater. Med.* **1,** 9–13 (1990).

127. (CSA), C. S. A. International Standard ISO Specification 10993-5: Biological evaluation of medical devices – Part 5: Tests for in vitro cytotoxicity. *Int. Organ.* **2009,** 1–11 (2009).

128. Mosmann, T. Rapid colorimetric assay for cellular growth and survival: Application to

proliferation and cytotoxicity assays. *J. Immunol. Methods* **65,** 55–63 (1983).

129. Matos, A. *et al.* Minocycline-loaded acrylic bone cement – in vitro release, biochemical and biological assessment. *Mater. Sci. Eng C* **38,** 218–226 (2014).

130. Žilnik, L. F., Jazbinšek, A., Hvala, A., Vrečer, F. & Klamt, A. Solubility of sodium diclofenac in different solvents. *Fluid Phase Equilib.* **261,** 140–145 (2007).

131. Lobo, S. E. & Arinzeh, T. L. Biphasic calcium phosphate ceramics for bone regeneration and tissue engineering applications. *Materials (Basel).* **3,** 815–826 (2010).

132. INFARMED. Folheto informativo - Diclofenac Alter 50mg comprimidos revestidos. *Instr. use* 1–8 (2014).

133. Sidney, L. E. *et al.* Investigation of Localized Delivery of Diclofenac Sodium from Poly(D,L-Lactic Acid- *co* -Glycolic Acid)/Poly(Ethylene Glycol) Scaffolds Using an *In Vitro* Osteoblast Inflammation Model. *Tissue Eng. Part A* **21,** 362–373 (2015).

134. Dan, Y. *et al.* Development of Novel Biocomposite Scaffold of Chitosan-Gelatin/Nanohydroxyapatite for Potential Bone Tissue Engineering Applications. *Nanoscale Res. Lett.* **11,** 1–6 (2016).

135. Karuna, D. *et al.* Preparation And Evaluatıon Of Chitosan Succinate Pellets Using Extrusion-Spheronization Technology: Processing And In Vitro Characterization. *Turkish J. Pharm. Sci.* **13,** 68–86 (2016).

136. Berzina-Cimdina, L. & Borodajenko, N. Research of Calcium Phosphates Using Fourier Transform Infrared Spectroscopy. *Infrared Spectrosc. - Mater. Sci. Eng. Technol.* (2012). doi:10.5772/36942

137. Topete, A., Saramago, B. & Serro, A. P. Effects of sterilization on drug loaded soft contact lenses. (2015).

6. ANNEX

Annex A – FTIR spectra

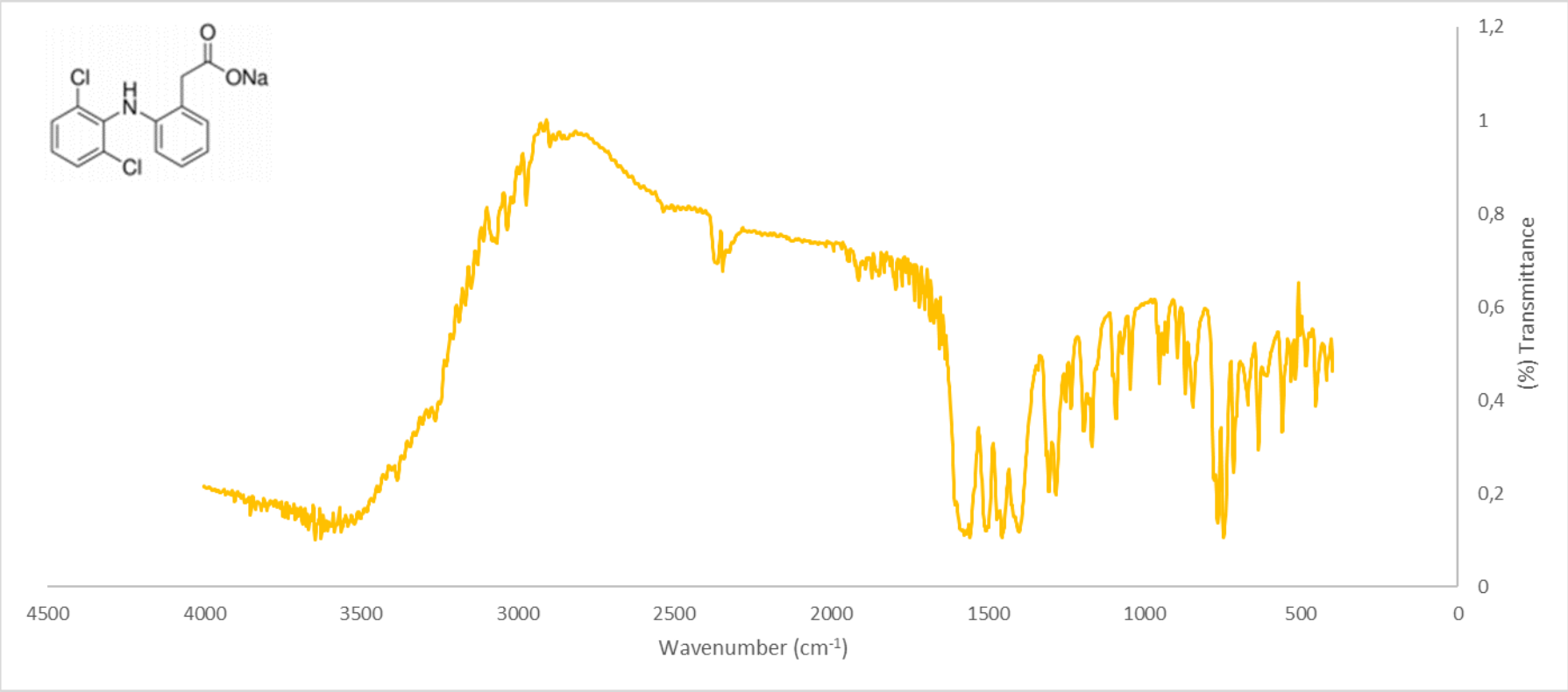

Figure 48 - FTIR spectra corresponding to DF.

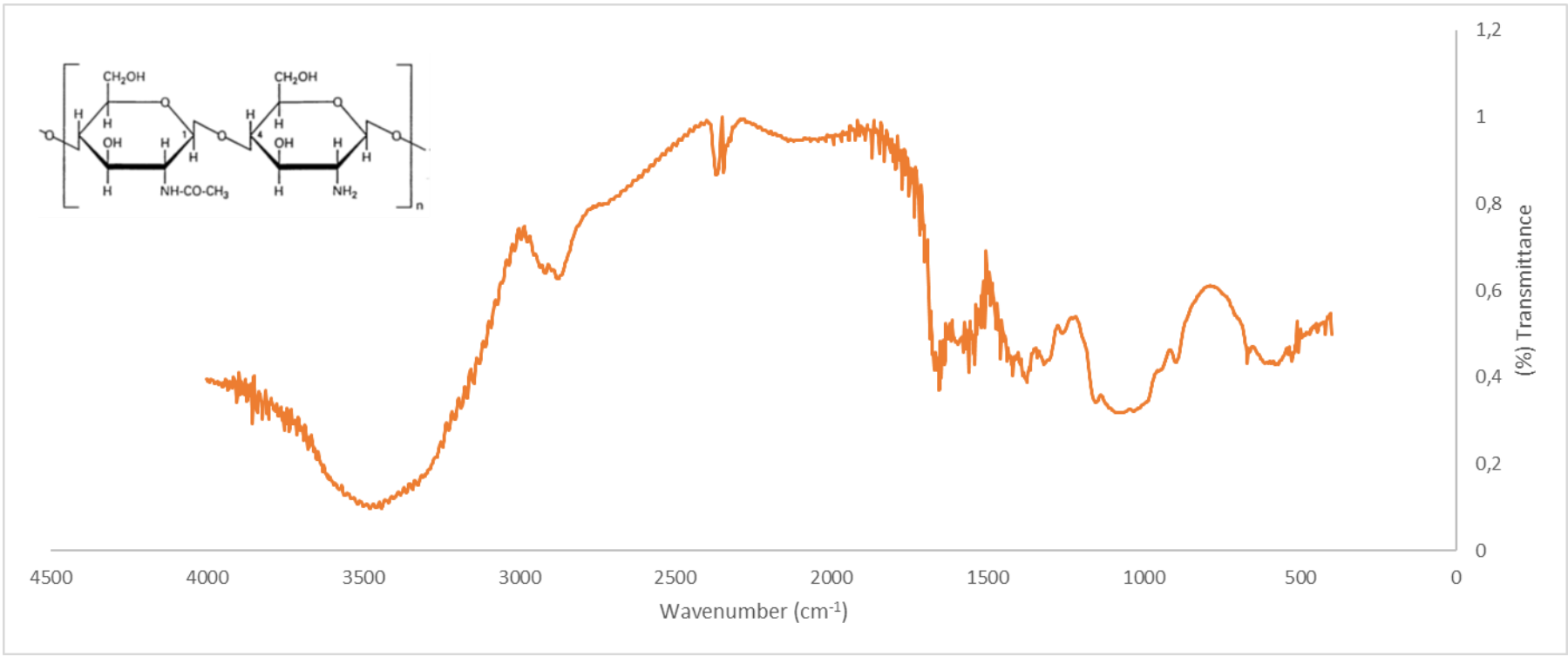

Figure 49 - FTIR spectra corresponding to CS.

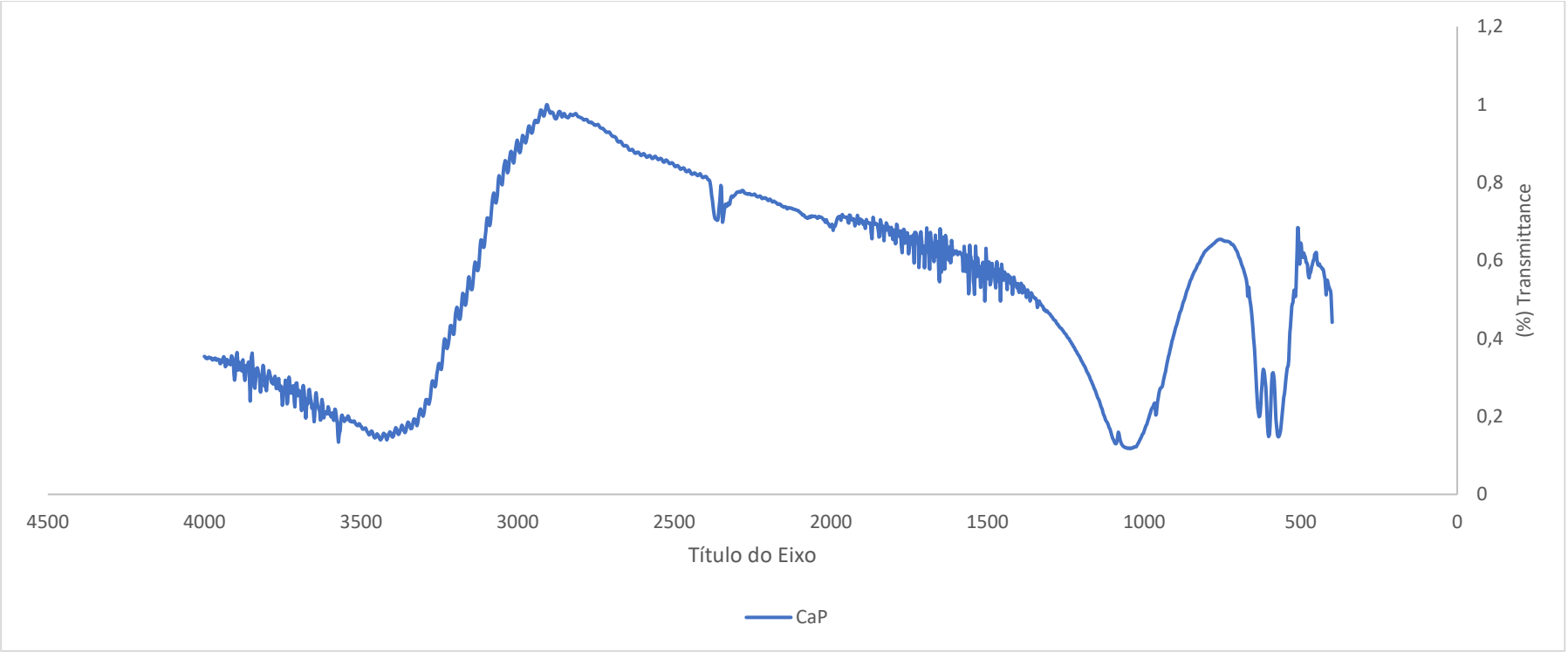

Figure 50 - FTIR spectra corresponding to CaPs.